Discovering New Physics at the Large Hadron Collider

A Dissertation

Presented to the Faculty of the Graduate School

of Cornell University

in Partial Fulfillment of the Requirement for

the Degree of Doctor of Philosophy

by

Joshua Berger

August 2012

Discovering New Physics at the Large Hadron Collider

Joshua Berger, Ph.D.

Cornell University 2012

A new era of major particle physics discoveries has begun at the Large Hadron Collider (LHC). Theorists have devised models that suggest a wide range of phenomenology. The goal of this work is to present techniques for seeing signatures of new physics at the LHC. Our approach is threefold. First, we suggest new ways to see partner particles for the top quark that are required to solve the fine-tuning problem of the Standard Model (SM). We proceed to suggest ways to see CP violating in new states produced at the LHC, which could help explain baryogenesis. Finally, we discuss ways to study the flavor structure present in extensions of the SM.

Biographical Sketch

Josh was born in the midst of a Montreal winter storm. From there, he enjoyed a happy childhood filled with falling down stairs, smashing his teeth against beds, and falling of ski hill chairlifts. Perhaps all of these events knocked some sense into him, for he went on to pursue an academic career.

His formal education began at Westpark elementary school in suburban Montreal. From there, he moved on to West Island College, where his mother teaches. He began to show an interest and proficiency in the arts and sciences, but when forced to choose a career path for college, he went with science. The more physics courses he took, the more he leaned toward studying that discipline. For CÉGEP, the intermediate college between high school and university in Québec, he chose to study Pure and Applied Science. While originally intending to go on to study engineering, he ultimately went with his heart and entered the Honours Mathematics and Physics program at McGill University. There, he began his research career by working on a project looking for evidence of cosmic strings under the supervision of Professor Robert Brandenberger. He graduated in May of 2006 with a B.Sc.

For graduate school, he moved the USA and studied at Cornell University. There, he pursued his nascent interest in high energy particle physics. While he originally worked in experimental particle physics on the Compact Muon Solenoid experiment, he switched to theoretical work upon the arrival of Professor Yuval Grossman, who became his supervisor. The results of this collaboration are presented in this Thesis.

To my parents who have supported me throughout my career despite my decision to keep moving further away from Montreal.

Acknowledgements

I would like to begin by thanking my thesis adviser, Yuval Grossman, without whose guidance this work would not be possible. Beyond steering my development as a physicist, he has provided inumerable lessons about life and the academic world. I would also like to thank my many collaborators in the completion of the work making up this thesis: Monika Blanke, Csaba Csáki, Yuval Grossman, Ben Heidenreich, Jay Hubisz, Maxim Perelstein, Shamayita Ray, Michael Saelim, and Andrew Spray. The entire high energy theory group at Cornell has been instrumental to my successes, as friends, mentors, and resources for discussions about physics. I would like to thank all the many other physicists whose discussions were instrumental to this work: Gala Nicolas Kaufman, Yossi Nir, Michael Peskin, Javi Serra, João Silva, Yael Shadmi, Natalia Toro, Jay Wacker. I have had the pleasure to visit several institutions during my studies and I would like to thank all my hosts, particularly during my extended visits to the TASI and Cargese summer schools. I would like to acknowledge the financial support of the Cornell physics department, NSF grants PHY-0355005, PHY-0757868, and CAREER award PHY-0844667. My collaborators have been supported by DOE grant DE-FG02-85ER40237 and the National Sciences and Engineering Research Council for Canada (NSERC).

In addition, I would like to thank my parents, Josif and Tessa Berger, for their support and for putting up with me living so far from Montreal. I would also like to thank the various people with who have had extended stays at my home in Ithaca for providing entertaining breaks from work when necessary. Lastly, I would to thank the Cornell High Energy espresso club and Gimme! Coffee for providing the caffeine necessary to complete this work.

Contents

CHAPTER 1

Introduction

In the 1960s and '70s, several important works [1, 2, 3, 4, 5, 6] completed the development of a model describing the universe up to and beyond the shortest distances yet probed. Known now as the Standard Model (SM), this model was tested [7, 8, 9, 10, 11, 12, 13, 14] in exquisite detail and, within experimental and theoretical uncertainties, succeeded in describing all observed phenomena observed up to the time of this writing[1]. Yet the SM is an effective model that can only be good down to a certain unknown distance scale. There are compelling reasons to believe that it needs to be extended to describe physics that will be probed shortly at the Large Hadron Collider (LHC). The work done in completing this thesis focused on constructing and studying such extensions, as well as their implications for the experiments at the LHC. The goal, in the end, is to determine the effective Lagrangian that describes nature at the TeV scale.

We begin in this introduction by discussing the SM itself, its successes and its failures. We then continue by discussing the LHC experiments and how they will try to discover new physics. Finally, before delving into specific studies, we give an overview of the most relevant extensions of the SM.

[1]The only uncontroversial exception is the observation of neutrino mixing. As discussed below, these results can be naturally accommodated using non-renormalizable operators.

Field	$SU(3)_C$	$SU(2)_L$	$U(1)_Y$
Q_{Li}	3	2	$\frac{1}{6}$
U_{Ri}	3	1	$\frac{2}{3}$
D_{Ri}	3	1	$-\frac{1}{3}$
L_{Li}	1	2	$-\frac{1}{2}$
E_{Ri}	1	1	-1
H	1	2	$\frac{1}{2}$

Table 1.1: The Standard Model field content. The first rows indicate Weyl fermions, while the last row is the scalar field. Each Weyl fermion comes in three copies. The subgroup $SU(2)_L \times U(1)_Y$ is spontaneously broken in the vacuum of the Higgs field potential.

1.1 THE STANDARD MODEL

1.1.1 Describing the model

The Standard Model (SM), like any relativistic field theory, can be described by specifying the gauge groups, the field content, and the pattern of spontaneous symmetry breaking[2]. Then, the Lagrangian describing the theory is simply the most general renormalizable one compatible with the symmetries.

Following this procedure, we describe the SM as follows. The gauge group is $SU(3)_C \times SU(2)_L \times U(1)_Y$. The field content for any renormalizable theory consists entirely of Weyl fermions and scalar fields (as well as the gauge bosons). The Weyl fermions come as three copies, or generations, which transform identically under the gauge group. The fermions are distinguished further based on their transformation properties under $SU(3)_C$. Those that transform (Q_L, U_R, D_R) are known as quarks and those that do not (L_L, E_R) are known as leptons. There is a single scalar field, known as the Higgs field. The transformation properties of this fields are described in Table 1.1.

The final essential piece to the SM picture is the use of the Higgs Field to spontaneously breaks the electroweak symmetry $SU(2)_L \times U(1)_Y$ to its $U(1)_{\rm EM}$ subgroup. The most general renormalizable Higgs potential compatible with gauge symmetries can be written as

$$V(H) = \mu^2 H^\dagger H + \lambda (H^\dagger H)^2. \tag{1.1}$$

[2]In principle, one needs to specify the amount of supersymmetry as well, but the SM does not have any supersymmetry.

The signs of μ^2 and λ are thusfar unspecified. In order for the potential to have a stable minimum, $\lambda \geq 0$ is requried. The sign of μ^2, however, can go either way. If $\mu^2 > 0$, then the potential has a minimum at 0 and the gauge symmetries of the SM remain unbroken, up to effects induced if the gauge groups become strongly coupled. If $\mu^2 < 0$, then we must have $\lambda > 0$ and there is a minimum of the potential at

$$H^\dagger H = -\frac{\mu^2}{\lambda}. \tag{1.2}$$

The Higgs fields gets a Vacuum Expectation Value (VEV). The excitations about this vacuum correspond to four degrees of freedom. Three are eaten gauge bosons, resulting in massive spin 1 particles Z^0 and $W^\pm$. The remaining scalar degree of freedom is called the Higgs boson.

After electroweak symmetry breaking (EWSB), the fermion $SU(2)_L$ doublets are split in two. Their quadratic terms can be diagonalized by unitary rotations, resulting in the so-called mass basis. The spectrum can then be described in terms of transformation properties under $SU(3)_C$ and $U(1)_{\rm EM}$. In the mass basis, the full physical spectrum of the SM is as follows: one scalar $h(1)_0$; 3 fermionic generations each of charged leptons $\ell(1)_{-1}$, neutrinos $\nu(1)_0$, up-type quarks $u(3)_{2/3}$, and the down-type quarks $d(3)_{-1/3}$; the massless gauge bosons for $U(1)_{\rm EM}$, the photon γ, and for $SU(3)_C$, the gluon g; and the massive gauge bosons $W^\pm$ and Z from $SU(2)_L \times U(1)_Y$ breaking.

This completes the most basic description of the SM. The only remaining step is to write down the most general renormalizable Lagrangian. On the other hand, this model leads to extremely rich phenomenology. A few important properties of the model that we will revisit frequently include:

- The renormalizable Lagrangian has four accidental global $U(1)$ symmetries: three corresponding to rotations of the L_{Li} and E_{Ri} fields for each generation separately, known as lepton family number, and one corresponding to simultaneous rotations of all Q_L, U_R and D_R fields, known as baryon number. This ensures the stability of the lightest state carrying each type of quantum number. The case of baryon number is particularly important as it ensures the stability of the proton.

- The fermions in the model only get mass via EWSB. There are three neutral components of the L_{Li} fields that do not get mass at all in the SM and are known as neutrinos. There is

only one mass scale that appears in the Lagrangian, which is the parameter μ^2 of the Higgs potential.

- The coupling constants for the fermion-Higgs interactions, known as Yukawa couplings, are all smaller than about 1/100 with the exception of the coupling of the heaviest up-type quark, the top quark. Without these Yukawa couplings, the SM enjoys a large $U(3)^5$ global symmetry known as flavor and a $SU(2)$ in the Higgs potential known as custodial symmetry. These approximate symmetries ensure important relations between various observables.

- The coupling corresponding to the $SU(3)_C$ color gauge group, denoted by g_s, becomes non-perturbatively large at a small energy scale of $\Lambda_{\rm QCD} \sim 200$ MeV. The strong coupling in the infrared (IR) leads to the phenomenon of confinement: would-be low energy states carrying $SU(3)_C$ quantum numbers form color-neutral bound states. Quark-antiquark bound states are known as mesons and triquark bound states are known as baryons.

- In the mass basis, the off-diagonal couplings of the quarks with the Higgs get transferred into the couplings with the W gauge boson. The flavor structure of this interaction is described by a 3×3 unitary matrix known as the Cabibbo-Kobayashi-Maskawa (CKM) matrix [15, 16] which contains three mixing angles and one CP-violating phase. This is the only source of CP violation (other than the unmeasured strong CP phase) in the SM. All of the flavor-changing and CP-violating interactions come through the W boson charged current interactions, given by the Lagrangian terms:

$$\mathcal{L} = -\frac{g}{\sqrt{2}} V_{ij} \overline{u}_{L,i} \not{W} d_{L,j} + \text{h.c.}, \tag{1.3}$$

  where V_{ij} is the CKM matrix and g is the $SU(2)_L$ coupling constant.

1.2 QUANTIFYING THE SUCCESS

In addition to containing exactly the spectrum of particles observed in experiments, there are several quantitative predictions of the SM that match accurately with experiment. It is particularly useful to construct observables that vanish at leading order in the couplings. These observables are

predicted to be small, so they are most sensitive to deviations from SM prediction.

In this section, we provide a brief overview of such quantitative predictions. It is important to note that we have compelling reasons to expect new physics to enter around the 1 TeV scale. These reasons will be outlined below, but the bounds imposed on new symmetry-violating operators should be taken in with this expectation in mind.

Since the states that we have observed in nature thusfar are all consistent with the spectrum of the SM, we can quantify bounds imposed by the following observables as constraints on higher dimension operators consistent with the gauge symmetries of the SM. We do not, on the other hand, assume the global symmetries, which are expected on general grounds to be violated in high-energy (UV) completions. We can look for violations of the SM symmetries by constructing appropriate observables sensitive to these operators. This provides stringent bounds on the scales at which symmetry breaking enters. We consider only the most important dimension 5 and 6 operators.

The only dimension 5 operator that can be written down that is consistent with gauge symmetries is the lepton-number violating operator

$$\lambda^{\nu}_{ij}\frac{(\overline{L^c}_{Li}H)(\tilde{H}^{\dagger}L_{Lj})}{\Lambda}, \tag{1.4}$$

where L^c denotes the charge conjugate field of L, $\tilde{H}$ is $(\epsilon H)^{\dagger}$ using the Levi-Civita symbol ϵ and fields in parantheses are $SU(2)_L$ contracted. After the Higgs gets a VEV, this operator corresponds to neutrinos acquiring a Majorana mass. This is not the only way in which neutrinos could acquire mass. If an additional set of SM gauge singlet fields is introduced and lepton number is imposed, then it is possible to give neutrinos as Dirac mass. To settle between the two possibilities, we must observe or exclude neutrinoless double beta decay, an explicitly lepton-number violating process.

For the moment, we assume that neutrinos acquire a Majorana mass via this dimension 5 operator. Neutrino oscillation measurements [17] place a lower bound on the largest eigenvalue of the operator 1.4. In addition, cosmological data [18] place an upper bound on this operator. These combine to impose

$$10^{14}\text{ GeV} \lesssim \frac{\Lambda}{\lambda^{\nu}_3} \lesssim 6\times 10^{14}\text{ GeV}. \tag{1.5}$$

In addition to the dimension 5 operator, there are several dimension 6 operators that are either not allowed or are highly suppressed.

For instance, there are dimension 6 operators that violate both baryon and lepton number. Such operators the most highly constrained in the entire model since they would lead to proton decay, which has been not been observed even on time scales much longer than the age of the universe. The operators in question have the following structures [19]:

$$\lambda^{B1}_{ijk\ell}\frac{(\overline{Q^c}_{Li}Q_{Lj})(\overline{Q^c}_{Lk}L_{L\ell})}{\Lambda^2}, \qquad \lambda^{B2}_{ijk\ell}\frac{\overline{D^c}_{Ri}U_{Rj}\overline{U^c}_{Rk}E_{R\ell}}{\Lambda^2},$$
$$\lambda^{B3}_{ijk\ell}\frac{(\overline{Q^c}_{Li}Q_{Lj})\overline{E^c}_{Rk}U_{R\ell}}{\Lambda^2}, \qquad \lambda^{B4}_{ijk\ell}\frac{\overline{D^c}_{Ri}U_{Rj}(\overline{Q^c}_{Lk}L_{L\ell})}{\Lambda^2}. \tag{1.6}$$

The most stringent bounds come on those operators involving the first generation of SM, which contribute to the proton decay amplitude. For example, the strongest bound is on $p \to \pi e$ at $\tau_{p\to\pi e} \geq 8.2 \times 10^{33}$ years [11], leading to

$$\frac{\Lambda}{\sqrt{|\lambda^B|}} \gtrsim 10^{16} \text{ GeV}. \tag{1.7}$$

As these bounds are enticingly close to the scale of Grand Unification, it has long been assumed that new baryon number violation comes in at this scale. The other possibility is that the structure of baryon number violating couplings is highly non-trivial.

As mentioned previously, flavor is an approximate symmetry of the SM, broken only by the Yukawa couplings. In the mass basis, flavor changing is mediated exclusively by the charged W boson. That is, they are exclusively charged current interactions. Flavor changing neutral currents (FCNCs) only occur starting at one loop and are therefore highly suppressed. Large FCNCs are not observed in experiments, which are thusfar in exquisite agreement with SM predictions, so contributions to FCNCs from new physics are highly suppressed.

There are many dimension 6 operators which contribute to FCNCs. On the other hand, flavor changing properties of the K, D and B mesons are very well measured. For example, operators of the form

$$c\frac{(\bar{s}d)(\bar{s}d)}{\Lambda^2} \tag{1.8}$$

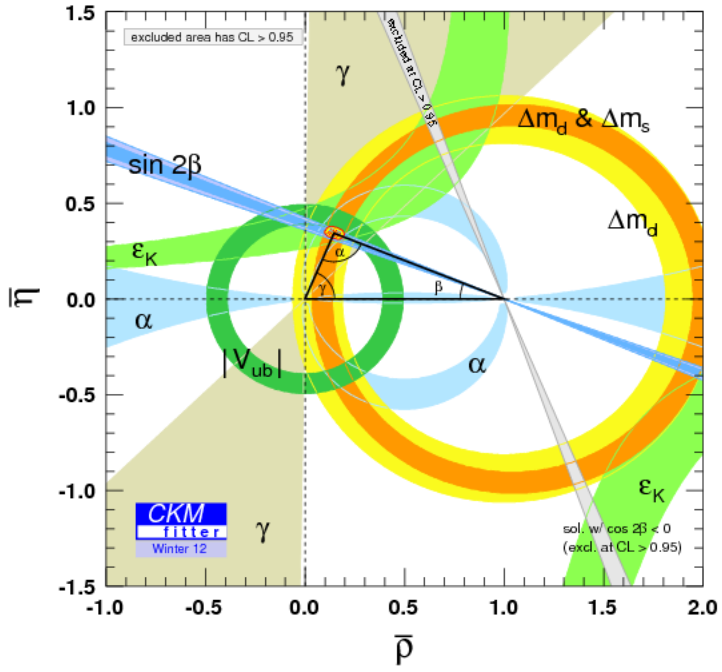

Figure 1.1: The unitarity triangle fit as performed by the CKMfitter group [10].

contributes to the CP-violating kaon system observable ϵ_K. On the other hand, ϵ_K is measured to have a value of 2.228×10^{-3} [7, 20], giving a bound on this operator of

$$\frac{\Lambda}{\sqrt{c}} \gtrsim 10^4 \text{ Tev} \tag{1.9}$$

The bounds on FCNCs in the B and D systems are only slightly weaker at around 10^3 TeV.

The success of the SM flavor description can also be summarized by comparing with a determination of the unitarity triangle [10], as shown in Fig. 1.1. Since the SM predicts a unitary mixing matrix amongst the quark flavors, we can verify that unitarity holds. This verification is generally presented visually, as it demands that the sum of three complex numbers, say $\sum_i V_{id} V^*_{id'}$, is zero; in the complex plane, the three numbers then form a triangle.

There is one final class of operators that are well constrained, yet appear in the SM only at loop level. These are operators involve the interactions of the electroweak gauge bosons W, Z and γ.

There are at total of 7 such operators, but the two most constrained are generally described in terms of the S and T Peskin-Takeuchi parameters [21]. If we define operators

$$c_S \frac{H^\dagger W^{\mu\nu} B_{\mu\nu} H}{\Lambda_S^2}, \qquad c_T \frac{|H^\dagger D_\mu H|^2}{\Lambda_T^2} \tag{1.10}$$

then the S, T and U parameters can be written, under the assumption that the Higgs sector consists solely of $SU(2)_L$ doublets, as [22]

$$\alpha S = 4 s_W c_W c_S \frac{v^2}{\Lambda_S^2}, \qquad \alpha T = -c_T \frac{v^2}{2\Lambda_T^2}. \tag{1.11}$$

These parameters can be constrained by doing a fit to all of the electroweak observables measured primarily at the LEP experiments. They are somewhat correlated and depend on the Higgs mass, but the bounds are roughly [7]

$$\frac{\Lambda_S}{\sqrt{c_S}} \gtrsim 8 \text{ TeV}, \qquad \frac{\Lambda_T}{\sqrt{c_T}} \gtrsim 4 \text{ TeV} \tag{1.12}$$

It is important to note that the T parameter is protected by an approximate symmetry of the SM, called custodial symmetry. The Higgs potential alone has an $SU(2)_L \times SU(2)_R$ symmetry, of which the $SU(2)_L$ is gauged, but the $SU(2)_R$ is an accidental global symmetry. The VEV of the Higgs breaks this symmetry to a single $SU(2)_C$ symmetry, which prevents a T parameter from developing. The Yukawa couplings explicitly break this symmetry, allowing for the development of a non-zero T parameter at loop level in the SM. The S parameter has no such symmetry protection and can generally face large corrections.

1.3 PROBLEMS WITH THE STANDARD MODEL

There are several problems with the SM that have been found. Several of these hint at scales for new physics that are being probed in current experiments. In this section, we give a brief overview of the various issues with the SM and what they say about new physics. There are several important problems that we will not discuss in detail, but that we mention here, including those

related to the strong CP phase, grand unification, and quantum gravity. The following problems have the most direct impact on the work of this thesis.

The first problem, which leads to several additional puzzles, is the hierarchy problem. Most of the parameters of the SM Lagrangian are renormalizable in that they receive quantum corrections logarithmically sensitive to physics at the cutoff of validity of the SM. There is, however, one parameter that is quadratically sensitive to physics at the UV scale, the quadratic μ^2 term in the Higgs potential (1.1). On the other hand, the scale of electroweak symmetry breaking is now known to be $v \approx 246$ GeV. Unless there is some precise cancelation, known as fine-tuning, between the Higgs quadratic Lagrangian parameter and its various loop corrections, we expect that the scale of physics should be not too far above v.

To make this more precise, we consider the largest loop contribution to μ^2. Among SM particles, the top quark couples most strongly to the Higgs and so gives the largest contribution:

$$\delta\mu^2 = -\frac{3}{8\pi^2} y_t^2 \Lambda^2. \tag{1.13}$$

For $\mu^2 \gtrsim 1.4$ TeV, the Higgs would have non-perturbative couplings. Since $y_t \sim 1$, we then have a fine-tuning dependent bound on physics of

$$\Lambda \lesssim 7 \text{ TeV}. \tag{1.14}$$

We expect Λ to be even smaller to evade fine-tuning, since there are now many compelling hints for a light Higgs boson. Electroweak precision measurements and now direct LHC measurements both favor $m_h \sim 125$ GeV [8, 23]. This would imply a scale of new physics in the top sector around

$$\Lambda \lesssim 400 \text{ GeV}. \tag{1.15}$$

The W and Z bosons are next most strongly coupled and new physics in the electroweak sector is bounded to come in at around 1.2 TeV.

One of the primary goals of the LHC will be to discovery new top and electroweak sector physics

if it is out there and a primary focus of the work in this thesis is to study possible extensions of the SM in general that are not fine-tuned, yet leave distinct signatures at the LHC.

Another oft discussed problem is that of dark matter. There is now overwhelming astrophysical evidence [24, 25, 26] for a new class of stable particles that makes up over 80 % [24] of the matter in the universe. Very little is known about these particles for they have only been observed gravitationally at the time of this writing. The following properties are known to some degree of certainty. Dark matter is

- Stable [27]
- Particulate [25]
- Weakly interaction with SM (e.g. no electromagnetic or color charge) [28]
- Gravitationally interacting.

We further know its abundance in the present day universe, generally written as a ratio with the critical density [24]:

$$\Omega \approx 0.22. \tag{1.16}$$

Under the most rudimentary set of assumptions, however, there is a tie between dark matter and TeV scale physics. Supposing that dark matter was in thermal equilibrium with SM matter when the universe was a temperatures higher than the dark matter mass scale and then froze out as the temperature decreased below that scale, to explain the observed density of dark matter in the universe, the cross-section would have to be given by [29]

$$\langle \sigma v \rangle \sim 3 \times 10^{26} \text{ cm}^2 \approx 1 \text{ pb} \times \frac{v}{c}, \tag{1.17}$$

which is around what is expected for a particle that couples via the $SU(2)L$ "weak" coupling constant and has a mass around the TeV scale. This so-called WIMP miracle constitutes the second piece of evidence pointing to the TeV scale.

The SM also has a problem explaining the observed abundance of baryonic matter in the universe. When combined with general relativity on cosmological distances, the SM explains the

history of the universe back to very early times. On the other hand, there are a few gaping holes. Some, such as those solved by inflation [29], are expected to be at very high energies that can only be probed astrophysically and may be related to theories of quantum gravity. The problem of baryogenesis, on the other hand, is likely a problem of our particle physics model.

Inflation would tend to wash out any charge asymmetries in the universe that were present by initial conditions, leaving a universe that was symmetric [29]. In particular, the post-inflation universe is expected to have negligible baryon-antibaryon asymmetry at first. The observed asymmetry should then be generated dynamically. Baryogenesis, as this procedure is known, requires three conditions set out by Sakharov [30]:

1. Baryon number violation;

2. C and CP violation;

3. Out-of-equilibrium dynamics.

While the SM history contains all of these ingredients, it turns out to be insufficient to generate the observed asymmetry. In particular, CP violation is extremely suppressed, leading to the proposal that there are additional sources of CP violation beyond those present in the SM. Many models contain such sources, but they are also highly constrained by low energy flavor [10, 31] and electric dipole moment [32, 33] observables.

The final issue that we mention is the SM flavor puzzle. The flavor-violating interactions of the SM follow an unexpected pattern. They are determined by dimensionless couplings, which we naively expect to be $\mathcal{O}(1)$. On the other hand, the masses determined by the Yukawa eigenvalues span almost six order of magnitude, while the Cabibbo mixing angle that is the dominant factor in flavor-changing interactions is small. If neutrino mass and mixing is included, the picture becomes even further muddled: the masses are extremely small compared to the weak scale, which may be explained by implementing the see saw mechanism, and the mixing angles are large. This leads to the expectation that some high energy dynamics explains the particular flavor pattern observed in the SM.

1.4 THE EXPERIMENTAL FRONTIER

The success of the SM remains somewhat incomplete: the Higgs boson remains to be observed conclusively in experiment. In additon, several of the problems discussed in Section 1.3 may see their solution at energies of order 1 TeV, as indicated primarily by the hierarchy problem.

In order to rectify this situation, the Large Hadron Collider (LHC) is colliding protons at high energy. Currently, the highest energy collisions have been at 8 TeV. Two general purpose detectors, CMS [34] and ATLAS [35], and two specialized detectors, ALICE [36] and LHCb [37], are placed around the accelerator ring.

The experiments have thusfar provided enticing hints of a Higgs boson with a mass of around 125 GeV with properties consistent with SM predictions [38, 39]. If these hints are confirmed later in 2012, then the goals of the LHC will shift slightly.

The first goal of future analyses will be to study the properties of the Higgs in detail. A 125 GeV Higgs is ideal for these purposes: many decay modes are measurable, allowing for a precise determination of the relative branching fractions.

The second goal will be to determine what, if anything, solves the hierarchy problem. Since the biggest hierarchy problem is due to the top quark loops, much of the focus is on discovering so-called top partners that provide additional virtual contributions to the Higgs potential and render a light Higgs natural. The discovery of such a top partner may be challenging and we have devoted chapters 2 and 3 of this thesis to studying the discovery prospects of top partners.

Beyond the hierarchy problem, several other problems have direct impacts on the physics of the weak scale. The strong constraints on flavor, CP, baryon number, and lepton number violation restrict the couplings in models of new physics, as discussed in Section 1.2. The flavor structure of models beyond the SM is studied directly in Chapter 4, while methods for studying CP violation at the LHC are explored in Chapter 5.

In addition, exciting new results are expected in both dark matter and neutrino experiments.

Dark matter experiments come in two varieties: direct and indirect detection. The former looks for collision of dark matter with baryonic matter in a detector, while the latter looks for the

resulting products of dark matter annihilation or decay. These experiments provide complimentary constraints on the physics of the TeV scale, where we might expect to see dark matter because of the WIMP miracle.

Neutrino experiments have recently measured the third mixing angle in the active neutrino mixing matrix [40, 17] and can soon hope to probe CP violation [41] and lepton number violation via Majorana masses [42]. The neutrino sector appears to have a very different structure from the quark sector, motivating the construction of flavor models such as that studied in Chapter 6.

1.5 MODELS OF NEW PHYSICS

The problems discussed in Section 1.3 and the experiments discussed in Section 1.4 have motivated the construction of new models that solve one ore more of the problems, while providing observable consequences at future experiments. In this section, we provide a brief overview of some of the models most relevant for the work in this thesis.

The primary motivation for new models at the LHC is the hierarchy problem. There are two known classes of models that alleviate the fine-tuning issues of the SM: supersymmetry and strong dynamics.

Supersymmetry (SUSY) [43] is a powerful extension of the Poincaré symmetry of the SM. It transforms bosons into fermions and vice versa, such that spin 0 bosons are afforded the chiral protection that fermions enjoy; the contributions to their masses can then be at most logarithmically divergent. On the other hand, SUSY cannot be an exact symmetry of nature and much of the interresting phenomenology of such models is due to the variety of ways in which it can be broken. From the point of view of a TeV scale phenomenologist, viable models of SUSY breaking can be parametrized by new dimensionful parameters in the Lagrangian that only involve the spin 0 partners of Weyl fermions and the fermionic partners of gauge bosons. They introduce a large number of new parameters that drastically affect LHC phenomenology.

In addition to these SUSY breaking effects, there are two important SUSY-conserving effects, aside from the alleviation of the fine-tuning problem. The first is the introduction of a more complicated Higgs sector, with an extra doublet of bosons. The new bosons may be observable

at the LHC. In addition, the couplings of the Higgs are now restricted such that it is favored to have a very light Higgs, well below the current bounds. Loop corrections will tend to raise the mass of the Higgs, but simultaneously introduce fine-tuning. The second SUSY conserving effect is the introduction of a new approximate symmetry. The renormalizable SUSY conserving Lagrangian contains terms that would induce rapid proton decay. Some new principle must prevent the problematic terms. The most often studied solution is to introduce a symmetry known as R-parity, defined as

$$R = (-1)^{3B+L+2S}, \tag{1.18}$$

where B is baryon number, L is lepton number, and S is spin. Current LHC results place a lot of strain on R-parity conserving models. In this thesis, we will study one recent alternative to this paradigm that evade many of the current bounds.

Strong dynamics models [44] are also under severe constraints, this time from low energy precision measurements and the hints of a light Higgs. Such models typically induce large corrections to already well constrained dimension 6 electroweak operators, such as S and T [45]. Furthermore, they often do not have a light Higgs state. Both of these issues can be solved by either using nearly conformal dynamics [46] (which are dual to the existence of an extra dimension via the AdS/CFT correspondence [47, 48]) or by making the Higgs a pseudo-Nambu-Goldstone boson of a spontaneously broken symmetry, a so-called Little Higgs [49]. In either case, to have a light Higgs without fine-tuning, a fermionic top partner must exist in these models and we devote a Chapter 2 to the study of this possibility.

With this survey of the status of high-energy particle physics, we are ready to delve into the core material of this thesis. The content of the remaining chapters is based on work presented in Ref. [50, 51, 52, 53, 54]. Chapter 2 is devoted to the study of fermionic top partners in Little Higgs models. In Chapter 3, we look at stop production in R-parity conserving models, again using jet substructure to help. In Chapter 4, we study the effects of flavor symmetries on the structure of models of new physics. In Chapter 5, we begin our study of CP violation at the LHC. In Chapter 6, we turn to the neutrino sector and show how spontaneously broken continuous symmetries can be used to explain the observed structure of their masses and mixing angles.

CHAPTER 2

A Fermionic Top Partner: Naturalness and the LHC

2.1 INTRODUCTION

The Standard Model (SM) of particle physics postulates the existence of an elementary scalar field, the Higgs, which is responsible for electroweak symmetry breaking. Precision measurements of the properties of electroweak gauge bosons are consistent with this picture, and favor a light ($\sim$ 100 GeV) Higgs boson. Recently, experiments at the Large Hadron Collider (LHC) reported preliminary evidence for a new particle with properties roughly consistent with the SM Higgs and a mass of about 125 GeV [23].

In the SM, the contribution of quantum loops to the Higgs mass term is quadratically divergent. To avoid fine-tuning, new physics beyond the SM must appear and cut off this divergence at a scale of order 1 TeV or below. Precision electroweak data favors models where the divergence is cancelled by loops of new weakly-coupled states; such cancellations can occur naturally as a consequence of underlying symmetries of the theory. What is the minimal set of new particles that must appear below 1 TeV to avoid fine-tuning? It is well known that the only SM contribution to the Higgs mass that must be modified at sub-TeV scales is the one-loop correction from the top sector. All other SM loops are numerically suppressed by either gauge or non-top Yukawa couplings, by extra loop factors, or both. As a result, the states responsible for cutting off these loops can lie above 1 TeV with no loss of naturalness. Thus, the sub-TeV particles that soften the divergence in the top

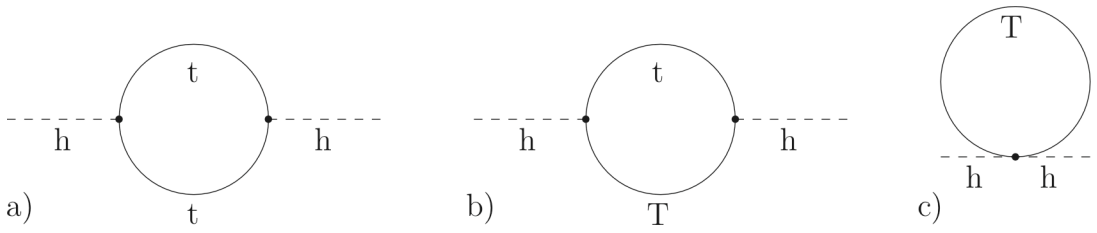

Figure 2.1: One-loop Higgs mass renormalization in a model with a fermionic top partner, such as the Littlest Higgs.

loop, the "top partners," provide a uniquely well-motivated target for searches at the LHC, and it must be ensured that a comprehensive, careful search for such partners is conducted.

The best-known mechanism for canceling the Higgs mass divergences is supersymmetry (SUSY). In SUSY models, the quadratic divergence in the SM top loop is cancelled by loops of scalar tops, or stops. Recently, a number of papers [55] emphasized the importance of stop searches at the LHC, and reinterpreted the published LHC results, based on the 1 fb^{-1} integrated luminosity data set, in terms of bounds on stop masses. It was found that completely natural spectra are allowed so far. On the other hand, incorporating a 125 GeV Higgs in the Minimal SUSY Model (MSSM) does require significant fine-tuning, of order 1% at best. (Fine-tuning can be reduced in non-minimal models [56].)

However, SUSY is not the only option for canceling the quadratic divergence in the SM top loop. An alternative is to introduce a spin-1/2 top partner T, a Dirac fermion with mass m_T, which is an $SU(2)_L$ singlet, color triplet, and has electric charge 2/3. In the Weyl basis, $T = (T_L, T_R)$. This field couples to the SM Higgs doublet H via

$$\mathcal{L} = -\lambda_T T_R^\dagger \tilde{H} Q_3 + \frac{\lambda_t^2 + \lambda_T^2}{2m_T}(H^\dagger H) T_L^\dagger T_R + \text{ h.c.}\,, \tag{2.1}$$

where Q_3 is the SM third-generation left-handed quark doublet, λ_t is the SM top Yukawa, λ_T is a new dimensionless coupling constant, and $\tilde{H} = (i\sigma_2 H)^\dagger$. The one-loop contribution to the Higgs mass in this model is shown in Fig. 2.1; the quadratic divergences present in each of the

three diagrams cancel in the sum. Even though the structure of the couplings in Eq. (2.1) looks completely ad hoc at first sight, it can emerge naturally if the Higgs is embedded as a pseudo-Nambu-Goldstone boson [57] of spontaneous global symmetry breaking at the TeV scale. The global symmetry must be broken explicitly to induce non-derivative Yukawa and gauge couplings of the Higgs; divergence cancellation is achieved if the explicit symmetry breaking terms obey the "collective" condition, such as in Little Higgs models [58, 59]. (A similar mechanism is operative in the 5-dimensional composite Higgs models [60], where the role of the top partner is played by the Kaluza-Klein excitations of the top.) In this chapter, we will focus on a minimal model that incorporates the top Yukawa via collective symmetry breaking and explicitly realizes the structure of Eq. (2.1). We will present direct and indirect bounds on the model and discuss their implications for naturalness in light of the 125 GeV Higgs. We will also consider predictions for the deviations of the Higgs and top properties from the SM.

Our model is basically identical to the top sector of the Littlest Higgs [58], and we will make use of many results derived in the context of that model. The original Littlest Higgs is severely constrained by precision electroweak data [61]. The constraints come almost entirely from the extra gauge bosons of the model, whose masses are required to be above 2-3 TeV. In itself, this is not a problem for naturalness. However, the structure of the Littlest Higgs imposes a tight relation between the gauge boson and top partner masses, so that multi-TeV top partners are required, which in turn implies strong fine-tuning. This problem can be avoided by modifying the model, by introducing an additional symmetry (T-parity) to forbid tree-level corrections to precision electroweak observables [62], by decoupling the top and gauge boson partner mass scales [63], or simply by slightly lowering the cutoff and getting rid of the extra gauge bosons altogether [64]. Thus, while the structure of the top sector is robust – it is in effect fixed by the naturalness requirement – the gauge and scalar sectors appear quite model-dependent, both in their structure and in the associated mass scale. Motivated by these considerations, we consider the top sector in isolation, and identify the predictions that are in a sense unavoidable once the cancellation mechanism in Fig. 2.1 is postulated. This approach is similar to the bottom-up attitude to SUSY phenomenology advocated in Refs. [55].

The work of this chapter is based on Ref. [54]. It is organized as follows. The minimal model for the fermionic top partner is presented in Section 2.2. Section 2.3 discusses naturalness of electroweak symmetry breaking in this model, assuming a 125 GeV Higgs boson. Section 2.4 summarizes existing experimental constraints on the model, divided in three groups: precision electroweak, flavor constraints, and direct searches at the LHC. Sections 2.5 and 2.6 discuss the expected deviations of the Higgs and top properties, respectively, from the SM predictions. We summarize our findings and conclude in Section 2.7. A number of useful formulas are collected in Appendix A.

2.2 MINIMAL MODEL FOR FERMIONIC TOP PARTNER

We begin with a non-linear sigma model describing spontaneous $SU(3) \to SU(2)$ global symmetry breaking by a fundamental vev. The sigma field is

$$V = \exp\left(\frac{i\pi_a t_a}{f}\right) \begin{pmatrix} 0 \\ 0 \\ f \end{pmatrix}, \tag{2.2}$$

where t_a are the broken generators ($a = 1 \ldots 5$), π_a are the corresponding Goldstone bosons, and f is the symmetry breaking scale (we assume $f \lesssim 1$ TeV). We identify the $SU(2)$ doublet of Goldstone bosons with the SM Higgs doublet H, and ignore the remaining one which plays no role in our analysis:

$$\pi_a t_a = \begin{pmatrix} 0 & H \\ H^\dagger & 0 \end{pmatrix}. \tag{2.3}$$

To generate a top Yukawa coupling without introducing one-loop quadratic divergences, we introduce an $SU(3)$ triplet of left-handed Weyl fermions, $\chi_L = (\sigma^2 Q, U)^T_L$, and two $SU(3)$ singlet right-handed Weyl fermions, u_R and U_R. Here $Q_L = (t_L, b_L)$. These fields are coupled via [58, 65]

$$\mathcal{L} \;=\; -\lambda_1 u_R^\dagger V^\dagger \chi_L \;-\; \lambda_2 f U_R^\dagger U_L \;+\; \text{h.c.} \tag{2.4}$$

Expanding the sigma field up to terms of order $1/f^2$ gives

$$\mathcal{L} \,=\, -f\,(\lambda_1 u_R + \lambda_2 U_R)^\dagger\, U_L \,-\, \lambda_1 u_R^\dagger \tilde{H} Q_L \,+\, \frac{\lambda_1}{2f}(H^\dagger H) u_R^\dagger U_L + \text{ h.c. } + \ldots \tag{2.5}$$

where $\tilde{H} = (i\sigma_2 H)^\dagger$. The fermion mass eigenstates are

$$\begin{aligned} T_L = U_L, \quad T_R &= \frac{\lambda_1 u_R + \lambda_2 U_R}{\sqrt{\lambda_1^2+\lambda_2^2}}\,, \\ t_L = u_L, \quad t_R &= \frac{\lambda_2 u_R - \lambda_1 U_R}{\sqrt{\lambda_1^2+\lambda_2^2}}\,, \end{aligned} \tag{2.6}$$

where we neglected the Higgs vev v, assuming $v \ll f$. (The mixing angles and masses with full v dependence are given in Appendix A.) We identify $t = (t_L, t_R)$ with the SM top quark, b_L with the SM left-handed bottom, and $T = (T_L, T_R)$ with the top partner, whose mass is

$$m_T = \sqrt{\lambda_1^2 + \lambda_2^2}\, f\,. \tag{2.7}$$

The interaction terms in the mass eigenbasis become

$$\mathcal{L}_{\text{int}} \,=\, -\lambda_t t_R^\dagger \tilde{H} Q_L \,-\, \lambda_T T_R^\dagger \tilde{H} Q_L \,+\, \frac{\lambda_1^2}{m_T}(H^\dagger H) T_R^\dagger T_L \,+\, \frac{\lambda_1\lambda_2}{2m_T}(H^\dagger H) t_R^\dagger T_L + \text{ h.c. } + \ldots \tag{2.8}$$

where we defined

$$\lambda_t = \frac{\lambda_1\lambda_2}{\sqrt{\lambda_1^2+\lambda_2^2}}\,, \quad \lambda_T = \frac{\lambda_1^2}{\sqrt{\lambda_1^2+\lambda_2^2}}\,. \tag{2.9}$$

The first term is simply the SM top Yukawa; the next two terms reproduce Eq. (2.1), ensuring the cancellation of the one-loop quadratic divergence (note that $\lambda_1^2 = \lambda_t^2 + \lambda_T^2$); while the last term does not contribute to the Higgs mass renormalization at one loop, and thus does not spoil the cancellation. The cancellation is also easy to understand in terms of symmetries of the model: the first term in (2.4) preserves the global $SU(3)$, so that in the limit $\lambda_2 \to 0$ the Higgs is an exact Goldstone boson and is therefore massless. On the other hand, the second term in (2.4) breaks the $SU(3)$ explicitly, but it does not involve the Higgs at all, and so cannot generate the Higgs mass on its own. Thus, both couplings need to enter any diagram contributing to the

Higgs mass renormalization, and at the one-loop level the diagrams involving both λ's are at most logarithmically divergent.

The Higgs can be given its usual SM gauge couplings by weakly gauging the $SU(2) \times U(1)$ subgroup of the $SU(3)$. As explained in the Introduction, we do not consider extended gauge sectors here: the gauge structure of our model is the same as SM. The new top-sector fields U_L, U_R have the same gauge quantum numbers as the SM right-handed top, $(\mathbf{3}, \mathbf{1})_{4/3}$.

Non-linear sigma model interactions become strongly coupled at a scale $\Lambda \approx 4\pi f$, where another layer of new physics must occur. The effects of that physics on weak-scale observables can be parametrized by adding operators of mass dimension > 4, suppressed by appropriate powers of Λ, to the lagrangian. The leading (dimension-6) operators are

$$\mathcal{L}_{\rm UV} = \frac{c_1}{(4\pi f)^2} \left(V^\dagger D_\mu V \right)^2 + \frac{g g' c_2}{(4\pi f)^2} W^a_{\mu\nu} B^{\mu\nu} (V^\dagger Q^a V) \,, \tag{2.10}$$

where D_μ is the covariant derivative including the $SU(2) \times U(1)$ gauge fields; W and B are the $SU(2)$ and $U(1)$ field strength tensors, respectively; c_1 and c_2 are dimensionless coefficients, which are unknown but expected to be of order 1; and

$$Q^a = \begin{pmatrix} \sigma^a & \\ & 0 \end{pmatrix} . \tag{2.11}$$

The two operators in Eq. (2.10) contribute to the T and S parameters, respectively, in precision electroweak fits (see Sec. 2.4.1). We do not include operators involving the top quark, since they are not strongly constrained at present.

2.3 HIGGS MASS AND NATURALNESS

An appealing feature of the class of models we're dealing with is a simple, rather predictive description of the electroweak symmetry breaking (EWSB). At tree level, the Higgs is a Goldstone boson and the Higgs mass parameter $\mu^2 = 0$. At one loop, the leading (log-divergent) contribution

to the Higgs mass parameter from the diagrams in Fig. 2.1 is given by

$$\delta\mu^2 = -3\frac{\lambda_t^2 m_T^2}{8\pi^2}\log\frac{\Lambda^2}{m_T^2}\,. \tag{2.12}$$

Naive dimensional analysis (NDA) suggests that this is the dominant contribution to the Higgs mass: two-loop quadratically divergent contributions are suppressed by a power of $\log(4\pi)^2 \approx 5$, while gauge boson loops (assuming that their quadratic divergences are canceled at a scale close to 1 TeV) are down by $(g/\lambda)^2$. Note that Eq. (2.12) automatically has the right (negative) sign to trigger EWSB.

If the LHC hint is correct and there is indeed a 125 GeV Higgs boson, then μ^2 can be treated as known, since $m_h = \sqrt{2}|\mu|$. In our model, this essentially fixes the top partner mass, up to logarithmic dependence on Λ. For definiteness, we take $\Lambda = 4\pi f$; to leading order in v/f,

$$\Lambda \approx \frac{2\pi}{\lambda_t}\, m_T \sin 2\alpha\,, \tag{2.13}$$

where α is the mixing angle in the right-handed top sector (at leading order at v/f, $\tan\alpha = \lambda_1/\lambda_2$). For example, for $\alpha = \pi/4$, we obtain

$$m_T \approx 236 \text{ GeV}. \tag{2.14}$$

Unfortunately, the top partner at this mass is excluded by precision electroweak constraints, see Section 2.4. The mild α dependence does not change this conclusion if α is varied within a reasonable range.

The only way to raise m_T and salvage the model is to assume that the gauge-loop and/or two-loop contributions to μ^2 are enhanced, and partially cancel the top-loop contribution.[1] This requires a certain degree of fine-tuning; we quantify it by defining

$$\Delta = \frac{|\delta\mu^2|}{\mu^2_{\text{obs}}}\,, \tag{2.15}$$

[1] In fact, Ref. [66] argued that the two-loop contribution in the Littlest Higgs is enhanced compared to the NDA estimate, and estimated that it is of the same order as the logarithmically divergent one-loop contribution. Since the two-loop contribution is UV-dominated, its magnitude (and sign) cannot be determined without specifying a UV completion and performing a calculation in a UV-complete model.

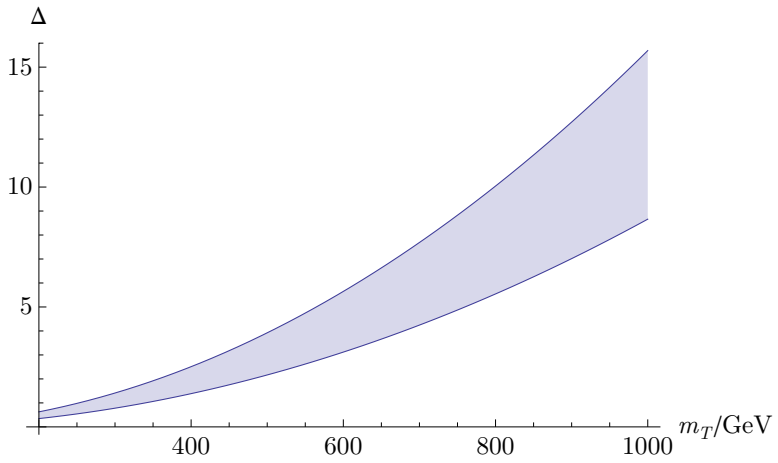

Figure 2.2: Fine-tuning as a function of the top partner mass (in GeV). We fixed $m_h = 125$ GeV. The band corresponds to varying the mixing angle α between 0.2 and 1.1.

where $\mu_{\rm obs} = m_h/\sqrt{2} \approx 88$ GeV. Required fine-tuning as a function of the top partner mass is shown in Fig. 2.2, where the band corresponds to varying the mixing angle α between 0.2 and 1.1, corresponding roughly to the range where both λ_1 and λ_2 are perturbative. This plot should be kept in mind as we discuss the experimental constraints on the model below.

A Higgs quartic coupling, $\lambda \approx 0.12$, is required to accommodate the Higgs vev $v = 246$ GeV along with a 125 GeV mass. In our model, there is no tree-level quartic, but at one loop the quartic is generated by quadratically divergent terms in the Coleman-Weinberg potential [58, 67]. In our minimal model, the quartic generated by the top-sector is in fact only logarithmically sensitive to the cutoff, and is thus expected to be small. However, the contributions to global symmetry breaking due to gauging the SM $SU(2)_L \times U(1)_Y$ do generate quadratically divergent contributions to the quartic. These diagrams are dominated by physics at the scale Λ, and hence cannot be computed without specifying a UV completion, but NDA estimates show that an $\mathcal{O}(g^2)$ quartic can be generated without tuning.

2.4 EXPERIMENTAL CONSTRAINTS

The model in Eq. (2.4) has three parameters: the symmetry breaking scale f and two dimensionless couplings $\lambda_{1,2}$. One combination of the couplings has to be fixed to reproduce the known top Yukawa, leaving two independent parameters. In our discussion of experimental constraints, we will use the top partner mass m_T and the rotation angle α between the gauge and mass eigenstates in the right-handed fermion sector. That is, α is defined by

$$t_R = \cos\alpha\, u_R - \sin\alpha\, u_R\,, \quad T_R = \sin\alpha\, u_R + \cos\alpha\, U_R\,. \tag{2.16}$$

The relation between (m_T, α) and the Lagrangian parameters, to leading order in v/f, is given in Eqs. (2.6), (2.7). In the analysis below, we will use generalizations of these formulas to all orders in v/f, see Appendix A. It is also worth noting that at order v/f, mixing between the left-handed fermion fields u_L and U_L is induced; the mixing angle β is approximately given by

$$\sin\beta \approx \tan\alpha\, \frac{m_t}{m_T}\,. \tag{2.17}$$

Again, we will use the exact expression for this mixing angle, given in Appendix A. This mixing induces the off-diagonal vector boson couplings to fermions, ZtT and WbT, which play a crucial role in the phenomenology of the model. Both couplings are proportional to $\sin\beta$.

2.4.1 Precision Electroweak Constraints

The top partner T does not induce tree-level contributions to precision electroweak observables. At one-loop, oblique corrections to the electroweak gauge boson propagators induced by diagrams

involving the T are given by [68]

$$\begin{aligned}
S_T &= \frac{s_\beta^2}{2\pi}\left[\left(\frac{1}{3}-c_\beta^2\right)\log x_t + c_\beta^2\frac{(1+x_t)^2}{(1-x_t)^2} + \frac{2c_\beta^2 x_t^2(3-x_t)\log x_t}{(1-x_t)^3} - \frac{8c_\beta^2}{3}\right], \\
T_T &= \frac{3}{16\pi}\frac{s_\beta^2}{s_w^2 c_w^2}\frac{m_t^2}{m_Z^2}\left[\frac{s_\beta^2}{x_t} - 1 - c_\beta^2 - \frac{2c_\beta^2}{1-x_t}\log x_t\right], \\
U_T &= -\frac{s_\beta^2}{2\pi}\left[s_\beta^2\log x_t + c_\beta^2\frac{(1+x_t)^2}{(1-x_t)^2} + \frac{2c_\beta^2 x_t^2(3-x_t)\log x_t}{(1-x_t)^3} - \frac{8c_\beta^2}{3}\right],
\end{aligned} \tag{2.18}$$

where $x_t = m_t^2/m_T^2$, and s_w is the sine of the Weinberg angle. In addition, there is a contribution due to the shift of the Higgs couplings to the electroweak gauge bosons from their SM values [69]:

$$\begin{aligned}
S_h &= -\frac{1}{3\pi}\frac{m_W^2}{g^2 f^2}\log\frac{m_h}{\Lambda}, \\
T_h &= \frac{3}{4\pi c_w^2}\frac{m_W^2}{g^2 f^2}\log\frac{m_h}{\Lambda},
\end{aligned} \tag{2.19}$$

where Λ is the scale where the Higgs loops are cut off. We will assume $\Lambda = 4\pi f$. Furthermore, the operators induced by the new physics at scale Λ, given in Eq. (2.10), contribute [70]

$$\begin{aligned}
S_{\rm UV} &= \frac{4c_s m_W^2}{\pi g^2 f^2}, \\
T_{\rm UV} &= -\frac{c_t m_W^2}{2\pi e^2 g^2 f^2}.
\end{aligned} \tag{2.20}$$

The only important non-flavor-universal correction is the top-partner loop contribution to the $Zb_L\bar{b}_L$ vertex. To leading order in the limit $m_T \gg m_t \gg m_W$, this is given by [68]

$$\delta g_L^{b\bar{b}} = \frac{g}{c_w}\frac{\alpha}{8\pi s_w^2}\frac{m_t^4}{m_W^2 m_T^2}\frac{\lambda_1^2}{\lambda_2^2}\log\frac{m_T^2}{m_t^2}. \tag{2.21}$$

The correction to the $Zb_R\bar{b}_R$ vertex is negligible since it is not enhanced by the top Yukawa coupling.

The results of a fit to the precision electroweak observables [71] are shown in Fig. 2.3, where we also included contours of constant fine-tuning computed according to Eq. (2.15). We conclude that:

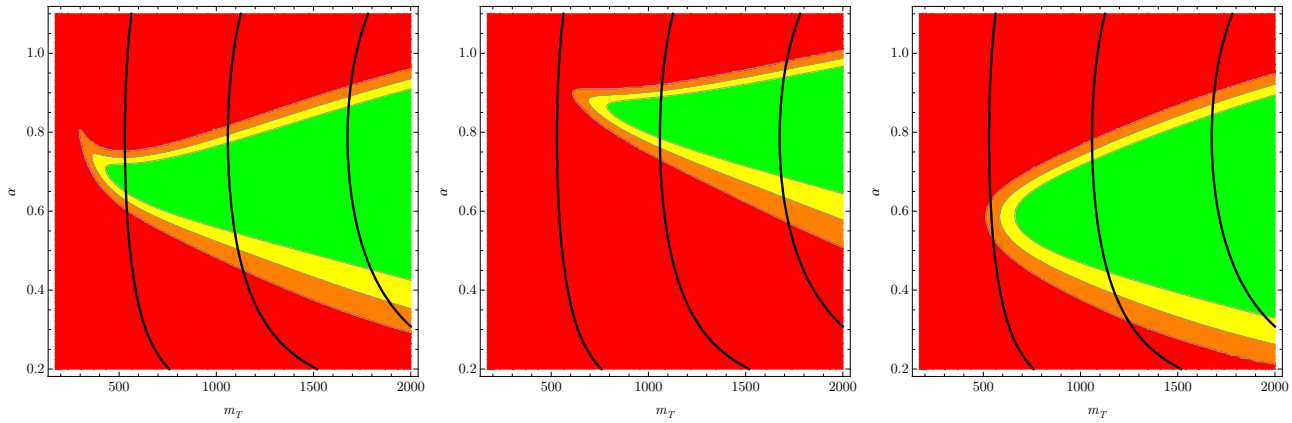

Figure 2.3: Precision electroweak constraints on the minimal fermionic top partner model, in the (m_T, α) plane. The three panels display the variation of the bounds depending on the coefficients of the UV operators: (a) $c_s = c_t = 0$; (b) $c_s = c_t = 1$; (c) $c_s = +1$, $c_t = -1$. Thick black lines represent constant fine-tuning contours: from left to right, 20%, 5%, and 2% fine tuning.

- The lower bound on the top partner mass from precision electroweak observables is approximately 500 GeV;
- The corresponding minimum level of fine-tuning on the Higgs mass is about 20%. This is significantly better than in the MSSM with a 125 GeV Higgs, and comparable to the NMSSM with large λ [56];
- These conclusions do not depend strongly on the operators induced by the UV completion of the model, as long as the size of these operators is roughly consistent with naive dimensional analysis.

2.4.2 Flavor Constraints

By selecting the top quark to be the only one with a partner, and introducing mixing between the SM top and its partner, our model explicitly breaks the approximate flavor symmetry of the SM, leading to potential constraints from flavor-changing processes. We investigate these constraints in this section.

Including the mixing between the three SM generations, the mass terms of the up-type quarks

in the gauge basis form a 4×4 matrix M_u^{IJ}, while the down-type mass terms are described by a 3×3 matrix M_d^{ij}. (Here and below, capital indices run from 1 to 4, and the lower case indices from 1 to 3.) Diagonalizing these matrices requires

$$\begin{aligned} M_u &\to L_u M_u R_u^\dagger \,, \\ M_d &\to L_d M_d R_d^\dagger \,, \end{aligned} \tag{2.22}$$

where L and R matrices rotate the left-handed and right-handed quark fields, respectively. The charged-current interactions in the gauge basis have the form

$$\begin{aligned} \mathcal{L}_{c.c.} &= g W_\mu^- J^{+\mu} + \text{ c.c.} \,, \\ J^{+\mu} &= \frac{1}{\sqrt{2}} \bar{U}_L^I \gamma^\mu (P_3)_I^j (D_L)_j \,, \end{aligned} \tag{2.23}$$

where

$$(P_3)_I^j \equiv \begin{pmatrix} 1_{3\times 3} \\ \vec{0} \end{pmatrix} . \tag{2.24}$$

In the mass basis, the charged current becomes

$$J_\mu^+ = \frac{1}{\sqrt{2}} \bar{u}_L^I \gamma^\mu (L_u^\dagger)_I^J (P_3)_J^k (L_d)_k^l (d_L)_l \,, \tag{2.25}$$

so that the generalization of the CKM matrix in our model is

$$(\tilde{V}_{CKM})_I^j = (L_u^\dagger)_I^K (P_3)_K^k (L_d)_k^j . \tag{2.26}$$

The elements of this matrix should in principle be determined by a fit to data. We will not attempt such a fit here. Since the SM CKM matrix provides an excellent description of flavor-changing

processes for the first two generations and the b quark, we assume the following structure:

$$\tilde{V}_{CKM} = \begin{pmatrix} V_{ud} & V_{us} & V_{ub} \\ V_{cd} & V_{cs} & V_{cb} \\ c_\beta V_{td} & c_\beta V_{ts} & c_\beta V_{tb} \\ -s_\beta V_{td} & -s_\beta V_{ts} & -s_\beta V_{tb} \end{pmatrix} \tag{2.27}$$

where V_{ij} are SM CKM elements. With this assumption, all flavor-violating new physics effects in K and B systems appear at loop-level only.

Unlike the SM, rotations (2.22) induce tree-level flavor-changing neutral currents (FCNC) in the left-handed sector [72], since the weak-singlet U_L mixes with the SM up-type quarks. The Z boson couples to the current

$$J_\mu^{\rm NC} = (\bar{U}_L)^I \gamma^\mu \left(T_3 - s_w^2 Q\right)_I^J (U_L)_J, \tag{2.28}$$

where

$$(T_3)_I^J = \begin{pmatrix} 1_{3\times 3} & 0 \\ 0 & 0 \end{pmatrix}. \tag{2.29}$$

Rotation to the mass basis yields flavor-changing couplings, proportional to

$$V_{\rm FCNC} = L_u^\dagger \left(T_3 - s_w^2 Q\right) L_u \,. \tag{2.30}$$

These can generate tree-level contributions to rare D meson decays and anomalous $D_0 - \bar{D}_0$ mixing, and flavor-changing top decays. Such contributions are however completely absent if

$$L_u = \begin{pmatrix} 1_{2\times 2} & & \\ & c_\beta & -s_\beta \\ & s_\beta & c_\beta \end{pmatrix}, \tag{2.31}$$

since the only flavor-violating Z coupling in this case is ZtT. Eq. (2.26) then requires $L_d = V_{CKM}^{SM}$. We will assume this texture in our analysis. Note, however, that due to large theoretical uncer-

tainties associated with the D system and the highly suppressed rates for anomalous top decays, significant deviations from this texture can still be consistent with experimental constraints [72].

At the one-loop level, our model predicts new contributions to $\Delta F = 2$ and $\Delta F = 1$ processes in B and K systems. Let us first consider $\Delta F = 2$. The effective Hamiltonian that governs the $B_s^0 - \bar{B}_s^0$ system is

$$\mathcal{H}_{B_s} = \frac{G_F^2}{16\pi^2} M_W^2 \sum_{I,J=u,c,t,T} \lambda_I \lambda_J F(x_I, x_J; M_W) \times (\bar{b}s)_{(V-A)} (\bar{s}b)_{(V-A)}, \tag{2.32}$$

where we defined $\lambda_I \equiv V_{Ib}^* V_{Is}$ and $x_I \equiv M_I^2/M_W^2$. The F functions are given in the Appendix B. Hamiltonians for the K^0 and B_d^0 systems are obtained by simple substitutions, $b \to d$ and $s \to d$, respectively. At leading order in v/f expansion, our results agree with Refs. [73, 74, 75]; however, our expressions are exact in v/f. To a good approximation, the size of the new physics effects in $\Delta F = 2$ observables can be estimated as the fractional deviation of the Wilson coefficient in Eq. (2.32) from its SM value. (This estimate does not take into account some effects, such as the running of the Wilson coefficient between the scales m_T and m_t, which are however expected to be small.) We find that the maximum deviations on the parameter space of our model are: 0.5% for Δm_K; about 20% for ϵ_K; and about 35% for $|\Delta m(B_d)|$ and $|\Delta m(B_s)|$. Such deviations are currently easily allowed by data: see, for example, [76].

We next consider the two most constrained $\Delta F = 1$ decays, $b \to s\gamma$ and $B_s \to \mu^+\mu^-$. The $b \to s\gamma$ amplitude is proportional, in the leading-log approximation, to the coefficient C_7 of the operator $P_7 = \frac{e}{16\pi^2} m_b (\tilde{s}_L \sigma^{\mu\nu} b_R) F_{\mu\nu}$, evaluated at the scale m_b. The top-quark contribution to this coefficient is given by

$$X_t = -\frac{1}{2} A_0^t(x_t) \eta^{16/23} - \frac{4}{3} F_0^t(x_t) \left(\eta^{14/23} - \eta^{16/23} \right), \tag{2.33}$$

where the functions $A_0^t(x)$ and $F_0^t(x)$ can be found in Appendix B, and $\eta = \alpha_s(m_t)/\alpha_s(m_b)$. The

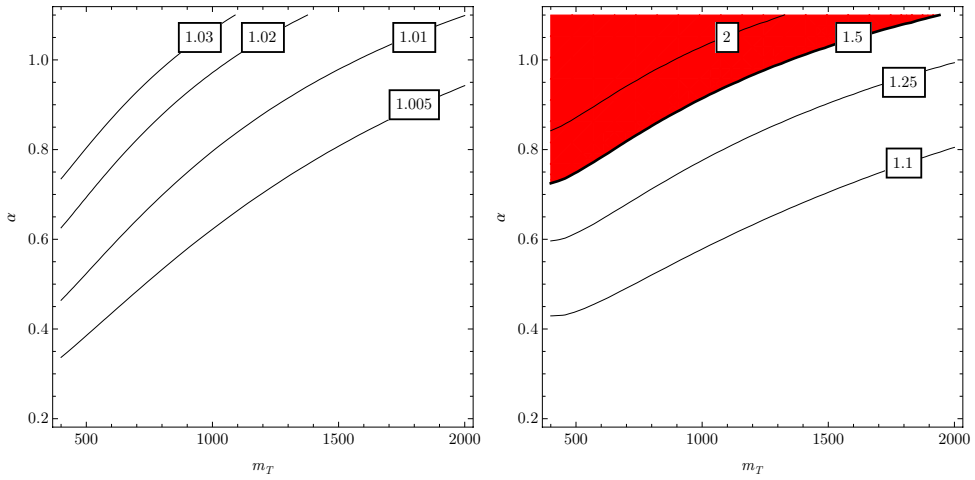

Figure 2.4: Fractional deviations of the $\bar{B} \to X_s\gamma$ (left panel) and $B_s \to \mu^+\mu^-$ (right panel) branching ratios from the SM predictions. The thick line on the right panel corresponds to the LHCb upper bound on $\mathrm{Br}(B_s \to \mu^+\mu^-)$; all points above the line are now ruled out.

only effect of the top partner is to replace

$$\begin{aligned} A_0^t(x_t) &\to c_\beta^2 A_0^t(x_t) + s_\beta^2 A_0^t(x_T), \\ F_0^t(x_t) &\to c_\beta^2 F_0^t(x_t) + s_\beta^2 F_0^t(x_T), \end{aligned} \tag{2.34}$$

in these expressions. (The first term in the v/f expansion of these formulas agrees with Refs. [77, 75]; however, our formulas are exact in v/f.) The resulting deviations of the $b \to s\gamma$ branching ratio from the SM are shown in the left panel of Fig. 2.4. In the region of interest, the deviations are at most about 5%. Given that both the experimental measurement [71] and the NNLO SM theoretical prediction [78] have uncertainties between 5 and 10%, such deviations cannot be currently ruled out. The right panel of the figure shows the deviation of the $B_s \to \mu^+\mu^-$ branching ratio from the SM prediction, evaluated using the formulas given in Ref. [79]. We also indicate the region ruled out by the recent LHCb bound [80], $\mathrm{Br}(B_s \to \mu^+\mu^-) < 4.5 \times 10^{-9}$ at 95% c.l., which is only a factor of 1.5 above the SM prediction. This is the strongest current bound on the top partner from flavor physics, even though it is still weaker than precision electroweak constraints. Notice that the

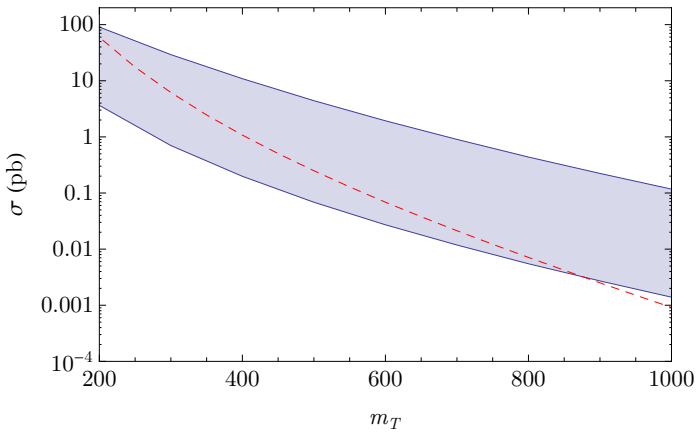

Figure 2.5: Production cross section of top partners at the 7 TeV LHC. For pair-production (red), we use `Hathor v1.2` [81] to calculate at NNLO in QCD. For single production (blue), we use `MadGraph5 v1.3.32` [82] to calculate at LO. The single production cross-section depends on α, with the band indicating the cross-sections for $0.2 < \alpha < 1.1$.

results of Ref. [79] are valid to leading order in the v/f expansion. Given the potential importance of this bound, a more precise calculation is desirable.

2.4.3 Direct Searches at the LHC

The two production mechanisms for the top partner are strong pair-production, $q\bar{q}/gg \to T\bar{T}$, and electroweak single production, $bq \to Tq'$ or $qq' \to Tb$. The production cross sections at the 7 TeV LHC are shown in Fig. 2.5. For pair-production the cross-section is calculated at NNLO in QCD using `Hathor v1.2` [81], with renormalization and factorization scales set to the top partner mass. For single-production the cross-section is calculated at LO using `MadGraph5 v1.3.32` [82], since a calculation beyond LO is not currently available for this process. In this case, we use the `MadGraph` default setting for renormalization and factorization scale, variable event-by-event. (For both pair- and single-production, varying renormalization and factorization scales within a factor of 2 leads to at most a few % variations in the cross sections.) At the 7 TeV LHC, due to the relatively small phase space for producing heavy particles, single production overcomes its electroweak suppression and can be comparable to pair production.

Decay channels of the top partner include th, tZ and bW [83, 65]. In the limit $f \gg v$, the branching ratios are 25%, 25%, and 50%, respectively, as can be easily seen from the Goldstone boson equivalence theorem. An explicit calculation of the partial widths yields [65]:

$$\begin{aligned}
\Gamma(bW) &= \frac{g^2 s_\beta^2 m_T^3}{64\pi m_W^2}\, f(x_W, x_b)\, g(x_b, x_W), \\
\Gamma(tZ) &= \frac{e^2 s_\beta^2 c_\beta^2 m_T^3}{128\pi c_w^2 s_w^2 m_Z^2}\, f(x_Z, x_t)\, g(x_t, x_Z), \\
\Gamma(th) &= \frac{m_T}{64\pi}\, f(x_t, x_h) \left[(1 + x_t^2 - x_h^2) \left((C_{Tth}^L)^2 + (C_{Tth}^R)^2 \right) + 4 C_{Tth}^L C_{Tth}^R x_t \right],
\end{aligned} \tag{2.35}$$

where $x_i \equiv m_i/m_T$, the kinematic functions are defined as

$$\begin{aligned}
f(x_i, x_j) &= \sqrt{(1 - (x_i + x_j)^2)(1 - (x_i - x_j)^2)}\,, \\
g(x_i, x_j) &= (1 - x_i)^2 + x_j^2 (1 + x_i^2) - 2x_j^4\,,
\end{aligned} \tag{2.36}$$

and the constants appearing in the tTh vertex are given in Appendix A.

There exist several searches for vector-like top partners at CMS and ATLAS [84, 85, 86, 87, 88, 89]. These searches focus on pair production and on one particular decay mode of the top partner, either bW or tZ, and assume 100% branching fraction to that mode. In our model, the signal is generally a mixture of pair and single production, and multiple decay channels are possible. As a result, the bounds on the top partner masses obtained by CMS and ATLAS are not directly applicable, but it is possible to "recast" the published analyses to estimate the bounds in our model. Below we present such an estimate, based on the CMS search in the $bbWW$ final state with 5.0 fb^{-1} integrated luminosity [84]. In the interesting parameter space of our model, the dominant decay mode for the T is bW, making $bbWW$ searches most sensitive. Furthermore, the CMS analysis places the strongest bounds as it is updated to use the full 2011 dataset.

The number of signal events expected in a given analysis can be written as

$$N_{\rm sig} = \sum_{ij} \sigma_i \mathcal{L} {\rm Br}_{ij} \epsilon_{ij} A_{ij}, \tag{2.37}$$

Final state	Raw $\mathrm{Br}_\ell \epsilon_i A_i$ (%)	Rescaled $\mathrm{Br}_\ell \epsilon_i A_i$ (%)	$\mathrm{Br}_i \mathrm{Br}_\ell \epsilon_i A_i$ (%)
$bWbW$	0.36	0.29	0.12
$bWtZ$	0.034	0.027	0.0046
$bWtH$	0.022	0.018	0.0011
$tZtZ$	0.0015	0.0012	8.5×10^{-5}
$tHtH$	9.9×10^{-4}	7.9×10^{-4}	7.5×10^{-6}

Table 2.1: Estimated raw $\mathrm{Br}_\ell \epsilon_i A_i$, rescaled $\mathrm{Br}_\ell \epsilon_i A_i$ and $\mathrm{Br}_\ell \mathrm{Br}_i \epsilon_i A_i$ for the various decays of pair produced $T\overline{T}$. All values assume $m_T = 400$ GeV and $\alpha = \pi/4$. See text for the definition of raw and rescaled efficiencies. Here Br_ℓ denotes the dileptonic branching fraction for WW, which is common to all decay modes.

where σ_i is the cross-section for each production channel, $\mathcal{L}$ is the integrated luminosity used in the search, Br_{ij} is the branching fraction for an event produced via channel i to result in the final state j after the decay of all unstable particles, ϵ_{ij} is the efficiency for detecting the final state j in a given analysis, and A_{ij} is the acceptance for the final state j. (Note that ϵ and A depend on the production channel, since final-state particles have different kinematic distributions depending on the production mechanism.) The efficiency and acceptance for the particular production and decay mode assumed in the CMS analysis ($T\bar{T}$, with $T \to bW$) can be found in [84]. We estimated the ϵA of all other relevant final states by modeling the acceptance and selection cuts of [84] on a sample of Monte Carlo (MC)-generated $T\bar{T}$ events. (Since the CMS analysis required two isolated leptons, and vetoed events with dilepton invariant mass close to the Z boson, the efficiencies for events with a single T to pass the cuts are extremely small, and we did not include the single production channel in our analysis.) For this estimate, we generated parton-level events using `MadGraph 5 v1.3.32` [82], showered and hadronized them using `Pythia 6.426` [90], and applied simplified detector simulation using `PGS 4.0` [91]. Unfortunately, `PGS 4.0` significantly underestimates the efficiency of b-tagging, compared to the TCHEM algorithm used by the CMS in this analysis.[2] To address this issue, we ignored the b-tag information provided by `PGS`, and instead applied p_T-dependent TCHEM efficiencies [92] to the b-jets in our sample. This procedure yields the "raw" ϵA values for all possible final states, as a function of m_T and α. For example, values of ϵA for $m_T = 400$ GeV, $\alpha = \pi/4$ are listed in the first column of Table 2.1. The MC simulation and analysis

[2]This can be easily seen by comparing PGS and TCHEM efficiencies on an SM $b\bar{b}$ sample. The peak efficiencies are 0.4 for PGS and 0.7 for TCHEM.

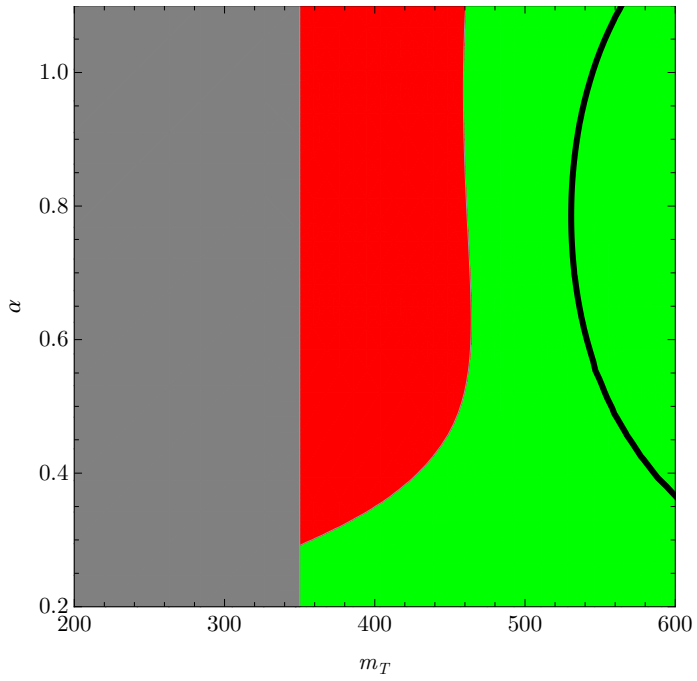

Figure 2.6: The estimated 95% excluded region from the CMS $T \to Wb$ search [84] in terms of M_T and α is shown as the red contour. The green is the allowed region. The thick black line corresponds to 20% fine-tuning. The CMS analysis does not quote efficiencies below top partner masses of 350 GeV, so no bound is shown (grey region). This low-m_T region is in any case already ruled out by precision electroweak fits.

procedure was validated on a sample of events with the final state considered by CMS, $WbWb$ with 2 leptonic W's. We found that the ϵA determined using our simulation for a 400 GeV top partner is 0.36%, compared with the value of 0.29% quoted in the CMS analysis. Given the crude nature of our MC simulations, this level of agreement is very reasonable. Even so, in deriving the bounds, we rescale the raw MC estimates of BrϵA by a correction factor of 0.29/0.36; in other words, we use the ϵA quoted by CMS for the $WbWb$ channel, and use the MC to estimate the relative ϵA of other channels with respect to $WbWb$. The resulting estimates are collected in Table 2.1. It is clear that the rates of events from final states other than $WbWb$ that pass the analysis cuts are quite small. While our estimates of those rates suffer from significant systematic uncertainties due to the crude detector simulation used, it is reassuring that even if the rates were inflated by a factor of two they would remain subdominant. Thus, our bounds on the top partner mass are robust.

The estimated 95% C.L. exclusion region as a function of m_T and α is presented in Fig. 2.6.

The typical bound on the top partner mass is about 450 GeV, with somewhat weaker bounds for small α.[3] It is clear that direct collider searches are just beginning to probe the region that is not already ruled out by precision electroweak constraints. Note that the least fine-tuned parameter space regions will be probed by direct LHC searches in 2012.

2.5 HIGGS PROPERTIES

If the LHC evidence for the Higgs boson at 125 GeV is correct, detailed measurements of the Higgs production cross section and branching ratios should be possible within the next few years. In our model, these properties deviate from the SM predictions. There are two important effects. First, the hWW and hZZ couplings are shifted,[4] leading to deviations in the WW and ZZ branching fractions and, via the W-loop contribution, in the $\mathrm{Br}(h \to \gamma\gamma)$. Second, loops of top partners produce corrections to the hgg and $h\gamma\gamma$ vertices, leading to deviations in the expected production cross section and, again, $\mathrm{Br}(h \to \gamma\gamma)$.

The production rate of h via gluon fusion is proportional to $\Gamma(h \to gg)$. Assuming that gluon fusion is the dominant Higgs production mechanism, the rates $\sigma(pp \to h \to VV)$ in our model, normalized to their SM values, are

$$R_V = \frac{\Gamma(h \to gg)\mathrm{Br}(h \to VV)}{\Gamma_{\mathrm{SM}}(h \to gg)\mathrm{Br}_{\mathrm{SM}}(h \to VV)}\,, \tag{2.38}$$

where $V = \gamma, Z, W$. The total Higgs decay rate at $m_h = 125$ GeV is dominated by the $b\bar{b}$ mode. The bottom Yukawa coupling can be incorporated in our model as an explicit breaking of the global symmetry; this would not spoil naturalness due to the small numerical value of y_b. At leading order in v/f, this results in the $h\bar{b}b$ coupling identical to the SM value. There may be corrections at higher orders in v/f; however, their form is not fixed by the symmetry, and is model-dependent. If

[3] A reanalysis of the published LHC searches in the context of the "Bestest" Little Higgs model appeared recently in Ref. [93], where similar bounds on the top partner mass were found.

[4] These shifts are due simply to the composite nature of the Higgs, and not to the presence of the top partners. They can be described within the framework developed in Refs. [94].

they are ignored, we simply get

$$R_V = \frac{\Gamma(h \to gg)\Gamma(h \to VV)}{\Gamma_{\rm SM}(h \to gg)\Gamma_{\rm SM}(h \to VV)} \,. \tag{2.39}$$

Note that the dropped terms in the $h\bar{b}b$ vertex are potentially of the same order as the corrections to the hgg and hVV couplings, so these predictions have an inherent $\mathcal{O}(1)$ ambiguity. Still, we compute them as an indication of the likely size of the effect. We should also note that our predictions for *ratios* of rates, such as for example R_γ/R_W, are free of this ambiguity.

The ratios of the $h \to WW$ and $h \to ZZ$ decay rates to the SM predictions are given by

$$\frac{\Gamma(h \to W^+W^-)}{\Gamma_{\rm SM}(h \to W^+W^-)} = \frac{\Gamma(h \to ZZ)}{\Gamma_{\rm SM}(h \to ZZ)} = 1 - \frac{2m_W^2}{g^2 f^2} \,. \tag{2.40}$$

The $h \to \gamma\gamma$ decay rate is [95, 96]

$$\Gamma(h \to \gamma\gamma) = \frac{\alpha^2 g^2}{1024\pi^3} \frac{m_h^3}{m_W^2} \left| F_1(\tau_W) + \sum_{i \neq t} Q_i^2 N_{c,i} F_{1/2}(\tau_i) + 3Q_t^2 \mathcal{A}_{\rm top} \right|^2 , \tag{2.41}$$

where $\tau_i = 4m_i^2/m_h^2$; the sum runs over all SM fermions except the top; Q_i is the electric charge of the i-th fermion and $N_{c,i}$ its color multiplicity (3 for quarks, 1 for leptons). The top contribution to the decay amplitude in our model is given by

$$\mathcal{A}_{\rm top} = \frac{\sqrt{2} m_W}{g m_t} \left(C_{tth} F_{1/2}(\tau_t) + \frac{m_t}{m_T} C_{TTh} F_{1/2}(\tau_T) \right) , \tag{2.42}$$

where the constants C are given in Appendix A; while in the SM, $\mathcal{A}_{\rm top} = F_{1/2}(\tau_t)$. Here we used

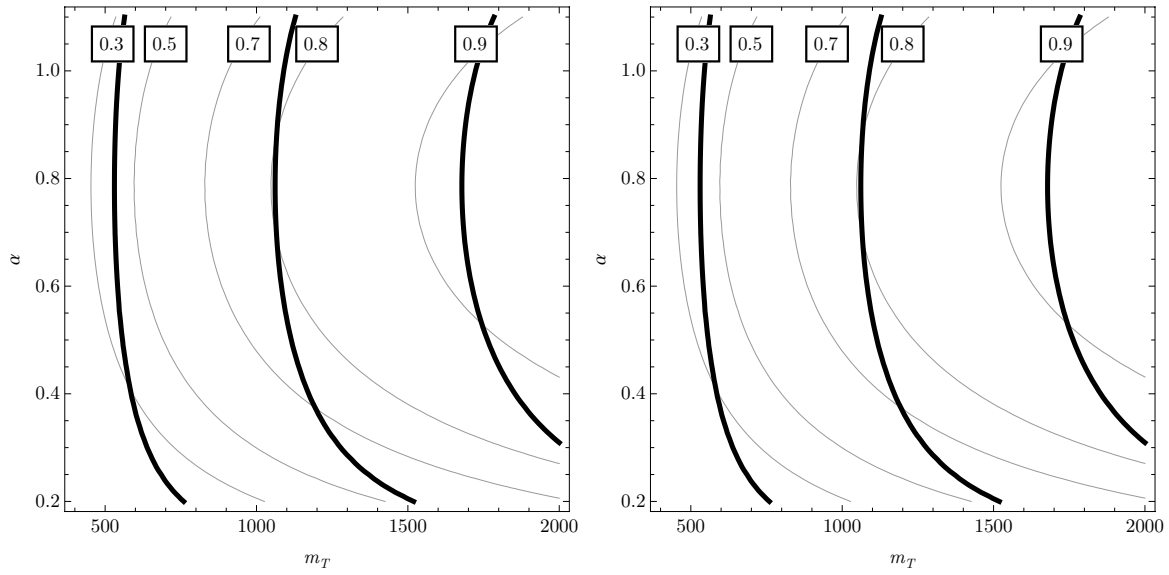

Figure 2.7: Event rates for $h \to \gamma\gamma$ (left) and $h \to WW$ (right), normalized to the corresponding SM rates, for $m_h = 125$ GeV. Thick black lines represent constant fine-tuning contours: from left to right, 20%, 5%, and 2% fine tuning.

the standard notation for the loop functions,

$$\begin{aligned} F_1(x) &= 2 + 3x + 3x(2-x)f(x)\,, \\ F_{1/2}(x) &= -2x\left(1 + (1-x)f(x)\right)\,, \\ f(x) &= \left[\sin^{-1}\left(\sqrt{\frac{1}{x}}\right)\right]^2 \quad \text{if } x > 1, \\ &\quad -\frac{1}{4}\left[\log\left(\frac{1+\sqrt{1-x}}{1-\sqrt{1-x}}\right) - i\pi\right]^2 \quad \text{if } x < 1. \end{aligned} \tag{2.43}$$

The $h \to gg$ decay rate is given by [95]

$$\Gamma(h \to gg) = \frac{\alpha_s^2 g^2}{512\pi^3}\,\frac{m_h^3}{m_W^2}\left|\sum_{i\neq t} F_{1/2}(\tau_i) \,+\, \mathcal{A}_{\rm top}\right|^2 . \tag{2.44}$$

The predicted rates $R_W = R_Z$ and R_γ are shown in Fig. 2.7. Comparing with the precision electroweak constraints, we conclude that large suppression of the rates in both WW/ZZ and $\gamma\gamma$

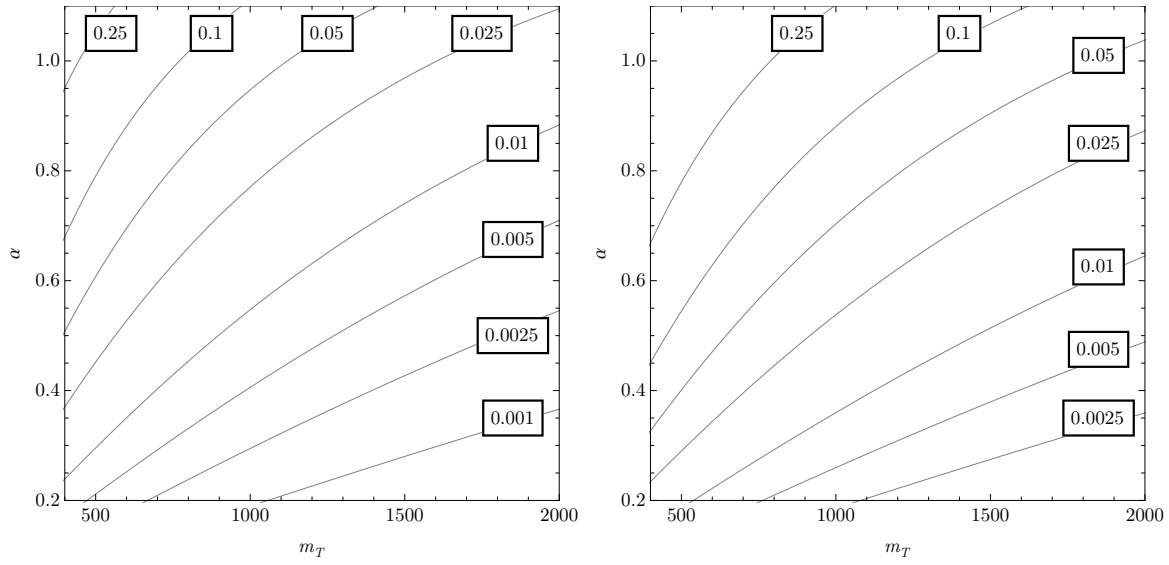

Figure 2.8: Fractional deviations of the axial (left) and vector (right) components of the $t\bar{t}Z$ coupling from their SM values.

channels is possible: the rates can be as low as 30% of the SM prediction. Deviations are the strongest for the least fine-tuned regions of parameter space: for example, if we demand EWSB fine-tuning of 5% or better, the minimal possible deviation in R_W and R_γ is 20%. As noted above, these predictions should be taken with a grain of salt, since they can be modified by the model-dependent $\mathcal{O}(v/f)$ terms in the $hb\bar{b}$ coupling. Still, it is interesting that large, potentially observable deviations from the SM may occur throughout the natural parameter space.

As remarked above, the ratio R_γ/R_W provides a robust test of the structure since it's insensitive to the model-dependent embedding of the bottom Yukawa. Unfortunately, throughout the parameter space of our model, the deviations of this ratio from the SM prediction are well below 1%, too small to be observed. The reason is that to a very good approximation, the fractional deviations of the hWW coupling and the top loop contributions to hgg and $h\gamma\gamma$ are the same.

2.6 TOP PROPERTIES

At order v/f, the lighter top eigenstate, which we identified with the SM top, actually contains an admixture of the $SU(2)$-singlet left-handed field U_L. As a result, the chiral structure of the top couplings to the Z deviates from the SM predictions at this order. To quantify this effect, in Fig. 2.8 we plot the ratio of the vector and axial components of the $t\bar{t}Z$ coupling expected in our model, normalized to their SM values. Deviations of order 10% or more in g_A, and up to 30% in g_V, are possible in regions consistent with precision electroweak constraints. It was estimated that the 14 TeV LHC with 3000 fb^{-1} integrated luminosity would be able to probe g_A at the 5-10% level and g_V at the 15-30% level [97]. A proposed 500 GeV linear electron-positron collider would reach precision of 2% on g_A and 5% on g_V [98, 99]. Though we would expect the top partner to be discovered in direct searches before these measurement become possible, they would still be of great interest to confirm the structure of the model.

2.7 CONCLUSIONS

Naturalness, together with evidence that electroweak-symmetry breaking sector remains weakly coupled up to scales well above 1 TeV, implies that a light Higgs must be accompanied by new particles that cancel the quadratically divergent Higgs mass contribution from the SM top loop. In SUSY, these particles are scalar top (stop) quarks, and LHC phenomenology of stops has been a subject of much work recently. In this chapter, we studied an alternative which has not received as much attention so far: naturalness restoration by spin-1/2 top partners. We focused on a minimal model where this mechanism is realized, which is essentially the top sector of the Littlest Higgs model. We explored current experimental constraints on this model from all relevant sources: precision electroweak fits, flavor physics, and direct LHC searches. We found that the current bound on the top partner mass is about 500 GeV, and is dominated by precision electroweak data, although direct searches are rapidly entering the hitherto allowed mass range. Given these bounds, accommodating a 125 GeV Higgs boson in this model requires only a modest level of fine-tuning, of order 20%. Thus, we conclude that natural EWSB is possible in theories with sub-TeV-scale

spin-1/2 top partners.

In the near future, direct searches for the top partners at the LHC will continue, gaining more sensitivity as more data is collected. The decay channels of the top partner include bW, tZ and th, all of which have order-one branching ratios; this situation is not special to our model but is in fact quite generic. Also, while existing searches focus on pair-production of the top partners, in our model single production dominates in parts of the parameter space. To maximize sensitivity to top partners, experiments should extend the menu of searches to encompass all available production and decay modes. Another interesting handle not used in the top partner searches so far is jet substructure: the top partner decay products, such as t, Z, W and h, are typically relativistic in the lab frame in the relevant mass range, so that their hadronic decays can be identified as jets with unusual substructure. Recent phenomenological studies [100, 101] show interesting potential of such searches.

As a complementary handle, measurements of the Higgs and top properties at the LHC may be sensitive to deviations from the SM predicted by our model. While these predictions are quite model-dependent, our study indicates that large deviations in $h \to WW/ZZ$ and $h \to \gamma\gamma$ rates are possible.

CHAPTER 3

Boosted Tops from Gluino Decays

3.1 INTRODUCTION

Recently, experiments at the Large Hadron Collider (LHC) have begun searching for new physics beyond the Standard Model (SM). Among the many theoretical ideas about the possible nature of this new physics, supersymmetry (SUSY) is the most popular one: it provides an appealing solution to the gauge hierarchy problem of the SM, contains an attractive dark matter candidate, and fits naturally in the framework of grand unification and string theory. SUSY models predict a number of new particles, "superpartners" of the known SM particles, which may be produced at the LHC. In the simplest SUSY models, all superpartners are odd under a discrete symmetry, R-parity, while all SM particles are R-even. This implies that the lightest SUSY particle (LSP) is stable, and that any other superpartner will decay to the LSP and one or more SM particles. Cosmological considerations strongly prefer the LSP to be electrically neutral and uncolored, so that at the LHC the LSP passes through the detector without interactions, leading to an apparent transverse momentum imbalance, or "missing transverse energy" (MET). The presence of MET provides a distinct signature which can be used to distinguish SUSY events from the (far more numerous) SM backgrounds.

At the time of writing, the LHC experiments have presented searches for events with anomalous MET using a data set of approximately 1 fb^{-1} collected in 2010-11 at the center-of-mass energy of

$\sqrt{s} = 7$ TeV. No evidence for anomalous MET has been found, and limits on superpartner masses have been set. Barring accidental features such as spectrum degeneracies, gluinos $\tilde{g}$ and squarks of the first two generations $\tilde{q}_{1,2}$ have been ruled out for masses up to about 1 TeV [102]. In models where all squarks have a common mass at some energy scale, this bound implies that a significant amount of fine-tuning would be necessary to accommodate the observed electroweak symmetry breaking scale [103]. On the other hand, fine-tuning can be avoided if the third-generation squarks, stops $\tilde{t}$ and sbottoms $\tilde{b}$, are significantly lighter than $\tilde{q}_{1,2}$ [104, 105, 106]. The LHC bounds on third-generation squarks are quite weak: stops above 200-300 GeV are currently allowed. The only other superpartner whose mass is significantly constrained by naturalness is the gluino [104]; at present, gluinos above 600 GeV are allowed if decaying only via the 3rd generation. With this motivation, we will focus on a scenario where gluinos, third-generation squarks, and a neutralino LSP are the only particles relevant for the LHC phenomenology, with other squarks being too heavy to be produced. An explicit example of a complete theory realizing this spectrum is the "accidental SUSY" models of Refs. [107].

The lack of discovery so far also implies that traditional SUSY searches using the MET signature will become more difficult, since the large-MET tails of SM backgrounds will need to be calculated (or extrapolated) with increasingly high precision to obtain sensitivity to lower SUSY cross sections. This motivates the question: Can any handles other than MET be used to identify SUSY events in the presence of large SM backgrounds? In this chapter, we explore an alternative signature. Gluino cascade decays to the LSP via intermediate stops produce two top quarks, so that gluino pair-production events may result in final states with four tops [108, 109]. If the gluino-stop and stop-LSP mass differences are sufficiently large, each of these tops will typically be relativistic in the lab frame, and its hadronic decay products will be merged into a single jet. Recently, much work has been done on distinguishing such top jets from the usual hadronic jets using the energy distribution inside the jet, and several well-tested algorithms for "tagging" top jets are now available [110]. The original motivation was to search for decays of the Kaluza-Klein gluon in models with extra dimensions [111]; other proposed applications include a search for the string-Regge excitation of the gluon [112], and a search for direct stop production in SUSY [113]. Here,

we point out that this technique can also be used to search for the SUSY gluino, and is particularly promising in scenarios with a light third generation, since $\tilde{g}$ decays to tops have large branching fractions in this case. The work presented in this chapter is based on Ref. [53].

3.2 ANALYSIS SETUP

In the spirit of the "simplified model" approach [114, 115], we assume that a gluino $\tilde{g}$, one stop $\tilde{t}$, and a single neutralino $\tilde{\chi}^0$ are the only superpartners relevant for the LHC phenomenology. This is the minimal set of particles required to produce our signature. In the Minimal Supersymmetric Standard Model (MSSM), this setup can be realized if the second stop and the left-handed sbottom are heavier than the gluino. (Note that naturalness considerations in the MSSM prefer spectra with a few hundred-GeV splitting among the two stop mass eigenstates [116].) If this is not the case, the branching ratios of the decays producing our signature would be reduced (e.g. from 1 to 2/3 if all three squarks are degenerate), resulting in a somewhat decreased rate, but qualitatively the picture is unchanged. We assume that the neutralino is the stable LSP, and set its mass to 60 GeV throughout the analysis. The LHC signal is dominated by gluino pair-production, followed by the cascade decay

$$\tilde{g} \to \tilde{t} + \bar{t}, \quad \tilde{t} \to t\tilde{\chi}^0 , \tag{3.1}$$

or its charge conjugate. We assume that $m(\tilde{g}) - m(\tilde{t}) > m_t$, $m(\tilde{t}) - m(\tilde{\chi}^0) > m_t$, so that all four tops in the event are on-shell. (It may be possible to relax one of these conditions, as long as the other one is satisfied strongly so that at least two tops in the event are boosted; we will not study that possibility here.) We compute gluino pair-production cross sections at next-to-leading order (NLO) using `PROSPINO` [117]. To study cut efficiencies, we generate event samples for gluino pair-production followed by the decays (3.1) using `MadGraph/MadEvent v5 1.3.27 (MG/ME)` [118] for a large set of parameters $(m(\tilde{g}), m(\tilde{t}))$. We then simulate top decays, showering and hadronization with `PYTHIA 8` [119]. To identify jets, we use the anti-k_T algorithm implemented in the `FastJet` code [120, 121]. Top tagging of jets in our sample is simulated using the implementation of the Hopkins algorithm [122] available at [121]. In the top tagger, we use two sets of parameters, "tight"

and "loose" tags; they are defined precisely as in Ref. [110].

We require at least 4 jets with $p_T > 100$ GeV in each event, and require that some of the jets be top-tagged. (The optimal number of top-tagged jets required depends on the LHC energy and luminosity, see below.) In the signal, tagged jets are typically due to hadronic decays of boosted tops, which produce 3 collimated partons that cannot be resolved. The backgrounds include SM processes with boosted tops, as well as ordinary jets mistakenly tagged as top-jets. (The mistag probability is typically of order 1% [110].) We also require the presence of substantial missing energy. The irreducible backgrounds may contain MET from invisible Z decays, leptonic W decays, or semileptonic top decays. We include the following irreducible backgrounds: $nt + (4-n)j$ with $n = 1 \ldots 4$; $Z + nt + (4-n)j$, with $n = 0, 2, 4$; and $W + nt + (4-n)j$, with $n = 0, 2, 4$. Here each t may be a top or an anti-top, j denotes a jet due to a non-top quark or a gluon, and $Z \to \nu\bar{\nu}$ or $W \to \ell\nu$ is required. We do not include reducible backgrounds, other than the light jets mistagged as tops. We simulated the backgrounds at parton level with `MG/ME`, and used these samples to compute p_T and MET cut efficiencies. We use leading-order (LO) cross sections for all background processes. The two dominant backgrounds, $2t + 2j$ and $Z + 4j$, have been recently computed at NLO. In both cases, the NLO correction to the cross section is negative: K-factors of 0.73 for $2t + 2j$ [123] and 0.95 for $Z + 4j$ [124] have been reported, so that using LO cross sections for these processes is conservative. No other backgrounds are currently known beyond the LO.

Unfortunately, due to large QCD rates and small mistag probabilities, we were not able to generate Monte Carlo samples large enough to measure top-tag efficiencies directly in the background channels. Instead, we estimate these efficiencies by multiplying the p_T-dependent tag and mistag probabilities for individual top and non-top jets reported in Ref. [110]. This estimate assumes that the tag and mistag probabilities for each jet are independent of the presence of other objects in the final state (the probabilities in [110] were computed using $t\bar{t}$ and $2j$ samples). The probability to tag a true top jet as such is clearly reduced by the presence of other jets in the event: for example, the tag efficiency for our signal approximated in this way is typically about a factor of two higher than that obtained by a full simulation. So, our estimate of backgrounds involving tops, such as $2t + 2j$, is certainly conservative. It is less clear how the mis-tag probability would be affected; we

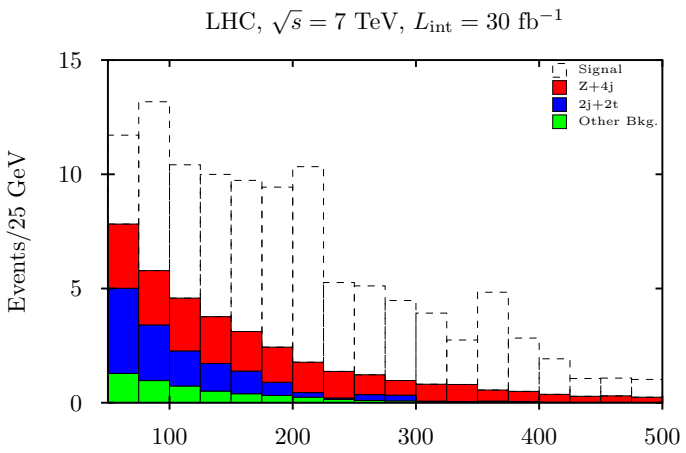

Figure 3.1: Signal at the benchmark point, $(m(\tilde{g}), m(\tilde{t})) = (800, 400)$ GeV, and background rates as a function of MET, at 7 TeV LHC. Four jets with $p_T > 100$ GeV and two top-tagged jets are required.

leave this issue for future work.

3.3 LHC SENSITIVITY AT $\sqrt{s} = 7$ TeV

To keep the analysis simple, we optimize the selection cuts for a single "benchmark" point in the model parameter space, and do not vary them as we scan the masses. At 7 TeV, we choose the benchmark point $(m(\tilde{g}), m(\tilde{t})) = (800, 400)$ GeV. We studied all possible combinations of between 0 and 4 loose and tight top tags, and conclude that requiring 2 loose tags is the best strategy at this point. Analyses requiring more than 2 tags, or 2 or more tight tags, suffer from low event rate, making a search in the 7 TeV LHC run with $20 - 30$ fb^{-1} integrated luminosity impractical. Requiring fewer tags leads to significantly higher background rates, decreasing sensitivity [125]. The two top tag requirements strongly suppress the backgrounds, as illustrated in Table 3.1, but are not by themselves sufficient, so that an additional MET cut must be applied. The signal and principal backgrounds as a function of MET are shown in Fig. 3.1. We require $\not{E}_T > 100$ GeV; with this cut, we expect 32 signal events, $S/B = 2.4$, and statistical significance of 6.8 at the benchmark point with 30 fb^{-1} integrated luminosity. The reach of the LHC with this data set is shown in Fig. 3.2. (The 95% exclusion contour is calculated using the expected CL_s [126]. The discovery significance is determined using the expected log likelihood of consistency with the signal

Process	$\sigma_{\rm tot}$	Eff(p_T)	Eff(tag)	$\sigma_{\rm tag}$	Eff($\not{E}_T$)	$\sigma_{\rm all\ cuts}$
signal	61.5	37	6	1.31	81	1.06
$Z+4j$	2×10^5	0.2	0.1	0.44	66	0.29
$2t+2j$	5×10^4	3	0.3	5.7	2	0.10
$W+4j$	2×10^5	0.2	0.03	0.12	29	0.04
$Z+2t+2j$	50	4	1	0.02	72	0.02

Table 3.1: Signal and background cross sections (in fb) and cut efficiencies (in %) at the 7 TeV LHC. Acceptance cuts of $p_T > 20$ GeV, $|\eta| < 5$ for all jets are included in the total cross sections. The cuts are labelled as follows: "p_T": requiring 4 jets with $p_T > 100$ GeV; "tag": requiring 2 jets to be tagged as tops with "loose" parameters; "$\not{E}_T$": requiring $\not{E}_T > 100$ GeV. The signal is at the benchmark point, $(m(\tilde{g}), m(\tilde{t})) = (800, 400)$ GeV. Backgrounds not listed here are negligible.

plus background hypothesis [127].) Gluino masses of up to about 1 TeV can be probed at the 95% confidence level, as long as the gluino-stop mass difference exceeds 400 GeV. The 5-sigma discovery reach extends to a gluino mass of about 900 GeV for stop masses below 350 GeV. We should also note that $S/B \gtrsim 1$ throughout the probed region, so no extraordinarily precise predictions of the background are required.

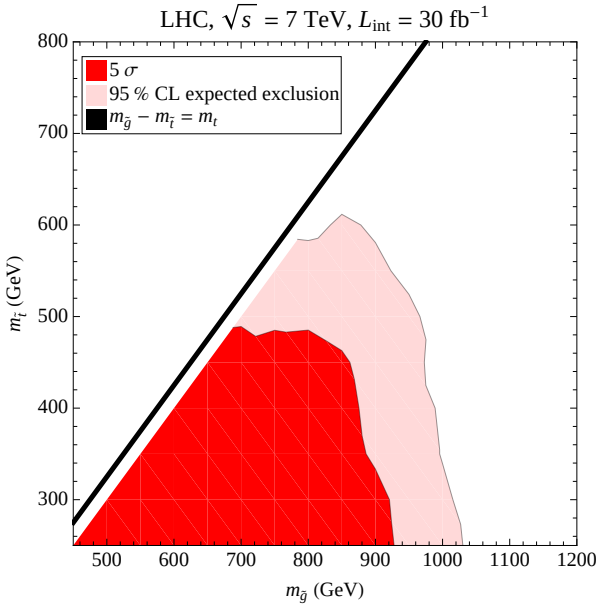

Figure 3.2: The 95% c.l. expected exclusion and 5-sigma discovery reach of the proposed search at the 7 TeV LHC run with 30 fb^{-1} integrated luminosity.

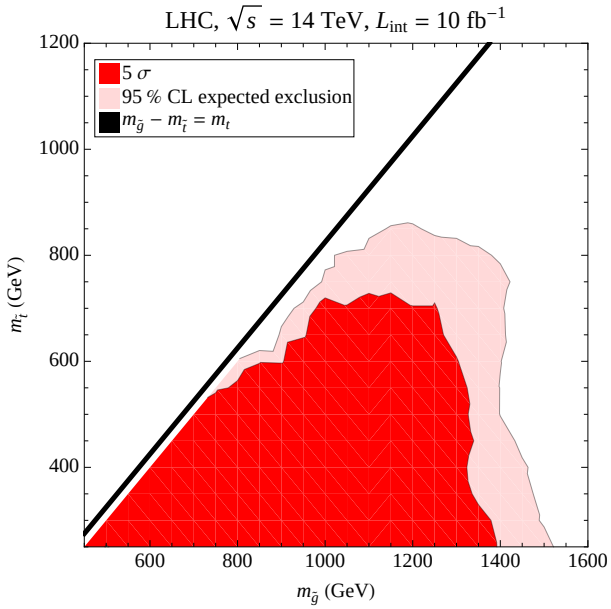

Figure 3.3: The 95% c.l. expected exclusion and 5-sigma discovery reach of the proposed search at the 14 TeV LHC run with 10 fb^{-1} integrated luminosity.

3.4 LHC SENSITIVITY AT $\sqrt{s} = 14$ TeV

Anticipating higher reach of the search at 14 TeV, we optimize the selection cuts for a benchmark point with higher masses, $(m(\tilde{g}), m(\tilde{t})) = (1200, 600)$ GeV. After again considering all possible combinations of loose and tight tag requirements, we conclude that the optimal strategy in this case is to require three loose tags. We further require $\not{E}_T \geq 175$ GeV. At the benchmark point, we expect 8.5 signal events to pass these cuts in a data set of 10 fb^{-1}, and with $S/B = 27.5$ the expected statistical significance of observation is 6.5. The reach of a search with these parameters is shown in Fig. 3.3. Discovery is possible up to $1.3 - 1.4$ TeV gluino masses with stops in the $300 - 700$ GeV mass range. In this case, $S/B \gtrsim 10$ throughout the discovery region.

Given how effective the top tagging technique is in suppressing backgrounds, it is natural to wonder whether, given enough data, a search for gluinos could be conducted with no MET requirement at all. Unfortunately, this is not possible. While the backgrounds studied above are sufficiently suppressed, a new irreducible background, pure QCD events with 4 hard jets ($p_T > 100$ GeV), must be included in the absence of a MET cut. The rate for this process is so large (5.3 nb at 14 TeV at tree-level) that, even including the small mistag probabilities for light jets, it overwhelms

the signal. We estimate that the most sensitive search without a MET cut is again one with 3 loose top tags required. For a 300 fb^{-1} data set, this search is sensitive to the benchmark point at about 4.5 sigma level (statistics-only), but with $S/B \sim 0.1$, systematic errors are probably too large to claim sensitivity.

3.5 DISCUSSION

Our analysis indicates that using tagged top jets as an additional handle to suppress SM backgrounds in the search for gluino decaying to stops leads to interesting reach, even in the 7 TeV run. In fact, the reach may be even higher than we estimate, since we did not perform a thorough cut optimization for various regions of the model parameter space, instead simply freezing the cuts to values that were found to be near-optimal for a single benchmark point.

While we made several simplifications in this exploratory study, the promising results in our opinion justify a more complete analysis. Most of the outstanding issues concern backgrounds. For irreducible backgrounds, the fixed-order (tree-level) simulations used here should be supplemented with showering and hadronization, although since the jets used in our analysis are required to have rather high p_T, we do not expect qualitative changes. Also, MC samples with higher statistics should be used to fully simulate top-tagging efficiencies on the backgrounds. Reducible backgrounds, which were ignored here, should be studied. The most important one of these is the pure QCD channel, $4j$ at parton level, which has a very high rate even with a 2 or 3 mistagged-jet requirement. The pure-QCD events passing our cuts lie far on the tail of the MET distribution for this channel, where the MET is entirely due to undetected or incorrectly measured jets. Correctly estimating this background would thus be a task for a complete detector simulation or a data-driven approach, which must be performed by the experimental collaborations. It is important to note, however, that large-MET QCD tails affect all SUSY searches at the LHC relying on MET, and in the purely hadronic searches this effect is typically subdominant to the reducible backgrounds once appropriate cuts are applied to eliminate events with MET aligned with one of the jets [102]. Similar techniques can be applied in our case.

3.6 CONCLUSIONS

If SUSY is realized in such a way that stops and sbottoms are the only squarks below the TeV scale, as favored by naturalness and recent negative results from the LHC, top-rich final states are a natural place to search for it. Our results indicate that the techniques to separate top jets from light jets, developed recently with a completely different motivation, can be employed to boost sensitivity of such searches. They can complement other proposed strategies for this scenario [109, 128], especially in the heavy gluino region. We encourage the experimental collaborations to incorporate this tool in the upcoming searches.

CHAPTER 4

Parameter counting in models with global symmetries

4.1 INTRODUCTION

When modeling a physical system, it is important to understand the relationship between the symmetries in the model and the number of physical parameters involved. Consider for example a hydrogen atom in a uniform magnetic field. Before turning on the magnetic field, the hydrogen atom is invariant under spatial rotations, which are described by the $SO(3)$ group. Furthermore, there is an energy eigenvalue degeneracy of the Hamiltonian: states with different angular momenta have the same energy. This degeneracy is a consequence of the symmetry of the system.

When magnetic field is added to the system, it is conventional to pick a direction for the magnetic field without a loss of generality. Usually, we define the positive z direction to be the direction of the magnetic field. Consider this choice more carefully. A generic uniform magnetic field would be described by three real numbers: the three components of the magnetic field. However, the magnetic field breaks the $SO(3)$ symmetry of the hydrogen atom system down to an $SO(2)$ symmetry of rotations in the plane perpendicular to the magnetic field. The one generator of the $SO(2)$ symmetry is the only valid symmetry generator now; the remaining two $SO(3)$ generators in the orthogonal planes are broken. These broken symmetry generators allow us to rotate the system

such that the magnetic field points in the z direction:

$$O_{xz}O_{yz}\begin{pmatrix} B_x \\ B_y \\ B_z \end{pmatrix} = \begin{pmatrix} 0 \\ 0 \\ B'_z \end{pmatrix}, \tag{4.1}$$

where O_{xz} and O_{yz} are rotations in the xz and yz planes respectively. The two broken generators were used to rotate away two unphysical parameters, leaving us with one physical parameter, the value of the magnetic field. That is, all measurable quantities in the system depend only on one new parameter, rather than the naïve three. In addition, the broken symmetry lifts the degeneracy of the energy eigenvalues.

The results described above are more generally applicable. Particularly, they are useful in studying the flavor physics of quantum field theories. Consider a gauge theory with matter content. This theory always has kinetic and gauge terms, which have a certain global symmetry G_f on their own. However, in adding a potential, which consists of a linear combination of all renormalizable operators that respect the imposed symmetries, the global symmetry may be broken down to a smaller symmetry group. In breaking the symmetry, there is an added freedom to rotate away unphysical parameters, as when a magnetic field is added to the hydrogen atom system. In order to analyze this process, we define a few quantities. The added potential has coefficients that can be described by N_{general} parameters in a general basis. The global symmetry H_f of the entire model has fewer generators than G_f and we call the difference in the number of generators N_{broken}. Finally, the quantity that we would ultimately like to determine is the number of parameters affecting physical measurements, N_{phys}. These numbers are related by the well-known rule [129] (for a review see, for example, Ref. [130])

$$N_{\text{phys}} = N_{\text{general}} - N_{\text{broken}}. \tag{4.2}$$

Furthermore, this rule applies separately for both real parameters (masses and mixing angles) and phases. A general, $n \times n$ complex matrix can be parametrized by n^2 real parameters and n^2 phases. Imposing restrictions like Hermiticity or unitarity reduces the number of parameters required to describe the matrix. A Hermitian matrix can be described by $n(n+1)/2$ real parameters and

$n(n-1)/2$ phases, while a unitary matrix can be described by $n(n-1)/2$ real parameters and $n(n+1)/2$ phases.

The rule given by (4.2) can be applied to the standard model. We consider only terms involving fermions, stating results for the Higgs field when they are relevant. The Yukawa potential for the interactions in terms of the quark $SU(2)_L$ doublet, Q_L, the lepton $SU(2)$ doublet, L_L, the $SU(2)_L$ singlet fields, U_R, D_R, E_R, and the Higgs doublet, H, is

$$V = Y^U_{ij}(\overline{Q_L})_i(U_R)_j H + Y^D_{ij}(\overline{Q_L})_i(D_R)_j \tilde{H} + Y^E_{ij}(\overline{L_L})_i(E_R)_j \tilde{H} + \text{h.c.}, \tag{4.3}$$

where Y^F are 3×3 complex matrices in a general basis. We use $\tilde{H} = \epsilon H^*$, where ϵ is the anti-symmetric matrix in $SU(2)_L$ space.

The interactions in this sector are parametrized by three complex 3×3 matrices, which contain a total of 54 parameters (27 real parameters and 27 phases) in a general basis. These parameters also break a large global symmetry of the kinetic and gauge terms in the model down to the familiar baryon number and lepton family number symmetries of the full standard model,

$$U(3)_Q \times U(3)_U \times U(3)_D \times U(3)_L \times U(3)_E \to U(1)_B \times U(1)_e \times U(1)_\mu \times U(1)_\tau. \tag{4.4}$$

hile $U(3)^5$ has 45 generators, the remaining symmetry group has only 4 and thus $N_{\text{broken}} = 41$. This broken symmetry allows us to rotate away a large number of the parameters by moving to a more convenient basis. Using (4.2), the number of physical parameters should be given by

$$N_{\text{phys}} = 54 - 41 = 13. \tag{4.5}$$

n addition, there are the three gauge couplings, the two Higgs parameters and the strong CP phase for a total of 19 parameters in the standard model. These parameters can be split into real parameters and phases. The five unitary matrices generating the symmetry of the kinetic and gauge terms have a total of 15 real parameters and 30 phases and the symmetry is broken down to

a symmetry with only four phase generators. Thus,

$$N^{(r)}_{\rm phys} = 27 - 15 = 12, \qquad N^{(i)}_{\rm phys} = 27 - 26 = 1. \tag{4.6}$$

e interpret this result by saying that of the 12 real parameters, 9 are the fermion masses and three are the CKM matrix mixing angles. The one phase is the CP-violating phase of the CKM mixing matrix.

In studying new models, it is particularly important to properly count the number of parameters. The number of physical parameters is, in principle, the number of measurements required in order to fully determine a model. Once these measurements are made, it should be possible to test the model with all further measurements. The standard model is so successful because all the parameters have been measured to some extent and further measurements have verified significant predictions of the model to high precision. The current parametrization appears to be sufficient to describe the quark sector at scales below 100 GeV [131]. The failure of the SM parametrization in the lepton sector have been used as indicators of new lepton flavor physics [131].

In this chapter, we present the work of Ref. [50]. We extend the rule for parameter counting to theories where global symmetries are imposed on the potential terms. In particular, we consider cases where part of the flavor symmetry present in the kinetic and gauge terms is restored. In section 2, a rule for analyzing these cases is presented. Simple toy examples are discussed to highlight the use of the rule. In section 3, the rule is applied to studying global symmetry constraints in the MSSM. The results of imposing symmetries are compared to the constrained MSSM (cMSSM).

4.2 RULES FOR PARAMETER COUNTING

In general, we distinguish between two ways in which one could impose a global symmetry. The symmetry can be imposed on the whole model, or only on a specific sector. Clearly, a symmetry of a specific sector is broken by higher order terms. Yet, in terms of parameter counting we care about the tree level parameters. For example, in the SM the custodial symmetry is respected only by the Higgs sector and it is broken at one loop.

In the following, we study both cases and show that the general result is the same: the total number of parameters, N_{total}, needed to describe a model in a general basis is reduced compared to a model without such symmetries. The specific number of parameters needed in each case is different.

The most general type of terms on which we consider imposing a global symmetry has the form

$$Y_{ij}\phi_i^{(1)}\phi_j^{(2)}\ldots, \tag{4.7}$$

where $\phi^{(1)}$ and $\phi^{(2)}$ have n generations each, Y is an $n \times n$ mixing matrix and $\ldots$ represents other (flavor-singlet) factors that ensure that the term is a gauge group singlet. Multiple terms of the form (4.7) may be present. It is therefore possible that some of the symmetries imposed could hold for some terms, but be broken explicitly by others. Furthermore, if one or more of the gauge symmetries of the model is broken, then it is possible to allow the imposed symmetries to be broken by the gauge sector.

We start by looking at a simple toy model. Consider the leptonic sector of the standard model, but with an imposed $SU(2)$ symmetry such that two of the lepton masses are the same. Since the leptonic Yukawa matrix can be diagonalized without breaking any gauge symmetry, if the symmetry is imposed on the Yukawa sector, it will hold for the entire model. Thus, the cases of imposing the symmetry on the model and on the Yukawa sector only are the same for this choice of matter content. The only interaction term that it is necessary to consider for now is the third term in (4.3), $Y_{ij}^E(\overline{L_L})_i(E_R)_j\tilde{H}$. As we show below, the result is that the total number of parameters required to describe this term in an arbitrary basis, N_{total}, is reduced from 18 to 15.

In an arbitrary basis, we begin to decompose the matrix Y^E, first performing a polar decomposition [132]:

$$Y^E = R\Phi, \tag{4.8}$$

where R is Hermitian with positive eigenvalues and Φ is unitary. The next step is to perform a spectral decomposition on R:

$$Y^E = U^\dagger D U \Phi, \tag{4.9}$$

where U is unitary and $D = \mathrm{diag}(m_e, m_e, m_\tau)$ (recall that we choose $m_e = m_\mu$). Clearly, U can be taken to have unit determinant in general. The final step is to apply a Cartan decomposition [132] on U. The involution of choice here will allow us to break U into the product of a matrix in $U(2) \times U(1)$ and a matrix generated by the remaining generators of $SU(3)$. At this point, to illustrate the general procedure, we explicitly perform steps outlined in the Appendix. The Cartan decomposition theorem (see the Appendix for a statement of the theorem and more details) then allows us to write

$$U = k \exp(\mathbf{p}), \tag{4.10}$$

where $k \in U(2) \times U(1)$ and $\mathbf{p} = \sum_{j=4}^{7} i a_j \lambda_j / 2$, a_j are real numbers and λ_i are the Gell-Mann matrices. Note that $\mathbf{p}$ is described by 4 parameters, the a_j. The final form of the matrix R is then

$$\begin{aligned} R &= \exp(-\mathbf{p}) \begin{pmatrix} U_{2\times 2}^\dagger & 0 \\ 0 & e^{-i\alpha} \end{pmatrix} \begin{pmatrix} m_e & 0 & 0 \\ 0 & m_e & 0 \\ 0 & 0 & m_\tau \end{pmatrix} \begin{pmatrix} U_{2\times 2} & 0 \\ 0 & e^{i\alpha} \end{pmatrix} \exp(\mathbf{p}) \\ &= \exp(-\mathbf{p}) \begin{pmatrix} m_e & 0 & 0 \\ 0 & m_e & 0 \\ 0 & 0 & m_\tau \end{pmatrix} \exp(\mathbf{p}). \end{aligned} \tag{4.11}$$

The main result following from (4.11) is that it only 6 parameters are required to describe the matrix R in this way. They are the two eigenvalues and the 4 a_j. This is in contrast to the usual 9 for a general 3×3 Hermitian matrix.

The decomposition of R given by (4.11) demonstrates the fact that the value of N_{general} is reduced when symmetries are imposed. In this case, the usual 18 is decreased to 15, of which 7 are real parameters and 8 are phases. As a check, the symmetry breaking pattern is

$$U(3)_L \times U(3)_E \to U(2)_e \times U(1)_\tau. \tag{4.12}$$

Thus, there are 13 broken symmetry generators, $N_{\text{broken}} = 13$. Using the fact that $N_{\text{general}} = 15$

and using Eq. (4.2) we get

$$N_{\text{phys}} = N_{\text{general}} - N_{\text{broken}} = 15 - 13 = 2. \tag{4.13}$$

ndeed there are two flavor parameters in this model, m_e and m_τ.

Now consider a more general model with one term of the form in (4.7), $Y_{ij}\phi_i^{(1)}\phi_j^{(2)}$. Without any restrictions, $2n^2$ parameters would be required to describe Y in a general basis. Whenever symmetries are imposed on such terms, this number is reduced. The degeneracies of the matrix eigenvalues ensure that one can always parametrize the matrix with fewer parameters than one would naïvely expect. As a first step in proving the general formula, consider imposing an n_1-fold eigenvalue degeneracy on Y, with $1 < n_1 \leq n$. Since Y can be diagonalized, this is equivalent to imposing an $SU(n_1)$ symmetry. Using results obtained in the Appendix, the required number of parameters is reduced by $n_1^2 - 1$ and thus $N_{\text{general}} = 2n^2 - n_1^2 + 1$ out of which, $n^2 + 1 - n_1(n_1+1)/2$ are real and $n^2 - n_1(n_1-1)/2$ are phases.

With this result for an imposed $SU(n_1)$ symmetry, it is possible to iteratively extend the symmetry group to $SU(n_1) \times \cdots \times SU(n_k)$. For each imposed $SU(n_j)$, $n_j^2 - 1$ parameters can be removed. Thus, the most general result for an n general model with two n fields transforming in the (anti-)fundamental of the imposed symmetry group is

$$N_{\text{phys}} = 2n^2 - \sum_{j=1}^{k}(n_j^2 - 1). \tag{4.14}$$

n terms of real parameters, $N_{\text{phys}}^{(r)}$, and phases, $N_{\text{phys}}^{(i)}$, the result is

$$N_{\text{phys}}^{(r)} = n^2 - \sum_{j=1}^{k}\left(\frac{n_j(n_j+1)}{2} - 1\right), \qquad N_{\text{phys}}^{(i)} = n^2 - \sum_{j=1}^{k}\frac{n_j(n_j-1)}{2}. \tag{4.15}$$

Some complications arise when more terms are added to the potential, particularly when one field appears in multiple potential terms. The cases of a full model symmetry and a sector symmetry cease to be the same as the interaction matrices cannot always be diagonalized concurrently with the gauge interactions. The case of a sector symmetry is trivial to extend. In this case, the symmetry

must hold if the interaction matrices in the sector were diagonalized. In this diagonal basis, a certain number of eigenvalues need to be degenerate in order for the symmetry to be manifest. The case of an interaction matrix with degenerate eigenvalues was discussed above and applies also to this case. In particular, the rule (4.15) apply to each individual interaction matrix. For model-wide symmetries, there are correlations between the change of basis matrices allowed in different terms. We demonstrate a general procedure for determining the correlations below.

Consider a model with three fields $\phi^{(k)}$ that have n generations each. Suppose further that the non-gauge interaction terms have the form

$$L = Y^{(2)}_{ij}\phi^{(1)}_i\phi^{(2)}_j\cdots + Y^{(3)}_{ij}\phi^{(1)}_i\phi^{(3)}_j\cdots . \tag{4.16}$$

typical example of a part of a model with interactions of this form is the quark-sector Yukawa interactions in the standard model. An $SU(n_1)\times\cdots\times SU(n_k)$ symmetry is imposed with all fields having their first $n_1+\cdots+n_k$ components transform in the fundamental. Naïvely, one might expect the number of parameters to be simply twice that of the one-interaction-term model with the same symmetry. However, there is a reduction in the number of parameters due to the fact that the change of basis matrix U in (4.9) must be the same for both Yukawa matrices in order for the symmetry to hold in some basis. Of the physical parameters subtracted off in (4.15), $\sum_j(n_j-1)$ were real eigenvalues that are now degenerate and $\sum_j n_j(n_j-1)/2$ real parameters and phases were parameters in U. Thus, since n of the phases of U always multiply out independent of the symmetry, the U matrix has the same number of real parameters and phases

$$\frac{n(n-1)}{2} - \sum_{j=1}^{k}\frac{n_j(n_j-1)}{2}. \tag{4.17}$$

hus, we count twice the number of parameters as in the one term case, then subtract off the number of parameters in each repeated U matrix. Using this counting, we find that the total number of

parameters required is

$$N^{(r)}_{\text{general}} = \frac{n(3n+1)}{2} - \sum_{j=1}^{k} \frac{(n_j+4)(n_j-1)}{2}, \qquad N^{(i)}_{\text{general}} = \frac{n(3n+1)}{2} - \sum_{j=1}^{k} \frac{n_j(n_j-1)}{2}. \quad (4.18)$$

If the symmetry is only required to hold in the Yukawa sector, but may be broken by the weak interactions, then there really are twice as many parameters in this case as in the case with one interaction term. That is

$$N^{(r)}_{\text{general}} = 2n^2 - 2\sum_{j=1}^{k} \left(\frac{n_j(n_j+1)}{2} - 1 \right), \qquad N^{(i)}_{\text{general}} = 2n^2 - 2\sum_{j=1}^{k} \frac{n_j(n_j-1)}{2}. \quad (4.19)$$

Finally, if we demand only that the first term has such a symmetry, but allow the symmetry to be broken by the other term, then only $Y^{(2)}$ is restricted. In a general basis, we subtract off the parameters of U that are unnecessary for that matrix

$$N^{(r)}_{\text{general}} = 2n^2 - \sum_{j=1}^{k} \left(\frac{n_j(n_j+1)}{2} - 1 \right), \qquad N^{(i)}_{\text{general}} = 2n^2 - \sum_{j=1}^{k} \frac{n_j(n_j-1)}{2}. \quad (4.20)$$

Any other model can be handled by accounting for the appropriate relation among the U matrices, described in one of the cases (4.18), (4.19) or (4.20).

4.3 PARAMETER COUNTING IN THE MSSM

Even with imposed R-parity, the MSSM has 124 parameters, which is much more than the 19 of the standard model [133, 134]. In order to make any specific, quantitative predictions using the model, it is necessary to make some assumptions about the flavor structure of the model. One of the most popular models that does so is the constrained MSSM (cMSSM), which has only 4 new parameters and one undetermined sign. The cMSSM involves a number of arbitrary assumptions about the parameters that appear in the low-energy Lagrangian. A different approach is to start imposing symmetries on the interactions at some UV scale, which we can then run down to the scales being studied. In order to see how this approach works and how the rules derived in section

4.2 help us in studying the MSSM, we consider a toy version of the MSSM.

The toy model has only two generations of quarks, no leptons and exact R-parity. The superpotential for quark multiplets is

$$W = Y^U_{ij} Q_i U_j H_u + Y^D_{ij} Q_i D_j H_d, \tag{4.21}$$

here Y^Q_{ij} are 2×2 complex matrices. See for example [134] for the choice of conventions for representations under the MSSM gauge group. The SUSY-breaking potential for the squarks is given by

$$V_{\text{soft}} = (A^U_{ij} \tilde{Q}_i \tilde{U}_j H_u + A^D_{ij} \tilde{Q}_i \tilde{D}_j H_d + \text{h.c.}) + (M^2)^Q_{ij} \tilde{Q}^\dagger_i \tilde{Q}_j + (M^2)^U_{ij} \tilde{U}^\dagger_i \tilde{U}_j + (M^2)^D_{ij} \tilde{D}^\dagger_i \tilde{D}_j, \tag{4.22}$$

where A^Q_{ij} are complex 2×2 matrices, and $(M^2)^F_{ij}$ are Hermitian 2×2 matrices.

Before restricting the model, we compute the number of flavor parameters in this toy MSSM. There are four 2×2 complex matrices and three 2×2 Hermitian matrices, which in the absence of symmetries gives the counting

$$N^{(r)}_{\text{general}} = 25, \qquad N^{(i)}_{\text{general}} = 19. \tag{4.23}$$

The full $U(2)^3$ flavor symmetry is broken by the interaction terms

$$U(2)^3 \to U(1)_B. \tag{4.24}$$

Using (4.2), we then find that

$$N^{(r)}_{\text{phys}} = 22, \qquad N^{(i)}_{\text{phys}} = 11. \tag{4.25}$$

The non-supersymmetric model with the same gauge and matter content has only 5 real parameters in the quark sector.

As in the non-supersymmetric case, there are a number of ways to impose a symmetry. Obviously, we could require the symmetry to hold through all sectors of the model. However, the

symmetry could also be imposed on the SUSY-breaking sector and broken by the SUSY sectors. It could be imposed on the two potentials, but broken by weak interactions. Finally, it could be imposed on the up quarks only, but broken by the down quarks or vice versa.

Consider the various ways of imposing a $U(1)$ symmetry on the lighter generation of quarks. This symmetry will automatically guarantee a second $U(1)$ for the heavy quarks. The least restrictive ways to impose the symmetry are to demand either that it hold only for the up quarks or only in the soft SUSY-breaking potential. It turns out that both scenarios have the same number of parameters. In the case where symmetry is imposed only on the up quark matrices, the only restriction is that all the up quark interaction matrices be simultaneously diagonalizable. If the matrices are written in the form (4.9), then all their U and Φ matrices must be the same up to an overall diagonal phase matrix. The down interaction matrices are not affected by this restriction. If the symmetry is imposed for both types of quarks, but only in V_{soft}, then all the U matrices must be the same within the SUSY-breaking sector. Both cases lead to the counting:

$$N^{(r)}_{\text{general}} = 21, \qquad N^{(i)}_{\text{general}} = 15. \tag{4.26}$$

Since the imposed symmetry is broken by other sectors, the symmetry breaking is

$$U(2)^3 \to U(1)_B. \tag{4.27}$$

With (4.2), it is then easy to see that the number of physical parameters is given by

$$N^{(r)}_{\text{phys}} = 18, \qquad N^{(i)}_{\text{phys}} = 7. \tag{4.28}$$

The number of parameters is further reduced if we demand that the symmetry hold for both potentials and for both types of quarks. Not only are the U matrices now correlated, but so are the Φ matrices. The number of parameters in a general basis is

$$N^{(r)}_{\text{general}} = 18, \qquad N^{(i)}_{\text{general}} = 12. \tag{4.29}$$

There is no additional symmetry for the full model, and we count that

$$N^{(r)}_{\text{phys}} = 15, \qquad N^{(i)}_{\text{phys}} = 4. \tag{4.30}$$

The next more restrictive case is imposing the $U(1)$ throughout the model. Progressing to this case is as simple as extending the correlations from the previous cases to the entire model, so that

$$N^{(r)}_{\text{general}} = 17, \qquad N^{(i)}_{\text{general}} = 11. \tag{4.31}$$

The extra $U(1)$ symmetry now holds on the model so part of the flavor symmetry is restored

$$U(2)^3 \to U(1)_u \times U(1)_c. \tag{4.32}$$

Thus, the number of physical parameters is given by

$$N^{(r)}_{\text{phys}} = 14, \qquad N^{(i)}_{\text{phys}} = 4. \tag{4.33}$$

Next, we study models where we impose minimal flavor violation (MFV) on the Yukawas and their supersymmetry-breaking extensions. MFV is defined in the spurion formalism by saying that the only flavor-violating spurions are the standard model Yukawa matrices. To leading order, this forces $A^F = a^F Y^F$, where a^F is a complex number, and $(M^2)^F = (m^2)^F 1$, where $(m^2)^F$ is a real number. The parameter counting in the SUSY-breaking sector is as follows. There are two additional parameters for each three-scalar coupling and one extra for each mass. In the end, we find that in a general basis

$$N^{(r)}_{\text{general}} = 13, \qquad N^{(i)}_{\text{general}} = 10. \tag{4.34}$$

Only baryon number is left after breaking the symmetry, so that

$$N^{(r)}_{\text{phys}} = 10, \qquad N^{(i)}_{\text{phys}} = 2. \tag{4.35}$$

The cMSSM is a restriction of the MFV case. It is assumed that at some high scale all the

scalar masses are equal, all the three-scalar couplings a^F are equal and all the gaugino masses are equal. In the full model with leptons, these restrictions hold between baryons and leptons as well. Furthermore, the new interactions are assumed to be CP-conserving so that there are no new CP violating physical phases. With these conditions, the counting in a general basis is

$$N^{(r)}_{\text{general}} = 10, \qquad N^{(i)}_{\text{general}} = 8, \tag{4.36}$$

so that in the physical basis

$$N^{(r)}_{\text{phys}} = 7, \qquad N^{(i)}_{\text{phys}} = 0. \tag{4.37}$$

The non-supersymmetric analogue of this model had only 5 flavor parameters: four quark masses and a mixing angle. Thus, there are two new flavor parameters here which we can take to be the SUSY-breaking squark mass m_0^2 and the triscalar coupling a_0. These two additional parameters in the quark sector, together with the SUSY-breaking Higgs parameter b and the gaugino mass $m_{1/2}$, are the only new parameters. The superpotential mass parameter μ can be related to the Higgs VEV and is not counted as new. An extra undetermined sign comes from moving to a more convenient parametrization where the Higgs parameters μ and b are traded for m_Z and $\tan\beta$. The two sets of parameters contain the same information up to the sign of μ which is not fixed by fixing m_Z and $\tan\beta$. This ambiguity arises from the fact that the scalar Higgs potential of the MSSM depends only on $|\mu|^2$ and not on μ.

Most of the counting outlined in (4.23)-(4.37) above extends trivially to constraining the full MSSM. The main complication is the additional generation in the fermion sectors. The additional generation allows an $SU(2)$ flavor symmetry to be imposed. This type of symmetry can then be handled using the rules derived in section 4.2. Maintaining exact R-parity, the superpotential for the fermion multiplets is given by

$$W = Y^U_{ij} Q_i U_j H_u + Y^D_{ij} Q_i D_j H_d + Y^L_{ij} L_i E_j H_d, \tag{4.38}$$

where Y^F_{ij} are 3×3 complex matrices and μ is a complex number. The SUSY-breaking potential

Imposed Symmetry	Broken By	$N^{(r)}_{\text{general}}$	$N^{(i)}_{\text{general}}$	$N^{(r)}_{\text{phys}}$	$N^{(i)}_{\text{phys}}$
None		84	69	69	41
Fermion Family	SUSY Interaction	66	51	51	23
	Weak Interactions	51	36	36	10
	All	48	33	33	9
$SU(2)$ Flavor	SUSY Interaction	56	49	41	21
	Weak Interactions	37	30	23	6
	All	35	28	22	6
Leading MFV		35	30	20	4
$SU(3)$ Flavor		20	21	11	3

Table 4.1: Parameter counting in the chiral multiplet potentials of the MSSM with various imposed symmetries in the potentials only and in the entire Lagrangian for the model. The large $SU(N)$ symmetries are necessarily broken, possibly spontaneously [135].

for the fields in these multiplets is given by:

$$V_{\text{soft}} = (A^U_{ij}\tilde{Q}_i\tilde{U}_j H_u + A^D_{ij}\tilde{Q}_i\tilde{D}_j H_d + A^L_{ij}\tilde{L}_i\tilde{E}_j H_d + \text{c.c.}) + (M^2)^Q_{ij}\tilde{Q}^\dagger_i\tilde{Q}_j + (M^2)^U_{ij}\tilde{U}^\dagger_i\tilde{U}_j + (M^2)^D_{ij}\tilde{D}^\dagger_i\tilde{D}_j + (M^2)^L_{ij}\tilde{L}^\dagger_i\tilde{L}_j + (M^2)^E_{ij}\tilde{E}^\dagger_i\tilde{E}_j, \quad (4.39)$$

where A^F_{ij} are complex 3×3 matrices and $(M^2)^F_{ij}$ are Hermitian 3×3 matrices.

The results of the parameter counting for various imposed symmetries are described in table 4.1. The four columns show the number of real and imaginary parameters in a general basis and in the physical basis for the potential of the chiral flavored fields. The first row gives the counting for the case when no symmetry is imposed. This is the MSSM-124 model. The second through fourth lines describe the case where only $U(1)$ family symmetry is imposed. On the second line, the symmetry is broken by the superpotential. On the third line, it is broken by weak gauge interactions. On the fourth line, it holds through all renormalizable terms in the model. The fifth through seventh lines describe the case where $SU(2)$ is imposed with the first two generations transforming as a doublet and the third as a singlet. The same three symmetry-breaking possibilities are presented. On the eighth line, we present the case of MFV where only the leading term in powers of the Yukawa matrices is kept. Finally, the case with maximal $SU(3)$ flavor symmetry is presented.

4.4 CONCLUSIONS

It is clear that the Standard Model is a low energy description of a more fundumental theory. The introduction of new states and symmetries into the Lagrangian adds many new interaction matrices. The hierarchy of the SM Yukawa matrices as well as the new physics flavor puzzle [130] motivate the idea that new flavor symmetries or approximate symmetries could exist in more fundamental interactions. If such symmetries exist, then parameter counting may be non-trivial. The number of parameters required in a general basis is less than if the symmetries were not imposed. We derived rules for accounting for this reduction in the number of parameters. We demonstrated the analysis for a series of toy models, leading up to counting the number of parameters in the MSSM with various imposed flavor symmetries. The results obtained for the MSSM are summarized in Table 4.1. However, the methods used above are general and can be used to study other potential UV completions of the Standard Model.

CHAPTER 5

A new CP violating observable for the LHC

5.1 INTRODUCTION

The Standard Model (SM) of particle physics contains a single CP violating phase in the Cabibbo-Kobayashi-Maskawa (CKM) matrix [16]. Many different measurements have confirmed that the SM describes observed CP violation to extremely good accuracy [10, 31]. Particularly strong constraints on physics beyond the SM can be obtained from neutral kaon mixing, pushing the scale of generic new CP violation operators to at least $\mathcal{O}(10^5\,\text{TeV})$ [136]. Strong constraints have also been obtained from the non-observation of electric dipole moments (see [137] for a review). While one might be tempted to conclude that new physics must be CP conserving up to very high energy scales, this is not necessarily the case. In fact, it is sufficient to introduce the new sources of CP violation in such a way that they are hidden from flavor physics observables. A large new physics scale is not the only way to achieve this; other options include, for example, the introduction of flavor symmetries or decoupling the new sources of CP violation from the flavor sector. Consequently it is important to search for new physics CP violation not only indirectly in low energy observables, such as meson decays or electric dipole moments, but also directly in the production and decay of new heavy particles at colliders. Direct searches have the advantage of giving much cleaner access to the new CP violating phases in question.

In order to observe CP violation in heavy particle decays, asymmetries in the decay rates

corresponding to CP-conjugate processes can be measured:

$$\mathcal{A}_{\rm CP} = \frac{\Gamma(M \to f) - \Gamma(\overline{M} \to \overline{f})}{\Gamma(M \to f) + \Gamma(\overline{M} \to \overline{f})}. \tag{5.1}$$

For this asymmetry to be non-vanishing, the amplitude for the decay rate must be composed of at least two interfering amplitudes with different CP-even ("strong") and CP-odd ("weak") phases. (If the momenta, and possibly the helicities, of the final state particles can be determined, then it is possible to avoid the condition of requiring amplitudes with different strong phases by looking at triple product asymmetries. See e. g. Refs. [138, 139, 140, 141, 142, 143, 144, 145, 146].)

In the SM, the weak phase always depends on the CKM phase. More generally, it is related to complex phases of the Lagrangian parameters and, therefore, changes sign under CP conjugation. Strong phases are so-named because they often arise from strong-interaction rescattering of the final state. However, several cases are known where a calculable strong phase arises from the propagation of intermediate state particles. For instance when the two amplitudes arise due to mixing of states with the same quantum numbers, as in $B \to \psi K_S$ for example, the strong phase arises simply through the time evolution of the intermediate $B^0 - \bar{B}^0$ system. Another source of strong phases is finite width effects that have been considered in both particle production [147, 148] and decay [149, 150].

The requirement of the existence of a strong phase places a limitation on our ability to measure CP-violation. There is no reason to assume the strong phase is large. Furthermore, there is often no way to determine the strong phase for a given process, since it can involve complicated strongly coupled physics. It is therefore important to look for processes where either the strong phase can be divided out or calculated. Situations where the strong phase can be calculated arise most readily in processes involving a propagating intermediate unstable particle.

In order to see this, consider a diagram of the form shown in Fig. 5.1. The corresponding amplitude can generally be written in the form

$$\mathcal{M} = \mathcal{M}_1 \frac{1}{q^2 - m^2 + i\Gamma m} \mathcal{M}_2, \tag{5.2}$$

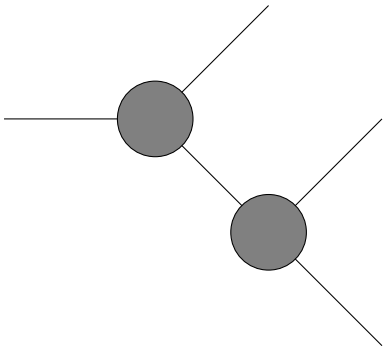

Figure 5.1: Diagram demonstrating the presence of a strong phase in the propagator of an intermediate state.

where $\mathcal{M}_{1,2}$ are, roughly, amplitudes for the upper and lower parts of the diagram and carry the weak phase, q is the off-shell momentum of the propagating particle, m is its mass, and Γ is its width. The Breit-Wigner denominator in this amplitude is CP-even; that is, in the CP-conjugate amplitude, the i in the denominator appears with the same sign. Thus, the propagating particle leads to a strong phase

$$\arg\left(\frac{1}{q^2 - m^2 + i\Gamma m}\right). \tag{5.3}$$

Recall that in order to have observable CP-violation in a decay process, it is necessary to have at least two amplitudes with different strong phases. If both amplitudes have a propagating particle, then there are two ways in which their strong phases can differ:

1. The propagating particles could be different, so that they have different mass and/or width;

2. The propagating particles could be the same, but off-shell by different amounts.

When studying SM physics, the first situation was considered [149, 150]. In this chapter, we study the second case, that is, strong phases that arise from different virtualities. Unlike the SM, this effect is a common feature of heavy particle decays leading to CP violating asymmetries in new physics models. In order to obtain a non-vanishing CP even phase the decay must proceed via two interfering diagrams with the same intermediate unstable particle but with different orderings of the final states. The examples studied in this chapter deal with neutral Majorana-like particle decays, i. e. particles that transform under real representations of all symmetry groups. While the

appearance of a CP even phase is very natural in such a situation, the mechanism in question is also present in charged particle decays.[1]

The work presented in this chapter is based on Ref. [52]. It is structured as follows. In Section 5.2, we discuss general considerations for having a non-vanishing strong phase difference as described above, using a toy model for concreteness. In Section 5.3, we present results of a study of CP violation via that mechanism within a model of new physics, the Minimally Supersymmetric Standard Model (MSSM). We discuss these results and conclude in Section 5.4.

5.2 CP-EVEN PHASES IN THE PROPAGATOR

As discussed in the introduction, three conditions must be satisfied in order for a CP-violating asymmetry to be observable in a given process:

1. the amplitude must be composed of at least two terms a_1 and a_2;
2. the two terms must have different CP-even ("strong") phases $\delta_1 \neq \delta_2$;
3. the two terms must have different CP-odd ("weak") phases $\phi_1 \neq \phi_2$.

In other words the amplitude must have the structure

$$\mathcal{M} = |a_1| e^{i(\delta_1+\phi_1)} + |a_2| e^{i(\delta_2+\phi_2)} \,. \tag{5.4}$$

The asymmetry $\mathcal{A}_{\rm CP}$ defined in (5.1) is then given by

$$\mathcal{A}_{\rm CP} \propto |a_1||a_2| \sin(\delta_1 - \delta_2) \sin(\phi_1 - \phi_2), \tag{5.5}$$

where we see explicitly that the three conditions must be satisfied.

As discussed in the introduction, two decay amplitudes can have different CP-even phases if the intermediate propagating particles are off-shell by different amounts. To make this statement more concrete, consider a three body decay $X_0^0 \to X_1^+ X_2^- X_3^0$. Suppose further that this decay can

[1] We would like to thank Alejandro Szynkman for useful discussion that led us to this observation.

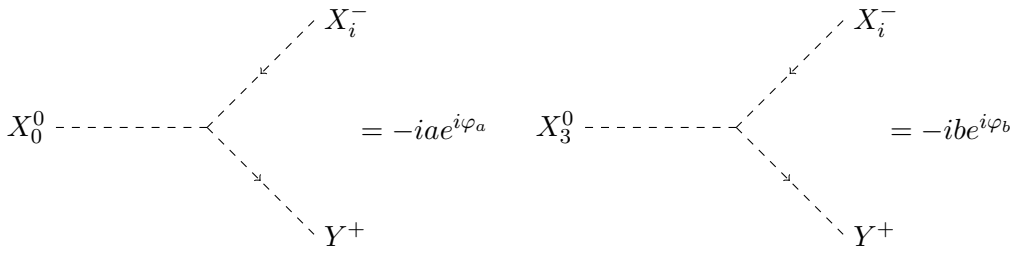

Figure 5.2: Feynman rules for the toy model.

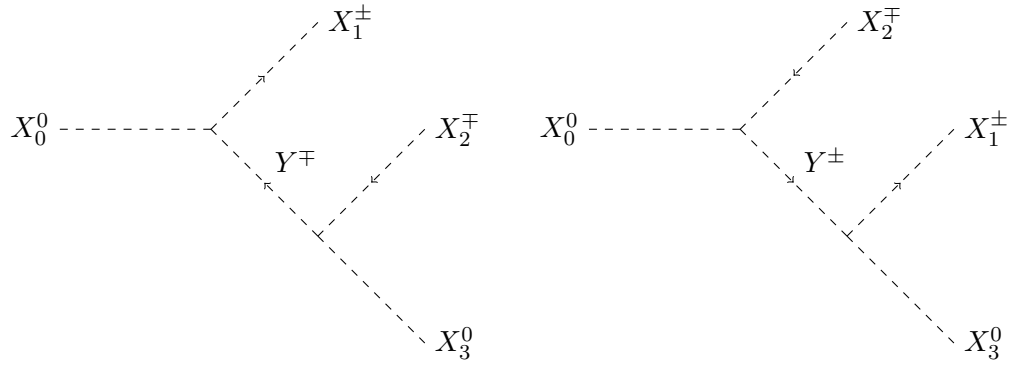

Figure 5.3: Diagrams for the decay $X_0^0 \to X_1^\pm X_2^\mp X_3^0$.

proceed in two ways

$$X_0^0 \to X_1^+ Y^{-*} \to X_1^+ X_2^- X_3^0, \qquad X_0^0 \to X_2^- Y^{+*} \to X_1^+ X_2^- X_3^0. \tag{5.6}$$

n both cases, the off-shell particle is Y and clearly has the same mass and width. However, its four-momentum in each case is different for a given point in the available phase space of the decay. The two decay modes contribute two different terms to the amplitude which have different strong phases at this point in phase space.

To demonstrate the new CP-even phase, we consider a simple toy model. We assume that all the particles involved are scalars and consider only cubic couplings. We further assume a universality of couplings: the X_0^0 and X_3^0 each couple to the charged particles with the same couplings. While this simplifying assumption is not a necessary condition, it is crucial that all four couplings of $X_{1,2}^\pm$ to $X_0 Y^\mp$ and $X_3 Y^\mp$ be non-vanishing so that two interfering diagrams with different final state orderings are present. The Feynman rules we consider are presented in Fig. 5.2. This toy model

has only one physical CP-odd phase,

$$\varphi = \varphi_b - \varphi_a. \tag{5.7}$$

he diagrams we consider are presented in Fig. 5.3. The differential decay width can be obtained from the Feynman rules in Fig. 5.2 and reads

$$\begin{aligned}\frac{d\Gamma}{dq_{13}^2 dq_{23}^2} &= \frac{a^2 b^2}{32(2\pi)^3 m_0^3} \times \frac{1}{(\Delta\hat{q}_{13}^2)^2 + \hat{\Gamma}_Y^2} \times \frac{1}{(\Delta\hat{q}_{23}^2)^2 + \hat{\Gamma}_Y^2} \times \\ &\Big[\Big((\Delta\hat{q}_{13}^2)^2 + (\Delta\hat{q}_{23}^2)^2 + 2\hat{\Gamma}_Y^2 \Big) \\ &\quad + 2\cos(2\varphi) \Big[\Delta\hat{q}_{13}^2 \Delta\hat{q}_{23}^2 + \hat{\Gamma}_Y^2 \Big] + 2\sin(2\varphi)\hat{\Gamma}_Y(\Delta\hat{q}_{13}^2 - \Delta\hat{q}_{23}^2) \Big]\end{aligned} \tag{5.8}$$

where m_0 is the mass of X_0, Γ ($\overline{\Gamma}$) is the rate for $X_0^0 \to X_1^+ X_2^- X_3^0$ ($X_0^0 \to X_1^- X_2^+ X_3^0$) and

$$q_{ij}^2 = (p_i + p_j)^2, \qquad \hat{q}_{ij}^2 = \frac{q_{ij}^2}{m_Y^2}, \qquad \hat{\Gamma}_Y = \frac{\Gamma_Y}{m_Y}, \tag{5.9}$$

here m_Y and Γ_Y are the mass and width respectively of $Y^\pm$. It is convenient to parametrize the differential decay width using

$$\Delta\hat{q}_{ij}^2 = \hat{q}_{ij}^2 - 1\,, \tag{5.10}$$

ince we will see that the asymmetry will be largest near the point $q_{13}^2 = q_{23}^2 = m_Y^2$ in phase space.

The first asymmetry that we calculate is the differential rate asymmetry before integrating over phase space:

$$\mathcal{A}_{\rm CP}^{\rm diff} = \frac{d\Gamma/dq_{13}^2 dq_{23}^2 - d\overline{\Gamma}/dq_{13}^2 dq_{23}^2}{d\Gamma/dq_{13}^2 dq_{23}^2 + d\overline{\Gamma}/dq_{13}^2 dq_{23}^2}, \tag{5.11}$$

It is given by

$$\mathcal{A}_{\rm CP}^{\rm diff} = \frac{2\sin(2\varphi)(\Delta\hat{q}_{13}^2 - \Delta\hat{q}_{23}^2)\hat{\Gamma}_Y}{2[1+\cos(2\varphi)]\hat{\Gamma}_Y^2 + |\Delta\hat{q}_{13}^2\, e^{i\varphi} + \Delta\hat{q}_{23}^2\, e^{-i\varphi}|^2}. \tag{5.12}$$

Note that this asymmetry is proportional to the sine of the weak phase as desired. Furthermore, it is proportional to $\hat{\Gamma}_Y(\Delta\hat{q}_{13}^2 - \Delta\hat{q}_{23}^2)$. When either $\Gamma_Y = 0$ or $q_{13}^2 = q_{23}^2$ the asymmetry vanishes. This factor in the numerator is proportional to the CP-even phase difference of the two diagrams. We thus demonstrate the occurrence of a CP-even phase due to the virtual $Y^\pm$ being off-shell by different amounts in the two diagrams.

The denominator of the asymmetry (5.12) is minimized when $\Delta\hat{q}_{13}^2 = \Delta\hat{q}_{23}^2 = 0$. That is, when the $Y^\pm$ is on-shell in both diagrams. The numerator, however, also vanishes at that point. We thus expect that the points in phase space where the size of the asymmetry is maximized are near the point $q_{13}^2 = q_{23}^2 = m_Y^2$, along the line $\Delta\hat{q}_{13}^2 + \Delta\hat{q}_{23}^2 = 0$ in order to be as far from the situation where $\Delta\hat{q}_{13}^2 = \Delta\hat{q}_{23}^2$ as possible. In this simple model, we can determine the points of maximum asymmetry analytically and obtain a simple result: the size of the asymmetry is maximized when

$$\Delta\hat{q}_{13}^2 = \pm\hat{\Gamma}_Y \cot(\varphi), \qquad \Delta\hat{q}_{23}^2 = \mp\hat{\Gamma}_Y \cot(\varphi), \tag{5.13}$$

matching our expectation. This result is modified in more complex situations. In particular, when the two interfering diagrams differ in size, the maximum asymmetry is pushed closer to one of the resonances.

Perhaps more telling than the asymmetry itself is the significance of a CP violating signal. The significance of a Dalitz plot asymmetry in a specific bin is given by [151]

$$\sigma_{\rm CP} = \frac{N(i) - \overline{N}(i)}{\sqrt{N(i) + \overline{N}(i)}}. \tag{5.14}$$

This quantity depends on the number of X_0 produced, N, so that it cannot be determined without providing further specifications. The relative significance of the bins, however, is of interest as it determines which bins are most important for confirming the existence of an asymmetry. These bins are not necessarily the ones with maximum asymmetry as the differential rate is enhanced near the resonances. There is a tension between the asymmetry which is largest away from the line $q_{13}^2 = q_{23}^2$ and the differential rate which is largest there. In the specific case we are considering, this significance can be written as

$$\frac{d\sigma_{\rm CP}}{\sqrt{dq_{13}^2 q_{23}^2}} = \sqrt{\frac{N}{\Gamma_{X_0}}} \frac{d\Gamma/dq_{13}^2 dq_{23}^2 - d\overline{\Gamma}/dq_{13}^2 dq_{23}^2}{\sqrt{d\Gamma/dq_{13}^2 dq_{23}^2 + d\overline{\Gamma}/dq_{13}^2 dq_{23}^2}}, \tag{5.15}$$

where Γ_{X_0} is the total width of the X_0^0.

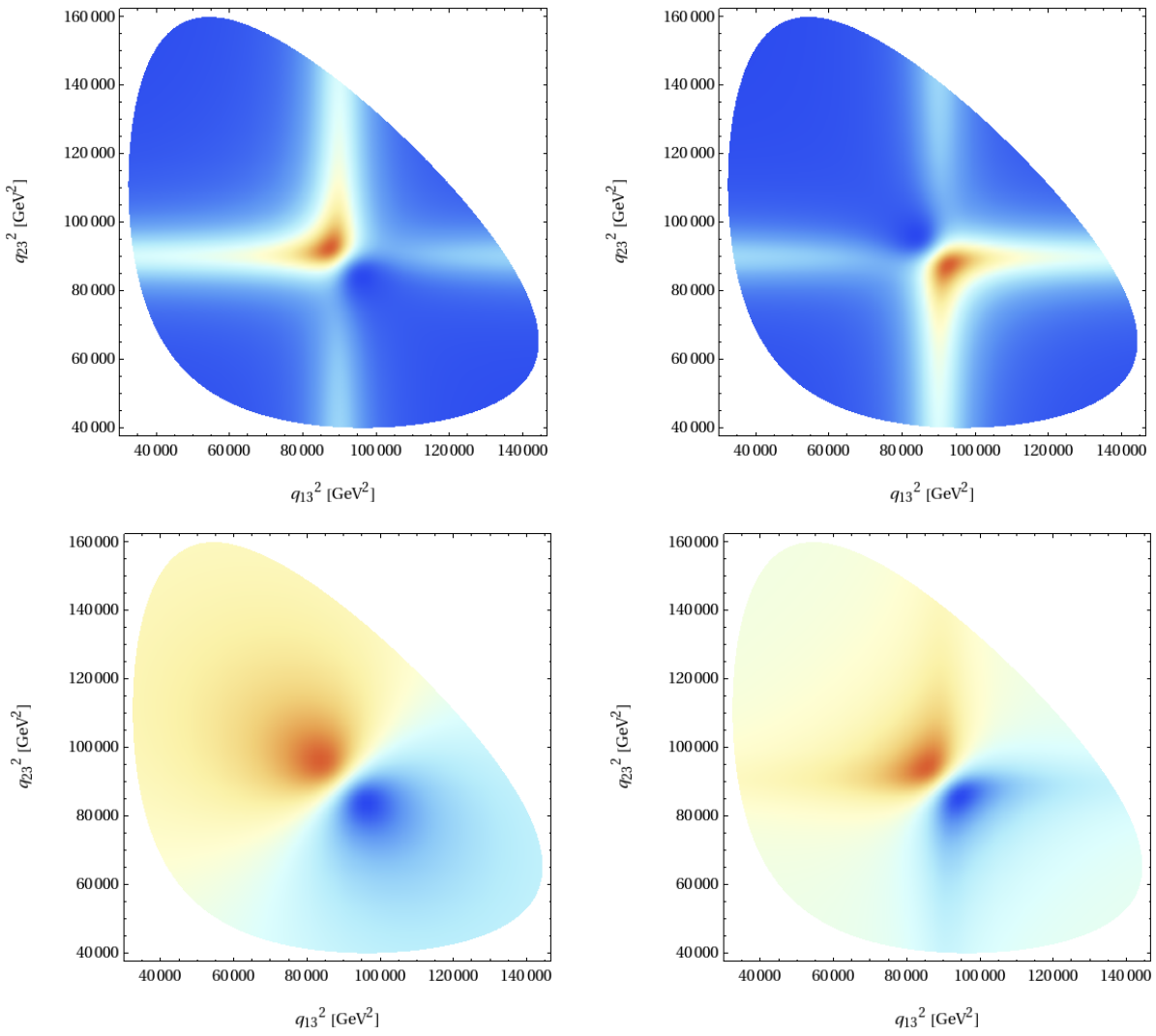

Figure 5.4: Dalitz plots for (a) the differential rate of $X_0 \to X_1^+ X_2^- X_3^0$, (b) the differential rate of the CP conjugate decay $X_0 \to X_1^- X_2^+ X_3^0$, (c) the asymmetry $\mathcal{A}_{\rm CP}$, and (d) the significance $\frac{d\sigma_{\rm CP}}{\sqrt{dq_{13}^2 dq_{23}^2}}\sqrt{\frac{\Gamma_{X_0}}{N}}$.

The Dalitz plots of the differential rate for X_0^0 decay, the rate for the CP conjugate decay, the rate asymmetry, and the significance are given in Fig. 5.4. To produce that plot we use the following parameters

$$m_0 = 500\,\text{GeV}, \quad m_1 = 100\,\text{GeV}, \quad m_2 = 120\,\text{GeV}, \quad m_3 = 80\,\text{GeV},$$
$$a = 20\,\text{GeV}, \quad b = 30\,\text{GeV}, \quad \varphi = \frac{\pi}{4}, \quad m_Y = 300\,\text{GeV}, \quad \hat{\Gamma}_Y = 7\%. \tag{5.16}$$

ll of the features discussed above are observed in these plots. The differential rate of X_0^0 decay is largest along two resonances at $q_{13}^2 = m_Y^2$ and $q_{23}^2 = m_Y^2$ with strong interference where the two resonances overlap. Interestingly the interference is constructive above the line $q_{13}^2 = q_{23}^2$ while destructive below this line. This feature is reversed for the differential rate of the CP conjugate decay: now the interference is constructive below $q_{13}^2 = q_{23}^2$ and destructive above that line, thus exhibiting a clear sign of CP violation. This is made even more explicit in Fig. 5.4 (c) showing the differential CP asymmetry. The maximum asymmetry is seen to be along the line $q_{13}^2 + q_{23}^2 = 2m_Y^2$, but away from the point $q_{13}^2 = q_{23}^2 = m_Y^2$. The maximum significance is located closer to the resonances along the lines $q_{13}^2 = m_Y^2$ and $q_{23}^2 = m_Y^2$.

It is instructive to consider how the obtained results change with the width of the intermediate state particle $Y^\pm$. The resonances visible in the Dalitz plot of the differential decay rate should get broader with increasing Γ_Y. Consequently also the differential CP asymmetry is expected to grow and spread further in phase space. These features are clearly visible from Fig. 5.5 where we show the differential decay rate and CP asymmetry for $X_0 \to X_1^\pm X_2^\mp X_3^0$ for $\hat{\Gamma}_Y = 3\%$, 15% and 30%, in addition to the corresponding plots for $\hat{\Gamma}_Y = 7\%$ shown in Fig. 5.4. We therefore expect the effect in question to be particularly pronounced in models which predict strongly coupled resonances.

We now turn to the discussion of integrated asymmetry variables. In general, it is expected that it will be easier to measure the integrated asymmetry. We first discuss the total integrated asymmetry defined as

$$\mathcal{A}_{\rm CP}^{\rm int} = \frac{1}{\Gamma + \bar{\Gamma}} \int dq_{13}^2 dq_{23}^2 \left(\frac{d\Gamma}{dq_{13}^2 dq_{23}^2} - \frac{d\bar{\Gamma}}{dq_{13}^2 dq_{23}^2} \right) . \tag{5.17}$$

Note that the integrated rate asymmetry vanishes in the limit where the particles X_1 and X_2 are degenerate. The asymmetry (5.12) is anti-symmetric under $q_{13}^2 \leftrightarrow q_{23}^2$, so if phase space is symmetric under such a transformation, the integrated rate asymmetry vanishes. In the case of degenerate charged daughters, phase space has such a symmetry. It is therefore beneficial to weigh the asymmetry above and below $q_{13}^2 = q_{23}^2$ with a relative minus sign and define

$$\mathcal{A}_{\rm CP}^{\rm wgt} = \frac{1}{\Gamma + \bar{\Gamma}} \int dq_{13}^2 dq_{23}^2 \, \mathrm{sgn}(q_{23}^2 - q_{13}^2) \left(\frac{d\Gamma}{dq_{13}^2 dq_{23}^2} - \frac{d\bar{\Gamma}}{dq_{13}^2 dq_{23}^2} \right) . \tag{5.18}$$

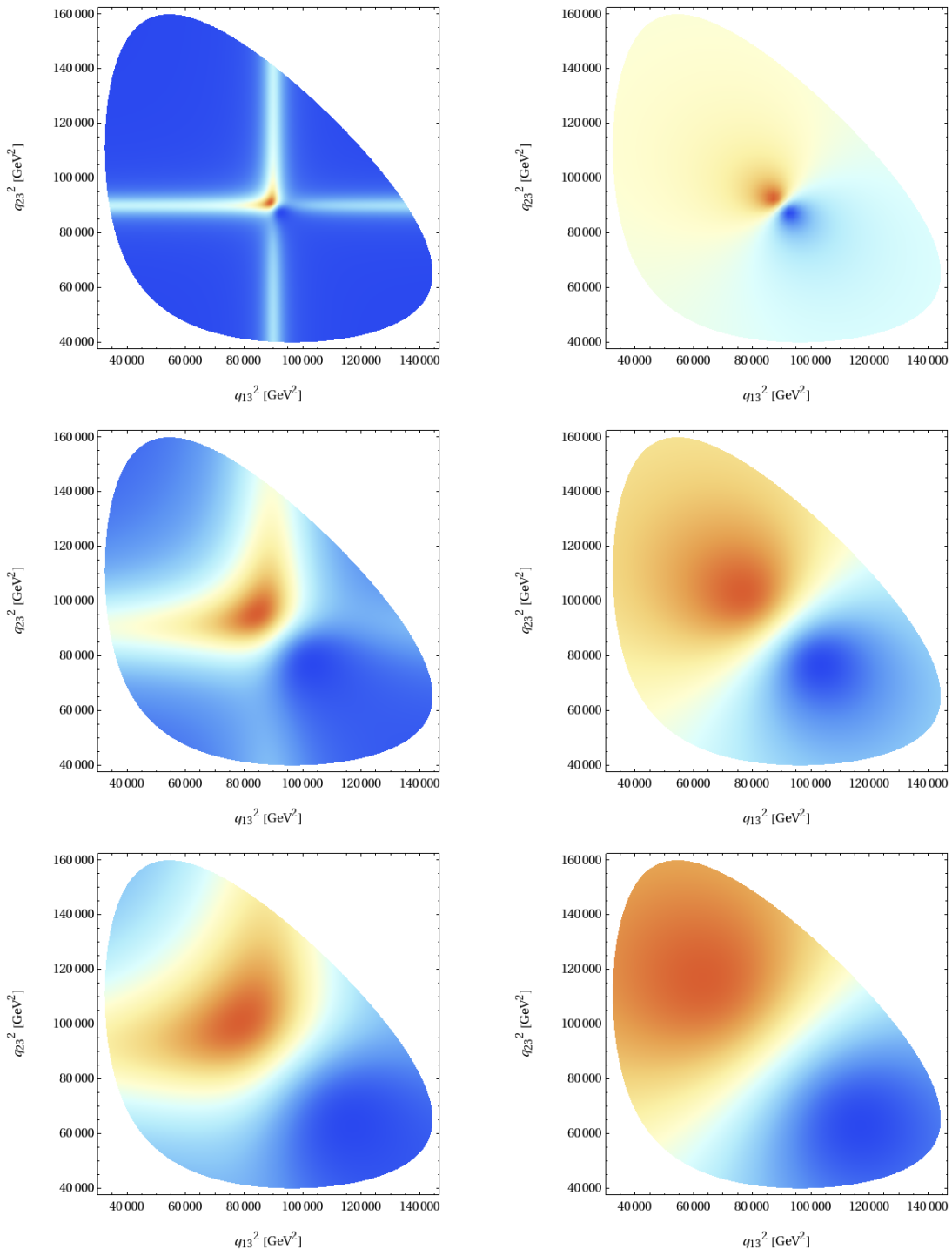

Figure 5.5: Differential decay rate and CP asymmetry for $X_0 \to X_1^{\pm} X_2^{\mp} X_3^0$ for $\hat{\Gamma}_Y = 3\%$, 15% and 30% (from top to bottom).

Whether or not this asymmetry can be measured is an experimental issue.

Even in this simplified model, we are unable to perform a full phase space integration, due to the rather complex nature of three body phase space. We can, however, integrate over a box around the point $q_{13}^2 = q_{23}^2 = m_Y^2$. The largest contributions to the rate asymmetry will come from within such a box. If the box is a square, then the region of phase space integration is again symmetric and the CP asymmetry vanishes. We could simply use an asymmetric phase space region, but we gain more sensitivity by taking advantage of the sign-weighted asymmetry defined in eq. (5.18). Integrating over a square box in phase space with width $2wm_Y^2$ centered at $q_{13}^2 = q_{23}^2 = m_Y^2$ and assuming that $\hat{\Gamma}_Y \ll w$, the resulting integrated asymmetry is given by

$$\mathcal{A}_{\rm CP}^{\rm wgt} \approx x \log x \sin(2\varphi), \qquad x = \frac{2\Gamma}{wm} \tag{5.19}$$

From the Dalitz plot, we conclude that most of the asymmetry effect is located within such a box. The full asymmetry will then be of the same order of magnitude, with $\hat{\Gamma}_Y \ll w \lesssim 1/4$ required by kinematics. The asymmetry is then proportional to the ratio of the width to some combination of mass scales, with a logarithmic enhancement. The asymmetry is larger for larger width.

In this section, we have worked with the simplest model that exhibits CP-violation where the difference in strong phase between the two diagrams for the process is due to the difference in virtuality of the off-shell particles. The model could be complicated by higher spin particles or by other diagrams. Independent of these complications, we can say a few things about the asymmetries. All of the asymmetries will of course be proportional to the sine of the weak phase difference between the diagrams. The differential rate asymmetry due to the effects described here will always vanish along the line $q_{13}^2 = q_{23}^2$. The integrated rate asymmetry will always vanish if the phase space is symmetric about $q_{13}^2 = q_{23}^2$. By doing a weighted integration over phase space, we can avoid this last constraint and enhance the asymmetry in cases where the two charged particles in the final state are nearly degenerate.

Another possible complication that could arise occurs in the large width limit. We have worked in the Breit-Wigner approximation, which will be valid in the new physics scenario we consider below. If the intermediate resonance is broad, the Breit-Wigner approximation breaks down. This

does not alter the qualitative fact that the resonance virtuality leads to a strong phase. We stress that this generic feature of unstable modes in any theory is the crucial one for our purposes.

5.3 CP VIOLATION IN THE CHARGED HIGGS CHANNEL IN THE MSSM

We now turn to study how this new source of CP violation could be relevant to the MSSM. The electroweak sector of the MSSM is described in Appendix C.1. That model is a good starting point, since in the limit we are considering it contains only one CP-violating phase, $\mathrm{Im}(\mu^* b M_2^*)$, defined in (C.8). Any CP violating observable must involve a process that includes mixing between the Higgs and the electroweak sectors. It turns out that the process

$$\chi_4^0 \to \chi_i^\pm \chi_j^\mp \chi_1^0, \qquad i \neq j, \tag{5.20}$$

is very instructive for studying the impact of the strong phases of interest. This process necessarily involves mixing between the Higgs and electroweak sectors. Note that we must be in the limit where the heaviest neutralino is sufficiently heavy that the decay (5.20) is kinematically allowed. This only occurs when the χ_4^0 is mostly Bino like and the Bino soft mass M_1 is large, that is

$$m_{\chi_4^0} \sim M_1 \gg m_{\chi_i^0}, m_{\chi_j^\pm} \sim \sqrt{|\mu M_2|} > m_Z, \tag{5.21}$$

for $i = 1, 2, 3$ and $j = 1, 2$. In order for the decay to be kinematically allowed, the hierarchy must be at least

$$M_1 \gtrsim 3\sqrt{|\mu M_2|}. \tag{5.22}$$

There are several diagrams for the process $\chi_4^0 \to \chi_i^\pm \chi_j^\mp \chi_1^0$, but we would like to focus on the diagram mediated by the charged Higgs as illustrated in Fig. 5.6. We further assume that the charged Higgs can decay on-shell in both cases, so that $m_{H^\pm} \gtrsim 2\sqrt{|\mu M_2|}$. In principle, there are also diagrams mediated by the neutral Higgses, the W, and the Z. Diagrams with intermediate W and Z can be neglected since the W and Z are too light to decay on-shell and thus the amplitudes

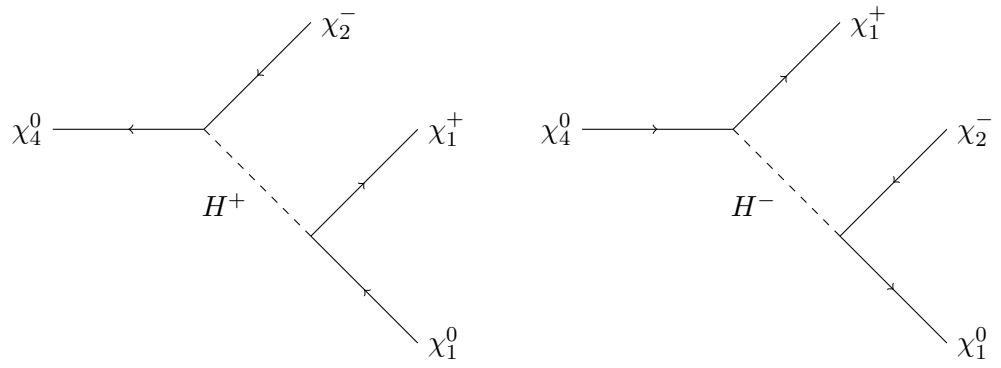

Figure 5.6: Decays of a neutralino through a charged Higgs. In this case, there are only two diagrams for the decay.

are suppressed compared to the nearly on-shell amplitudes for the Higgses. The lighter neutral Higgs and CP-odd Higgs will also generally be too light to decay on-shell, but the heavy neutral Higgs will generally have a mass $m_{H^0} \sim m_{H^\pm}$. We will, however, neglect all but the diagrams mediated by the charged Higgs for simplicity. If other diagrams were included, then the more familiar type of strong phase would contribute in the interference between these diagrams and the charged Higgs mediated ones.

Before performing some analytic and numerical calculations, we would like to get an idea of how large the CP asymmetry can be in this case. To perform this estimate, we take into account the three sources of suppression that the numerator has relative to the denominator: the weak phase, the strong phase, and, in the integrated case, the required phase space asymmetry. The CP odd effect is proportional to (C.8), that is to $|\mu b M_2|$. The relevant dimensionless quantity is normalized to the mass of the decaying particle, that is to some powers of M_1. Taking $b \sim M_1^2$, which is equivalent to taking $\sin\beta \sim 1$, we conclude that this gives a suppression of

$$\mathcal{A}_{\rm CP}^{\rm diff} \propto \frac{|\mu M_2|}{M_1^2}. \tag{5.23}$$

Numerically, this suppression due to the weak phase is at least about 1/9 due to the kinematic constraint, (5.22). The requirement of a non-vanishing strong phase implies that the asymmetry is large only in portion of the Dalitz plot with distance of order $m_{H^\pm}\Gamma_{H^\pm}$ from the point where the two resonances overlap. Thus, for the integrated asymmetry there is an extra suppression of order

$\Gamma_{H^\pm}/m_{H^\pm}$. When considering the fully integrated asymmetry, we get an additional suppression due to the fact that the phase space is nearly symmetric: $\Delta m_{\chi^\pm} \ll M_1$. This suppression is not there for the sign weighted asymmetry. This hierarchy gives a suppression of $\Delta m^2_{\chi^\pm}/M_1^2$. Putting these pieces together, we can say that for order one CP-odd phase, the asymmetry in integrated rates is roughly given by

$$\mathcal{A}_{\rm CP}^{\rm int} \sim \frac{\Gamma_{H^\pm} \Delta m^2_{\chi^\pm} |\mu M_2|}{m_{H^\pm} M_1^4}, \tag{5.24}$$

and the asymmetry in the weighted rates is roughly given by

$$\mathcal{A}_{\rm CP}^{\rm wgt} \sim \frac{\Gamma_{H^\pm} |\mu M_2|}{m_{H^\pm} M_1^2}. \tag{5.25}$$

From these results we conclude that, in order to enhance the asymmetry as much as possible, we would like to have the smaller parameters μ and M_2 as close as possible to the larger parameter M_1 without cutting into phase space.

We now present some more specific results. The tree-level differential decay rate induced by the diagrams Fig. 5.6 is given in Appendix C.2. In order to study this decay rate, we choose a specific point in MSSM parameter space. We arbitrarily parametrize the model such that the CP-violating phase is contained entirely in μ and the other parameters are real. The Bino mass M_1 is chosen to be much larger than the other weak-scale masses so that there is sufficient phase space to allow the relevant decay. The other new dimensionful parameters are chosen to be of order 100 GeV, but can be varied in absolute scale without changing the results significantly.

Parameter	Value
M_1	500 GeV
M_2	80 GeV
$\tan\beta$	5
$M^2_{H_u}$	$-(120\text{ GeV})^2$
$M^2_{H_d}$	$(250\text{ GeV})^2$
$\arg(\mu)$	$\pi/2$

Table 5.1: The choice of MSSM and soft SUSY-breaking parameters used to study CP-violation in the decays $\chi_4^0 \to \chi_1^\pm \chi_2^\mp \chi_1^0$. All other relevant parameters have been measured and are set to their values according to Ref. [7].

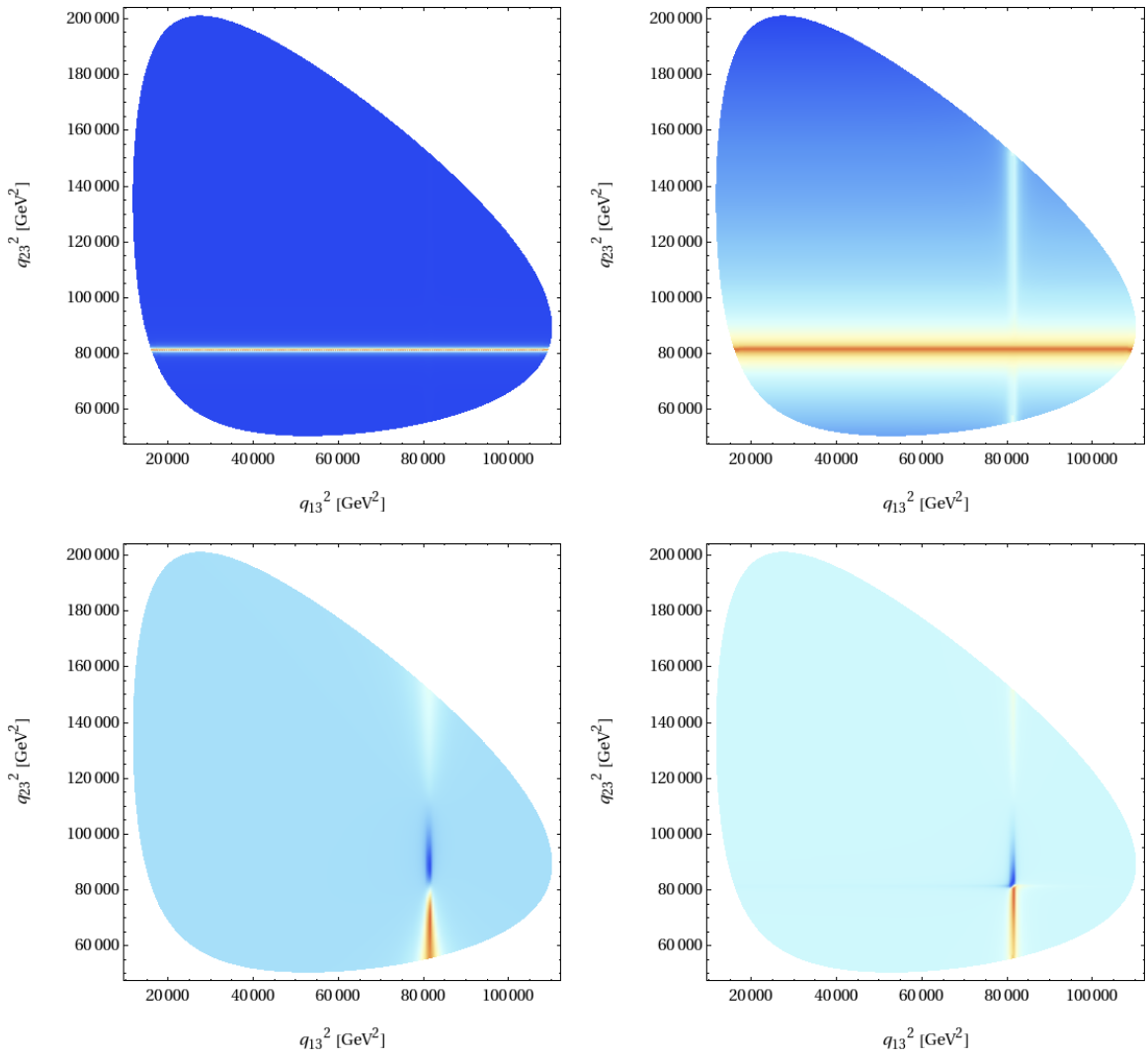

Figure 5.7: Dalitz plots for (a) the differential rate of $\chi_1^+\chi_2^-\chi_1^0$ decay, (b) the log of the differential rate, (c) the asymmetry $\mathcal{A}_{\rm CP}$, and (d) the significance $\frac{d\sigma_{\rm CP}}{\sqrt{dq_{13}^2 dq_{23}^2}}\sqrt{\frac{\Gamma_{\chi_4^0}}{N}}$. The indices $1, 2, 3$ refer to χ_1^+, χ_2^- and χ_1^0 respectively.

The particular choice of parameters used for this study is given in Table 5.1. All other superpartners are assumed to be heavy or otherwise negligible. Dalitz plots of the differential decay rate, relative asymmetry, and significance as defined in Sec. 5.2 of the asymmetry for the processes $\chi_4^0 \to \chi_1^\pm \chi_2^\mp \chi_1^0$, including only the amplitudes involving a virtual charged Higgs, are shown in Fig. 5.7. Many of the features that were obvious in the toy example are obscured here due to the fact that the resonance in the q_{13}^2 direction corresponding to the left diagram in Fig. 5.6 is

suppressed. In fact using a linear color function for the Dalitz plot (Fig. 5.7 (a)) this resonance is not even visible and only the dominant one in the q_{23}^2 direction shows up. In Fig. 5.7 (b) showing the log of the differential decay rate also the q_{13}^2 resonance shows up, but is suppressed by more than two orders of magnitude with respect to the dominant one. The pattern of constructive and destructive interference between the two resonances, which was clearly visible in the toy model decay, is not visible from these figures, suggesting that the relevant CP asymmetry is small. In Fig. 5.7 (c) we see the resulting differential CP asymmetry which appears "tilted" towards the weak q_{13}^2 resonance with respect to the toy model case. On top of this there is now a phase space dependence in the numerator of the amplitude due to the fact that the external states are not scalars. We also observe the suppression due to the narrowness of the $H^\pm$ resonance, $\Gamma_{H^\pm}/m_{H^\pm} \simeq 0.5\%$.

Next, we calculate CP-violating integrated asymmetries. As discussed in Section 5.2, an unweighted phase space integration can be improved upon by introducing a relative sign between the rates above and below the line $q_{13}^2 = q_{23}^2$ in phase space. In particular, for the scenario described in Table 5.1, the total rate asymmetry is calculated to be -3.5×10^{-5}, while introducing a relative sign improves the asymmetry to -6.5×10^{-4}. The improvement is a factor of almost 20, roughly obtained by eliminating the suppression $\Delta m_{\chi^\pm}^2/m_{\chi_4^0}^2 \sim 1/20$.

We have performed this study with the goal of demonstrating the potential relevance of such CP violation to models of physics beyond the Standard Model in general. As such, we have worked from a bottom up approach. In particular, we have worked with a tree-level SUSY Lagrangian with added soft SUSY breaking terms. Renormalization of the parameters from a UV SUSY breaking scheme can significantly alter the spectrum and couplings. Furthermore, a full study of this scenario should include a UV theory of SUSY breaking that gives a heavy, Bino-like neutralino at the weak scale. On the other hand, so long as the phase (C.8) is non-zero and the decay studied is allowed to proceed on-shell, the strong phase due to the virtuality of the intermediate charged Higgs will lead to a new source of CP violation independent of the model's details.

A detailed study of collider prospects of this model is beyond the scope of this work. We would, however, like to make a few remarks on what would be necessary to observe the asymmetry in question. At the level of theory, a more detailed study should also include the important heavy

Higgs contribution. Experimentally, there are several challenges that need to be overcome. Quite generally, the significance of signal depends on the following factors: the integrated luminosity, the production cross section for χ_4^0 and the branching ratio for $\chi_4^0 \to \chi_1^\pm \chi_2^\mp \chi_1^0$, all affecting the number of events. Due to the smallness of the asymmetry in question clearly a very large number of events is needed. Given a large production of these decays, it is then necessary to identify the events as having the correct structure. In the case where R-parity is conserved, this issue is exacerbated by issues of combinatorics as the heavy neutralino must be produced in conjunction with another superpartner that could have similar decay modes. Our inability to determine final state MSSM particle momenta ensures that we can only determine the integrated asymmetry, which suffers from the additional $\Delta m^2_{\chi^\pm}/m^2_{\chi_4^0}$ suppression. It might be possible to circumvent this suppression by studying asymmetries in kinematic observables, such as invariant masses of the SM decay products of the decaying charginos. We leave such investigations for future work.

5.4 CONCLUSIONS

The hope is that new physics will be soon discovered at the LHC. Once it is discovered, we can turn to study all the parameters describing it. In particular, we will study the masses, spins and couplings of the new particles. In doing so, we would like to look for signals of CP violation. In this chapter, we pointed out a new way to look for such signals: looking for asymmetries in the Dalitz plots of cascade decays with unstable intermediate particles. The new observation is the fact that a strong phases can arise even when there is only one intermediate particle. This phase is present when there are two amplitudes in which the intermediate particle has different virtuality.

This situation arises generally in cases where two interfering diagrams exist with different orderings of the final state particles. This effect can be present in both neutral and charged particle decays. The new observable we discuss is complementary to other observables that have been discussed before, such as triple product observables and CP violation associated with oscillations.

It is particularly important to account for the kind of strong phase described here in new physics models. Most of these models, and certainly ones in which we can hope to calculate any observables reliably, are weakly coupled at sufficiently low energies. In such cases, a sizable strong phase can

only come in processes involving unstable particles. This could be important in essentially any beyond the SM scenario, such as heavy neutrino decays, Kaluza-Klein state decays, and W' or Z' decays, to name just a few examples. Even within the weak sector of the MSSM, interference terms of the kind studied here are relevant to the asymmetry in $\chi_i^0 \to W^{\pm} H^{\mp} \chi_j^0$, where it is a subdominant contribution compared to chargino mixing. In many of these new physics scenarios, observables could be complicated, as in the MSSM weak sector, by the existence of several amplitudes for the decay, all with different strong phases.

The CP violating observable we have introduced could, in principle, be relevant for SM physics as well, but it is not easy to come up with a practical observable. In terms of fundamental particle decays, a possible channel would in principle be $t \to q_i q_j \bar{q}_k$ with an intermediate W exchange. However, the region where the W is approximately on shell in both diagrams lies outside the physical region of phase space. In addition, the weak phase is highly suppressed due to the hierarchical structure of the CKM matrix strongly favoring one decay channel over the other. We thus have to rely on decays of composite particles, namely hadrons. Indeed, there is a plethora of three body decays of K, D and B mesons at our disposal. Kaon decays, however, do not occur via a resonance. Neutral D and $B_{d,s}$ meson decays are not good examples either, since the same physics can be probed via oscillations in a more effective way. We are thus left with charged B and D meson decays. While it should be possible to find a decay channel for which the intermediate particle can go on shell in both diagrams, we are again confronted with the CKM hierarchy, leading to a strong suppression of one channel with respect to the other in many cases.

To conclude, most extensions of the SM include new particles whose decays can lead to the type of CP violation that we discuss here. Thus, we expect this type of CP violation to be relevant in finding CP violating signals at the LHC and future colliders in many of the possible scenarios for physics beyond the SM.

CHAPTER 6

Model of leptons from $SO(3) \to A_4$

6.1 INTRODUCTION

Recent experiments [152, 153, 154, 155, 156] have given an increasingly accurate picture of the neutrino sector of the new Standard Model (νSM). Current best measurements are summarized in Table 6.1. These pieces of evidence paint a picture radically different from that of the quark sector [10, 157, 158] that exhibits extremely small masses, small mass splittings and non-hierarchical mixing angles.

Many attempts were made to obtain the masses and mixing angles from a more fundamental theory. In this chapter, we concentrate on the lepton sector and consider the Pontecorvo-Maki-Nakagawa-Sakata (PMNS) mixing matrix, U [159, 160]. Using the data presented in Table 6.1, the current best fit for this matrix is

$$|U| = \begin{pmatrix} 0.823 & 0.554 & 0.126 \\ 0.480 & 0.558 & 0.677 \\ 0.305 & 0.618 & 0.725 \end{pmatrix}. \tag{6.1}$$

It has been pointed out that within 2σ this matrix is consistent with the Harrison-Perkins-Scott

Observable	Value	Main Source
$\sin^2\theta_{12}$	$0.312^{+0.019}_{0.018}$	Solar neutrino experiments
Δm^2_{21}	$7.67^{+0.16}_{-0.19}\times 10^{-5}$ eV^2	
$\sin^2\theta_{23}$	$0.466^{+0073}_{-0.058}$	Atmospheric neutrino experiments
$\lvert\Delta m^2_{32}\rvert$	$2.39^{+0.11}_{-0.08}\times 10^{-3}$ eV^2	
$\sin^2\theta_{13}$	$0.016^{+0.010}_{-0.006}$	Global fit with all current data
Δm^2_{31}	$2.39^{+0.11}_{-0.08}\times 10^{-3}$ eV^2	

Table 6.1: The current best fit values for neutrino mass splittings and mixing angles [165, 166]. All ranges are quoted at 1σ.

(HPS) mixing matrix [161]

$$U_{\rm HPS} = \begin{pmatrix} \sqrt{\frac{2}{3}} & \frac{1}{\sqrt{3}} & 0 \\ -\frac{1}{\sqrt{6}} & \frac{1}{\sqrt{3}} & \frac{1}{\sqrt{2}} \\ \frac{1}{\sqrt{6}} & -\frac{1}{\sqrt{3}} & \frac{1}{\sqrt{2}} \end{pmatrix}. \tag{6.2}$$

The HPS matrix has a definite pattern. This pattern has motivated explanations of the structure of U using non-Abelian discrete flavor symmetries. Of particular interest is a class of models postulating an A_4 family symmetry [162, 163]. In these models, the left-handed lepton doublet and the right-handed neutrino singlet transform in three dimensional irreducible representations, while the right handed charged leptons transform under distinct one dimensional representations. For a review of such models, see Ref. [164]. Such models, however, are typically plagued by two issues.

The first is that of vacuum alignment. The A_4 symmetry is broken to Z_3 by a scalar ϕ that couples to the charged leptons and to Z_2 by a scalar ϕ' that couples to the neutrinos. There is no reason, *a priori*, for this particular vacuum structure. One approach to resolving this problem is to add scalars and symmetries, possibly with supersymmetry, to enforce that vacuum alignment [167, 168]. Placing the scalars ϕ and ϕ' on separate branes of an extra-dimensional model [163, 169] is another possibility.

The second problem of A_4 based models, which is the problem that we attempt to solve in this chapter, is that of the origin of A_4. The symmetry group A_4 is chosen simply because it works, with no motivation from UV physics. This lack of motivation is exacerbated by the fact that gravity is believed to break global symmetries. Therefore, we look for possible motivations of the A_4 symmetry group. One possibility is that A_4 comes out as a subgroup of the modular group [170],

which often arises in string theory. Another possibility is that A_4 arises in the low-energy effective theory obtained by orbifolds of a six dimensional theory [171]. In this chapter we present a model where A_4 is obtained by spontaneously breaking a continuous symmetry which we take to be the minimal choice, $SO(3)$. The idea of embedding A_4 in $SO(3)$ has been discussed in [172]. Unlike in our case, where the $SO(3)$ is spontaneously broken, in [172] an explicit breaking of a global $SO(3)$ symmetry was introduced. The idea of spontaneously breaking a continuous symmetry to a discrete subgroup has been discussed in [173]. However, their procedure is different then ours.

The work presented is this chapter is based on Ref. [51]. In section 2, we briefly review the general structure of models of neutrino mixing using A_4 symmetry. In section 3, we review the vacuum structure of models with $SO(3)$ symmetry and how it can be broken to A_4. In section 4 we construct a model for the lepton sector based on spontaneously broken $SO(3) \to A_4$ symmetry. We conclude in section 5. Technical details are collected in the appendices. In appendix A, we summarize important properties of the group A_4 and introduce relevant group theory concepts. In appendix B, we describe one method for determining the vacua of a theory with $SO(3)$ symmetry and a scalar transforming in the **7** of the group.

6.2 MODELS WITH A_4 SYMMETRY

Implementing non-Abelian discrete flavor symmetries in a model generically leads to patterns in the mass matrices. These patterns yield patterns in the mixing matrices after changing to the mass basis. It is natural to try to obtain $U_{\rm HPS}$ using such symmetries. In fact, several models [174, 168] did it using A_4 symmetry. These models have several common features which we describe in this section.

We consider only the lepton sector. The basic required matter content are the νSM fermions (including the RH singlet neutrinos), the SM Higgs and two more scalars that are denoted by ϕ and ϕ'. The fermion field content is

$$\psi_\ell(2,3)_{1/2}, \qquad \psi_e(1,1)_{-1}, \qquad \psi_\mu(1,1')_{-1}, \qquad \psi_\tau(1,1'')_{-1}, \qquad \psi_n(1,3)_0, \tag{6.3}$$

nd the scalars are

$$H(2,1)_{1/2}, \qquad \phi(1,3)_0, \qquad \phi'(1,3)_0. \tag{6.4}$$

e use standard notation, $(S,A)_Y$, where S $[A]$ is the representation under $SU(2)_L$ $[A_4]$ and Y is the hypercharge. In specific models more fields are added in order to satisfy vacuum alignment conditions. In addition, further symmetries are usually required to forbid unwanted terms in the Lagrangian, as well as to obtain the correct vacuum alignment. The purpose of the two scalars ϕ and ϕ' is to break the A_4 symmetry down to its Z_3 and Z_2 subgroups respectively. For the standard basis described in Appendix D.1, this breaking is achieved by the VEVs:

$$\langle\phi\rangle = (v,v,v), \qquad \langle\phi'\rangle = (v',0,0). \tag{6.5}$$

The two scalars are then made (by symmetries, for example) to couple to different sectors of the model. The ϕ couples to the charged leptons, giving a Z_3 symmetric mass matrix, while the ϕ' couples to the neutrinos, giving a Z_2 symmetric mass matrix.

The Lagrangian for the fermions with the properties and fields described above is:

$$\mathcal{L} = -\frac{y_e}{\Lambda}\overline{\psi}_\ell\phi H\psi_E - \frac{y_\mu}{\Lambda}(\overline{\psi}_\ell\phi)' H\psi_\mu - \frac{y_\tau}{\Lambda}(\overline{\psi}_\ell\phi)'' H\psi_\tau - M\overline{\psi^c}_n\psi_n - x_\nu\overline{\psi^c}_n\psi_n\phi' - y_\nu\overline{\psi}_\ell H\psi_n, \tag{6.6}$$

where $(\overline{\psi}_\ell\phi)'$ $[(\overline{\psi}_\ell\phi)'']$ denotes that the product is taken such that the result transforms in the $1'$ $[1'']$. This Lagrangian provides an effective description up until a cutoff Λ. We assume that M is much larger than the weak scale. Notice that charged lepton masses would not be allowed without including non-renormalizable operators. We did not include terms that are suppressed by $1/\Lambda^2$.

We emphasize that the Lagrangian (6.6) is not the most general one. It is missing several terms allowed by the symmetries listed so far. Any of the terms coupling to ϕ is allowed with $\phi \to \phi'$ and vice-versa. For example, $\overline{\psi^c}_n\psi_n\phi$ is allowed. This issue is generally solved by including additional discrete or continuous Abelian symmetries. For example, ref. [168] describes a supersymmetric model with an additional Z_4 and $U(1)_R$ symmetry under which ϕ and ϕ' transform differently.

The heavy neutrino states present due to the see-saw mechanism can be integrated out. The

resulting low-energy Majorana mass matrix for the neutrinos has the form

$$m_\nu = \begin{pmatrix} a & 0 & 0 \\ 0 & b & d \\ 0 & d & b \end{pmatrix}, \tag{6.7}$$

where a, b, and d depend on the specifics of the model. The off-diagonal d entries are a reflection of the $A_4 \to Z_2$ breaking. It is made possible by the fact that a singlet can be formed out of the product of three triplets. The mass matrix for the charged leptons has the form

$$m_\ell = \begin{pmatrix} y_e & y_\mu & y_\tau \\ y_e & y_\mu\omega & y_\tau\omega^2 \\ y_e & y_\mu\omega^2 & y_\tau\omega \end{pmatrix}, \tag{6.8}$$

where $\omega \equiv e^{2\pi i/3}$ (see Appendix D.1 for more details). This mass matrix is diagonalized by multiplying on the left by

$$V = \frac{1}{\sqrt{3}} \begin{pmatrix} 1 & 1 & 1 \\ 1 & \omega & \omega^2 \\ 1 & \omega^2 & \omega \end{pmatrix}. \tag{6.9}$$

The rotation matrix V in (6.9) does not depend on any of the parameters of the theory. This fact helps ensure that no hierarchy will appear in the neutrino mixing matrix. No change of basis is required for the right-handed leptons. Performing the full diagonalization procedure, the physical PMNS matrix, U, is then given by U_{HPS}.

Specific implementations of the ideas described above have several obstacles to overcome. First, in general, A_4 based models only explain the mixing parameters and not the mass hierarchies. (Both mixing and masses can be obtained in an RS-type model [169].) Another issue, as we already discussed, is the fact that extra symmetries are needed in order to forbid problematic terms. There is also an issue of vacuum alignment, which has been discussed in the introduction. Finally, there is the issue of the origin for the A_4 symmetry group, which is the issue we discuss in this chapter.

Representation	Decomposition
1	**1**
3	**3**
5	$\mathbf{3}+\mathbf{1}'+\mathbf{1}''$
7	$\mathbf{3}+\mathbf{3}+\mathbf{1}$

Table 6.2: Decomposition of the four smallest representations of $SO(3)$ into irreducible representations of A_4.

6.3 SPONTANEOUS BREAKING OF $SO(3) \to A_4$

In order to motivate the use of A_4, we use a model where the group A_4 arises from spontaneous breaking of a continuous symmetry. The simplest choice of gauge group is $SO(3)$ [175, 176]. We discuss the representation necessary for a scalar to break $SO(3)$ to A_4 and write down a potential for this scalar to demonstrate how spontaneous symmetry breaking (SSB) is achieved.

Let T be a scalar that transforms under an irreducible representation of $SO(3)$. This irreducible representation of $SO(3)$ induces a representation of A_4 since A_4 is a subgroup of $SO(3)$. In Appendix D.1, we write down a general method for decomposing an irreducible representation of $SO(3)$ into irreducible representations of A_4. The decomposition of the four smallest representations is given in Table 6.2. For now, it is important to note that the smallest non-trivial representation of $SO(3)$ that contains a singlet of A_4 is the **7**. This is the smallest representation that could in principle result in an A_4 invariant vacuum. Thus, it is natural to start our attempt to construct a model using a scalar in the **7**.

A model with a scalar transforming in the **7** of $SO(3)$ has been described in [175, 176]. We summarize the results of [175]. The **7** of $SO(3)$ can be described by symmetric, traceless rank 3 tensors in 3D, denoted as T^{abc}. The most general renormalizable potential that can be written is

$$V = -\frac{\mu^2}{2} T^{abc} T^{abc} + \frac{\lambda}{4} (T^{abc} T^{abc})^2 + c\, T^{abc} T^{bcd} T^{def} T^{efa}. \tag{6.10}$$

Naively, there are other quartic terms that can be written down, but they are linear combinations of the two quartic terms in (6.10). Also note that cubic terms vanish since the cubic singlet is

Field	$SU(2)_L$	$U(1)_Y$	$SO(3)_F$	Z_2
ψ_ℓ	**2**	$-1/2$	**3**	$-$
ψ_f	**1**	-1	**3**	$-$
ψ_e	**1**	-1	**1**	$+$
ψ_m	**1**	-1	**5**	$+$
ψ_n	1	0	**3**	$-$
H	**2**	$1/2$	**1**	$+$
ϕ	**1**	0	**3**	$-$
ϕ'	**1**	0	**3**	$+$
ϕ_5	**1**	0	**5**	$-$
T	**1**	0	**7**	$-$

Field	VEV	Invariant Subgroup
H	v_H	none
ϕ	(v, v, v)	Z_3
ϕ'	$(0, 0, v')$	Z_2
ϕ_5	$\begin{pmatrix} 0 & v_5 & v_5 \\ v_5 & 0 & v_5 \\ v_5 & v_5 & 0 \end{pmatrix}$	Z_3
T	$\sim v_T$ (see text)	A_4

Table 6.3: Left: Matter content for the lepton and scalar sectors of the model. The blocks contain the left-handed fermions, right-handed fermions, and scalars respectively. Right: Vacuum expectation values for the scalars and the subgroup of $SO(3)_F$ under which they are invariant. The H gets the usual SM-like VEV and the T gets a VEV as described in Section 6.3

formed by an antisymmetric product of identical fields. A technique for minimizing the potential is presented in Appendix D.2. The results of the minimization are as follows. In order to have a stable potential we need $\lambda > 0$. In order to have a VEV at all we require $\mu^2 > 0$. Then, the residual symmetry depends on the relation between c and λ. For $c < -\lambda/2$, the potential becomes unstable. For $c > 0$, the residual symmetry is D_3. For $-\lambda/2 < c < 0$, the residual symmetry is A_4. We learn that there is a large area in parameter space where $SO(3)$ is broken to A_4. In our model we choose the parameters such that this is the case.

6.4 MODEL OF LEPTONS BASED ON $SO(3) \to A_4$

We move to describe the model. The symmetry of the model is

$$SU(2)_L \times U(1)_Y \times SO(3)_F \times Z_2. \tag{6.11}$$

t this stage we do not care if the $SO(3)_F$ is gauged or not. For the fermions, we consider only the leptons. The full matter content of the scalar and lepton sectors of the model are summarized in Table 6.3. We also describe the symmetry breaking induced by each of the scalars.

We start with the scalar sector of the model. There are five scalar fields in the model. Three of

them, H, ϕ and ϕ' are needed in the A_4 model. When extending the model to an $SO(3)_F$ symmetry, we add two scalars, T and ϕ_5. We need T as it is responsible for the $SO(3)_F \to A_4$ breaking. As we discuss later, ϕ_5 is needed because without it the tau and the muon would be degenerate. In term of scales, things are simpler if we decouple the $SO(3)_F \to A_4$ breaking (triggered by v_T) and the A_4 breaking (which is done by v, v' and v_5). That is, we assume the following hierarchies of scales

$$\Lambda \gg v_T \gg v \sim v' \sim v_5 \gg v_H. \tag{6.12}$$

We do not try to explain these hierarchies.

Next, we discuss the fermions. The fields ψ_ℓ, ψ_e, and ψ_n have the same representations under $SO(3)_F$ as under A_4. They correspond directly to fields in the A_4 model. Complications arise when considering the right handed muon and tau fields that transform as $\mathbf{1'}$ and $\mathbf{1''}$ respectively. The issue is that the $\mathbf{1'}$ and $\mathbf{1''}$ do not correspond to irreducible representations of $SO(3)_F$. Thus, they must be obtained as parts of $SO(3)_F$ representations that include extra singlets or triplets of A_4. Further complications arise from the fact that irreducible representations of $SO(3)$ are real and, therefore, $\mathbf{1'}$ and $\mathbf{1''}$ must be part of the same $SO(3)$ representation in the scenario with minimal matter content. The simplest choice of representation that contains both $\mathbf{1'}$ and $\mathbf{1''}$ is the $\mathbf{5}$. This explains why we introduce ψ_m, which is the field that after $SO(3)_F$ breaking gives us the right handed muon and tau fields.

A fermion that transforms in the $\mathbf{5}$ of $SO(3)_F$ decomposes into pieces that transform under the $\mathbf{1'}$, $\mathbf{1''}$, and $\mathbf{3}$ representations of A_4. A field transforming in the $\mathbf{5}$ can be written as a traceless, symmetric matrix. In this form, the decomposition is

$$\psi_m = \begin{pmatrix} \psi_\mu + \psi_\tau & \psi_h^3 & \psi_h^2 \\ \psi_h^3 & \omega\psi_\mu + \omega^2\psi_\tau & \psi_h^1 \\ \psi_h^2 & \psi_h^1 & \omega^2\psi_\mu + \omega\psi_\tau \end{pmatrix}, \tag{6.13}$$

where ψ_μ transforms as a $\mathbf{1'}$, ψ_τ transforms as a $\mathbf{1''}$, and ψ_h transforms as a $\mathbf{3}$. The use of a fermion in the $\mathbf{5}$ implies that further matter content is required. Without it, we end up with extra right-handed fields. These extra field can be "removed" by adding a triplet left-handed fermion

giving them a large Dirac mass. This is the reason we add the left-handed triplet, ψ_f.

The most general Lagrangian, including $1/\Lambda$ terms, that is responsible for charged lepton masses is given by

$$\begin{aligned}\mathcal{L} &= -y_e\overline{\psi_\ell^a}\frac{H}{\Lambda}\phi^a\psi_e - y_m\overline{\psi_\ell^a}\frac{H}{\Lambda}\phi^b\psi_m^{ab} - y_m^T\overline{\psi_\ell^a}\frac{H}{\Lambda}T^{abc}\psi_m^{bc} - y_e'\overline{\psi_f^a}\phi^a\psi_e \\ &\quad -y_m'\overline{\psi_f^a}\phi^b\psi_m^{ab} - y_m^{T\prime}\overline{\psi_f^a}T^{abc}\psi_m^{bc} - y_m^5\epsilon^{abc}\overline{\psi_\ell^a}\frac{H}{\Lambda}\phi_5^{bd}\psi_m^{cd} - y_m^{5\prime}\epsilon^{abc}\overline{\psi_f^a}\phi_5^{bd}\psi_m^{cd}. \qquad (6.14)\end{aligned}$$

he scalars get VEVs as indicated in Table 6.3. Consider the masses of the charged fermions. There are six left-handed and six right-handed fields that can mix. Working in the basis where the right handed fields are $(\psi_e, \psi_\mu, \psi_\tau, \psi_h^1, \psi_h^2, \psi_h^3)$ and the left-handed ones are (ψ_ℓ, ψ_f) the mass matrix is roughly

$$m_\ell \sim \begin{pmatrix} v_H v/\Lambda & v_H v_T/\Lambda \\ v & v_T \end{pmatrix}, \qquad (6.15)$$

where each block describes a 3×3 matrix. We see that there are three heavy states (of order v_T), three light states (of order $v_H v/\Lambda$), and that there is very small mixing between these two sets of states. We identify the light states as the three charged leptons, and we neglect the mixing between them and the heavy states. This procedure leaves a charged lepton Dirac mass matrix of the form (6.8), which is given by

$$m_\ell = \begin{pmatrix} y_e\frac{v_H v}{\Lambda} & y_m\frac{v_H v}{\Lambda} + y_m^5(\omega^2-\omega)\frac{v_H v_5}{\Lambda} & y_m\frac{v_H v}{\Lambda} + y_m^5(\omega-\omega^2)\frac{v_H v_5}{\Lambda} \\ y_e\frac{v_H v}{\Lambda} & \omega[y_m\frac{v_H v}{\Lambda} + y_m^5(\omega^2-\omega)\frac{v_H v_5}{\Lambda}] & \omega^2[y_m\frac{v_H v}{\Lambda} + y_m^5(\omega-\omega^2)\frac{v_H v_5}{\Lambda}] \\ y_e\frac{v_H v}{\Lambda} & \omega^2[y_m\frac{v_H v}{\Lambda} + y_m^5(\omega^2-\omega)\frac{v_H v_5}{\Lambda}] & \omega[y_m\frac{v_H v}{\Lambda} + y_m^5(\omega-\omega^2)\frac{v_H v_5}{\Lambda}] \end{pmatrix}, \qquad (6.16)$$

In order to diagonalize this matrix, we multiply on the left by V introduced in (6.9). The resulting diagonal mass matrix for the charged leptons is

$$m_\ell^{\rm diag} = \begin{pmatrix} \left|y_e\frac{v_H v}{\Lambda}\right| & 0 & 0 \\ 0 & \left|y_m\frac{v_H v}{\Lambda} - y_m^5 i\sqrt{3}\frac{v_H v_5}{\Lambda}\right| & 0 \\ 0 & 0 & \left|y_m\frac{v_H v}{\Lambda} + y_m^5 i\sqrt{3}\frac{v_H v_5}{\Lambda}\right| \end{pmatrix}. \qquad (6.17)$$

Two remarks are in order regarding the mass matrix for the charged leptons. First, note that the charged lepton scale is smaller then the electroweak scale by a factor of v/Λ. This implies that v and Λ are at most a factor of 10^2 apart. Recalling that we assume that $\Lambda \gg v_T \gg v$, we conclude that the different scales cannot be widely separated. That is, the ratio of scales is of order ten. Since this ratio is not very large, the fact that we neglected $1/\Lambda^2$ terms may not be justified.

The second remark is about the muon and tau masses. The matrix (6.17) leads degenerate muon and tau if the parameters of the theory are real or if $v_5 = 0$. Moreover, in order to reproduce the observed ratio of masses, $m_\mu/m_\tau \sim 1/16$, some amount of fine tuning is needed. Defining

$$a \equiv y_m v, \qquad b \equiv i\sqrt{3} y_m^5 v_5, \qquad \alpha \equiv \arg(ab^*), \tag{6.18}$$

e require

$$\frac{|a|^2 + |b|^2 - 2|a||b|\cos\alpha}{|a|^2 + |b|^2 + 2|a||b|\cos\alpha} \sim \frac{1}{16^2}. \tag{6.19}$$

hat is, the phase between y_m and y_m^5 must be very close to $\pi/2$ and the values of a and b must be very close to each other. Given this fine-tuning, it is clear that this model does not try to explain the fermion mass hierarchy: the tuning of the scales of the charged lepton sector is exchanged for a tuning of the scales a and b to be very close to each other.

The neutrino sector works just as in the low-energy A_4 model described in section 6.2. Since the neutrinos are in triplet representation, the Lagrangian is almost the same as in Eq. (6.6). One issue is that the off-diagonal terms in the Majorana mass matrix require a coupling to T. Coupling to ϕ and ϕ_5 are forbidden by the Z_2 symmetry used to forbid terms involving ϕ' in (6.14). Then the terms relevant for neutrino masses are

$$\mathcal{L} = -M\overline{\psi^c}^a_n \psi^a_n - \frac{x_\nu}{\Lambda}\overline{\psi^c}^a_n \psi^b_n \phi'^c T^{abc} - y_\nu \overline{\psi}^a_\ell H \psi^a_n. \tag{6.20}$$

Recalling that ϕ' gets a VEV $(v', 0, 0)^T$ and T^{abc} gets a VEV $v_T x^{(a} y^b z^{c)}$, the neutrino Majorana

mass matrix is given by

$$m_\nu^M = \begin{pmatrix} M & 0 & 0 \\ 0 & M & x_\nu v' \frac{v_T}{\Lambda} \\ 0 & x_\nu v' \frac{v_T}{\Lambda} & M \end{pmatrix}, \tag{6.21}$$

while the Dirac mass matrix is given by

$$m_\nu^D = y_\nu v_H \begin{pmatrix} 1 & 0 & 0 \\ 0 & 1 & 0 \\ 0 & 0 & 1 \end{pmatrix}. \tag{6.22}$$

The low-energy effective Majorana matrix is then

$$\tilde{m}_\nu^M = -m_\nu^D (m_\nu^M)^{-1} (m_\nu^D)^{-1} = \begin{pmatrix} -y_\nu^2 \frac{v^2}{M} & 0 & 0 \\ 0 & y_\nu^2 \frac{M v_H^2}{x_\nu v'^2 v_T^2 - M^2 \Lambda^2} & y_\nu^2 x_\nu \frac{v_H^2 v' v_T}{M^2 \Lambda^2 - x_\nu^2 v'^2 v_T^2} \\ 0 & y_\nu^2 x_\nu \frac{v_H^2 v' v_T}{M^2 \Lambda^2 - x_\nu^2 v'^2 v_T^2} & y_\nu^2 \frac{M v_H^2}{x_\nu v'^2 v_T^2 - M^2 \Lambda^2} \end{pmatrix}. \tag{6.23}$$

The matrix (6.23) has precisely the form (6.7). Taking into account the action of V on the left-handed handed fields, it can then be diagonalized by rotating the left-handed neutrinos by $U_{\rm HPS}$. The resulting diagonal mass matrix is

$$\tilde{m}_\nu^{\rm diag} = y_\nu^2 v_H^2 \begin{pmatrix} \frac{\Lambda}{M\Lambda + x_\nu v' v_T} & 0 & 0 \\ 0 & \frac{1}{M} & 0 \\ 0 & 0 & \frac{\Lambda}{M\Lambda - x_\nu v' v_T} \end{pmatrix}. \tag{6.24}$$

Two remarks are in order. First, we emphasis that the the result of the diagonalization is that the physical PMNS matrix is given by the HPS matrix, that is, $U = U_{\rm HPS}$. The second remark is about the mass splittings in the neutrino sector. The form of the neutrino masses in (6.24) constraints the scales in the theory. If $x_\nu v' v_T \ll M\Lambda$, then the splittings become very small, in contradiction to the $\mathcal{O}(100)$ factor difference in the measured values of Δm_{12}^2 and Δm_{23}^2. We then conclude that $x_\nu v' v_T \sim M\Lambda$. Since we require $\Lambda \gg v_T \gg v'$ and perturbative Yukawa couplings, we conclude that $v' \gg M$. This is not a problem, as both v' and M can be much above the weak

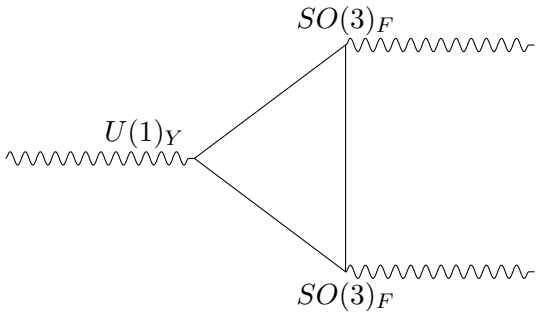

Figure 6.1: Triangle diagram contributing to a $U(1)_Y$ anomaly if the $SO(3)_F$ flavor symmetry is gauged.

scale.

6.5 DISCUSSION AND CONCLUSIONS

We have shown that, in principle, a model of lepton masses and mixings using an A_4 discrete symmetry can be obtained by spontaneously breaking a continuous symmetry. The model, however, is not very elegant. We already mentioned the problem of the fine tuning required to get the correct muon and tau masses. We discuss a few other problems below.

The first issue is that of vacuum alignment in the full scalar potential. In previous incarnations of the A_4 model, additional symmetries and, often, scalars are needed in order to ensure the correct vacuum alignment. The question is even trickier in our case. All four scalars in the model need very specific alignments. Without additional symmetries, there are many couplings in the potential between these scalars which affect the vacuum structure. In particular, a possibility is the case where the additional scalars force the scalar T away from the A_4 invariant vacuum. With the many additional degrees of freedom in this model, it is difficult to verify the vacuum alignment or to correct the alignment if it does not follow from the current iteration of the model.

The second is that of anomalies. The most natural way to implement the model would be to gauge the $SO(3)_F$ symmetry. This avoids possible issues with breaking due to gravity, as well as eating any massless Goldstone bosons. If $SO(3)_F$ were a global symmetry, there would be Goldstone bosons that would have to be extremely weakly coupled to the standard model fields in

order to not have been detected. Even though they are not directly coupled in this model, it is unclear that, at loop level, the couplings remain small enough to evade bounds. If the symmetry were gauged, however, it would induce a $U(1)_Y$ anomaly via the triangle diagram in Figure 6.1. Using the Casimir square operator for the 5 dimensional representation, $C(5) = 10$, the anomaly is given by

$$\mathcal{A}^{ab} = \sum_{\ell} Y_\ell \mathrm{Tr}\left(\{t_\ell^a, t_\ell^b\}\right) - \sum_{r} Y_r \mathrm{Tr}\left(\{t_r^a, t_r^b\}\right) = 12\delta^{ab}, \tag{6.25}$$

where ℓ are left-handed fermions and r are right-handed fermions. Such anomalies can be eliminated by introducing new fermions. Note the need to introduce new fermions in the full model once the quarks are included. The additional fermions may lead to new light states. It is beyond the scope of this work to resolve this issue and to present an anomaly-free model for an $SO(3)$ flavor gauge theory.

Our last remark is about possible variation of our model. Our model is minimal in many ways, like the choice of the gauge group, the scalars that breaks $SO(3)_F$, and the fields we choose. It is likely that in order to achieve the desired vacuum alignment further structure would be necessary, including addition symmetries and matter content. Furthermore, in our model, the origin of the Z_2 symmetry is unexplained. However, Abelian discrete symmetries are easier to produce naturally in the context of orbifolds or spontaneous symmetry breaking. Finally, no attempt has been made to incorporate solutions to the hierarchy problem or other extensions of the Standard Model. In particular, the model has not been made supersymmetric and is four dimensional, while many current models using A_4 symmetry work in supersymmetric theories [167, 168] or theories with extra dimensions [163, 169]. It should be possible to extend our model to fit within the structure of these theories.

APPENDIX A

Fermionic Top Partners: Naturalness and the LHC

A.1 MASSES, MIXING ANGLES AND COUPLING OF THE TOP AND ITS PARTNER

Ignoring the Goldstone fields that are eaten by the SM gauge bosons after EWSB, the sigma field V has the form

$$V = \exp(iaI) \begin{pmatrix} 0 \\ f \end{pmatrix} , \tag{A.1}$$

where

$$I = \begin{pmatrix} 0 & 1 \\ 1 & 0 \end{pmatrix} , \tag{A.2}$$

and

$$a = \frac{1}{\sqrt{2}} \frac{v+h}{f} . \tag{A.3}$$

Here v is the Higgs vev, and h is the physical Higgs boson. The exponent can be easily expanded using the fact that $I^2 = 1$:

$$\exp(iaI) = \cos a + i \sin a \, I . \tag{A.4}$$

The kinetic term of the sigma model has the form

$$\mathcal{L}_{\rm kin} = (D_\mu V)^\dagger \, (D_\mu V) \ , \tag{A.5}$$

where D_μ is the covariant derivative. This term contains a canonically normalized kinetic term for the Higgs, as well as masses for the SM gauge bosons; in particular,

$$m_W^2 = \frac{1}{2} g^2 f^2 \sin^2 \bar{a} \, , \tag{A.6}$$

where we defined $\bar{a} = v/(\sqrt{2}f)$. The measured value of m_W can be used to compute v from this formula; in the limit $f \to \infty$, v tends to its SM value, 246 GeV.

Using Eq. (A.4), the top mass terms take the form

$$\mathcal{L}_{\rm mass} = (u_R^\dagger \; U_R^\dagger) \, \mathcal{M} \begin{pmatrix} u_L \\ U_L \end{pmatrix} + \ \text{h.c.} \, , \tag{A.7}$$

where

$$\mathcal{M} \ = \ f \begin{pmatrix} \lambda_1 \sin \bar{a} & \lambda_1 \cos \bar{a} \\ 0 & \lambda_2 \end{pmatrix} . \tag{A.8}$$

Diagonalizing $\mathcal{M}^\dagger \mathcal{M}$, we find the masses of the top quark t and its partner T:

$$m_{t,T}^2 \ = \ \frac{(\lambda_1^2 + \lambda_2^2) f^2}{2} \left(1 \pm \sqrt{1 - \frac{4 \lambda_1^2 \lambda_2^2 \sin^2 \bar{a}}{(\lambda_1^2 + \lambda_2^2)^2}} \right) . \tag{A.9}$$

The rotation between gauge eigenstates (u, U) and mass eigenstates (t, T) is given by

$$\begin{aligned} t_L &= \cos\beta \, u_L - \sin\beta \, U_L, \qquad T_L = \sin\beta \, u_L + \cos\beta \, U_L \, ; \\ t_R &= \cos\alpha \, u_R - \sin\alpha \, U_R, \qquad T_R = \sin\alpha \, u_R + \cos\alpha \, U_R \, , \end{aligned} \tag{A.10}$$

and the mixing angles are

$$\begin{aligned}\alpha &= \frac{1}{2}\tan^{-1}\frac{2\lambda_1\lambda_2\cos\bar{a}}{\lambda_2^2-\lambda_1^2}\,,\\ \beta &= \frac{1}{2}\tan^{-1}\frac{\lambda_1^2\sin 2\bar{a}}{\lambda_2^2+\lambda_1^2\cos 2\bar{a}}.\end{aligned} \tag{A.11}$$

Mass and mixing angle formulas quoted in the main text are obtained by expanding in v/f and keeping the leading order terms only.

It is also useful to invert these formulas and express the Lagrangian parameters $(\lambda_1, \lambda_2, f)$ in terms of physical parameters (m_t, m_T, α):

$$\begin{aligned}f &= \left(\frac{\sqrt{2}m_W}{g}\right)\frac{1}{x_t^{1/2}}\left(\cos^2\alpha + x_t\sin^2\alpha\right)^{1/2}\left(\sin^2\alpha + x_t\cos^2\alpha\right)^{1/2}\,,\\ \lambda_1 &= \left(\frac{gm_t}{m_W}\right)\frac{1}{(1+x_t+(1-x_t)\cos 2\alpha)^{1/2}}\,,\\ \lambda_2 &= \left(\frac{gm_t}{m_W}\right)\frac{1}{(1+x_t-(1-x_t)\cos 2\alpha)^{1/2}}\,,\end{aligned} \tag{A.12}$$

where $x_t = m_t^2/m_T^2$. For example, together with the second line of Eq. (A.11), this expressions give the angle β in terms of the physical parameters, which was used in the calculation of precision electroweak parameters in Sec. 2.4.1:

$$\sin\beta = \frac{\sqrt{2}x_t^{1/2}\sin\alpha}{(1+x_t+(1-x_t)\cos 2\alpha)^{1/2}}\,. \tag{A.13}$$

The couplings of the top and its partner to electroweak gauge bosons are given by

$$\begin{aligned}\mathcal{L}_{\rm g} &= \frac{e}{\sqrt{2}s_w}\,b_L^\dagger\bar{\sigma}^\mu\left(\cos\beta t_L + \sin\beta T_L\right)W_\mu^- + \text{ c.c.}\\ &+ \left(g_{ttL}\,t_L^\dagger\bar{\sigma}^\mu t_L + g_{ttR}\,t_R^\dagger\bar{\sigma}^\mu t_R + g_{TTL}\,T_L^\dagger\sigma^\mu T_L + g_{TTR}\,T_R^\dagger\sigma^\mu T_R\right)Z_\mu\\ &+ g_{tTL}\,t_L^\dagger\bar{\sigma}^\mu T_L Z_\mu + \text{ c.c.}\,,\end{aligned} \tag{A.14}$$

where

$$\begin{aligned} g_{ttL} &= \frac{e}{c_w s_w}\left(\frac{\cos^2\beta}{2} - \frac{2s_w^2}{3}\right); \quad g_{ttR} = -\frac{2es_w}{3c_w}; \\ g_{TTL} &= \frac{e}{c_w s_w}\left(\frac{\sin^2\beta}{2} - \frac{2s_w^2}{3}\right); \quad g_{TTR} = -\frac{2es_w}{3c_w}; \\ g_{tTL} &= -\frac{e\sin 2\beta}{4s_w c_w}. \end{aligned} \tag{A.15}$$

Their couplings to the Higgs boson are

$$\mathcal{L}_{\rm yuk} = -\left(C_{tth} t_L^\dagger t_R - C_{TTh} T_L^\dagger T_R - C_{Tth}^L t_R^\dagger T_L - C_{Tth}^R T_R^\dagger t_L\right)\frac{h}{\sqrt{2}} + \text{ h.c.}, \tag{A.16}$$

where

$$\begin{aligned} C_{tth} &= \lambda_1 \cos\alpha \cos(\bar{a}-\beta); \quad C_{TTh} = -\lambda_1 \sin\alpha \sin(\bar{a}-\beta); \\ C_{Tth}^L &= -\lambda_1 \cos\alpha \sin(\bar{a}-\beta); \quad C_{Tth}^R = \lambda_1 \sin\alpha \cos(\bar{a}-\beta). \end{aligned} \tag{A.17}$$

Finally, the Higgs boson coupling to the electroweak gauge bosons are given by

$$\mathcal{L}_{hVV} = 2\cos\bar{a}\left(m_W^2 W^{+\mu} W_\mu^- + \frac{1}{2} m_Z^2 Z^\mu Z_\mu\right)\frac{gh}{2m_W}. \tag{A.18}$$

These couplings are suppressed compared to the SM values by a common factor,

$$\cos\bar{a} = \sqrt{1 - \frac{2m_W^2}{g^2 f^2}}. \tag{A.19}$$

A.2 LOOP FUNCTIONS APPEARING IN FLAVOR OBSERVABLES

The F functions that arise from calculating the box diagrams for $\Delta F = 2$ processes are given by [177]:

$$F(x_i, x_j, M_W) = \frac{1}{(1-x_i)(1-x_j)}\left(1 - \frac{7}{4}x_i x_j\right) + \frac{x_i^2 \log x_i}{(x_i - x_j)(1-x_i)^2}\left(1 - 2x_j + \frac{x_i x_j}{4}\right) + \frac{x_j^2 \log x_j}{(x_j - x_i)(1-x_j)^2}\left(1 - 2x_i + \frac{x_i x_j}{4}\right) \quad \text{(A.20)}$$

where the corresponding box diagrams have been calculated in Feynman-t'Hooft gauge. Since we computed the mass eigenvalues for the top sector at all orders in the v/f expansion, we also have the precise values for the F functions.

The loop functions appearing in the $b \to s\gamma$ amplitude are (see, for example, Ref. [178]):

$$\begin{aligned} A_0^t(x) &= \frac{-3x^3 + 2x^2}{2(x-1)^4}\log x + \frac{-22x^3 + 153x^2 - 159x + 46}{36(x-1)^3}, \\ F_0^t(x) &= \frac{3x^2}{2(x-1)^4}\log x + \frac{-5x^3 + 9x^2 - 30x + 8}{12(x-1)^3}. \end{aligned} \quad \text{(A.21)}$$

The $B_s \to \mu^+\mu^-$ branching ratio is given by [79]

$$\frac{\mathrm{Br}(B_s \to \mu^+\mu^-)}{\mathrm{Br}(B_s \to \mu^+\mu^-)_{\mathrm{SM}}} = \left|1 + \frac{\bar{Y}}{Y_{\mathrm{SM}}}\right|^2, \quad \text{(A.22)}$$

where

$$\begin{aligned} Y_{\mathrm{SM}} &= \frac{x_t}{8}\left[\frac{x_t - 4}{x_t - 1} + \frac{3x_t}{(x_t-1)^2}\log x_t\right], \\ \bar{Y} &= s_\beta^2\left[\frac{2 + 2x_t - 2x_t^2}{8(-1+x_t)} - \frac{x_t(2 - x_t + 2x_t^2)}{8(-1+x_t)^2}\log x_t + \frac{3 + 2x_t}{8}\log x_T + \frac{x_t}{8}\tan^2\alpha\right]. \end{aligned} \quad \text{(A.23)}$$

Note that these expressions are only valid to order $(v/f)^2$.

APPENDIX B

Parameter counting in models with global symmetries

B.1 CARTAN DECOMPOSITION OF A UNITARY MATRIX

The Cartan decomposition theorem is a theorem about semisimple Lie groups that gives a decomposition for elements of the group. In all the cases that we consider, the matrix we would like to decompose is an element of the semisimple Lie group $U(n)$. It is trivial to factor out the overall phase of such a matrix, and thus we consider below the decomposition of a matrix $U \in SU(n)$ for simplicity.

The mathematical definitions and theorems can be found, for example, in [132]. The specific decomposition process is inspired by the work of [179]. In order to understand the idea of a Cartan decomposition, we need to make some definitions.

Definition 1. Let $\mathfrak{g}$ be a semisimple Lie algebra. An automorphism θ of $\mathfrak{g}$ with square equal to the identity is called an involution. An involution is a Cartan involution if the symmetric bilinear form

$$B_\theta(X, Y) = -B(X, \theta Y) \tag{B.1}$$

is positive definite, where B is the Killing form of $\mathfrak{g}$.

The second definition is slightly technical, but for practical purposes, the involutions we use satisfy this condition. For more details, please see [132]. Since $\theta^2 = 1$, θ has eigenvalues ± 1 on

$\mathfrak{g}$. Thus, we can decompose $\mathfrak{g} = \mathfrak{l} \oplus \mathfrak{p}$, where $\mathfrak{l}$ and $\mathfrak{p}$ are the eigenspaces of θ corresponding to eigenvalues $+1$ and -1 respectively. This is the Cartan decomposition on a Lie algebra level. It is trivial to see by applying the involution that $[\mathfrak{l}, \mathfrak{l}] = \mathfrak{l}$; that is, the commutator of any two Lie algebra elements with eigenvalue 1 under θ has eigenvalue 1. This result means that the eigenspace $\mathfrak{l}$ is actually a Lie subalgebra. Extending this to the Lie group level is non-trivial and the theorem is due to Cartan.

Theorem 1. *Let G be a semisimple Lie group with Lie algebra $\mathfrak{g}$. Let θ be a Cartan involution on $\mathfrak{g}$. Let $\mathfrak{g} = \mathfrak{l} \oplus \mathfrak{p}$ be the eigenspace decomposition for θ. Finally, let K be the subgroup of G with Lie algebra $\mathfrak{l}$. Then*

1. *there exists a Lie group automorphism Θ of G with differential θ and with $\Theta^2 = 1$,*
2. *the subgroup of G that is invariant under Θ is K,*
3. *the mapping $K \times \mathfrak{p} \to G$ given by $(k, \mathbf{p}) \mapsto k \exp(i\mathbf{p})$ is a diffeomorphism.*

The first consequence can be interpreted as saying that for group elements infinitesimally different from the identity, the relation $\Theta(g) = 1 + i\epsilon\theta(\mathbf{g}) + O(\epsilon^2)$ holds. For any group element, this can be extended to $\Theta(g) = \exp(i\theta(g))$. The third consequence is the main result that we need in order to perform the decomposition. Effectively, it allows us to factor an element $g \in G$ into a product of an element $k \in K$ and another element of $SU(n)$ given by $\exp(i\mathbf{p})$ for $\mathbf{p} \in \mathfrak{p}$ by using the fact that the map defined in condition 3 is a diffeomorphism and that $\mathfrak{g} = \mathfrak{k} \oplus \mathfrak{p}$.

Now, consider the group $G = SU(n)$. Suppose we want to factor an element $g \in G$ into a product of an element k which is block diagonal with the first $n_1 \times n_1$ block an element of $SU(n_1)$ for $n_1 < n$ and another element $p \in SU(n)$ whose generators are all different from those of k. Along similar lines to [179], we choose an involution

$$\theta(\mathbf{g}) = \begin{pmatrix} -1_{n_1} & 0 \\ 0 & 1_{n-n_1} \end{pmatrix} \mathbf{g} \begin{pmatrix} -1_{n_1} & 0 \\ 0 & 1_{n-n_1} \end{pmatrix}. \tag{B.2}$$

This involution is in fact a Cartan involution. Furthermore, its eigenspace with eigenvalue $+1$ is all special unitary matrices that are block diagonal with blocks of size $n_1 \times n_1$ and $(n-n_1) \times (n-n_1)$.

This subalgebra is generated by matrices whose upper-left block are generators of $SU(n_1)$ and remaining entries are zero, whose lower-right block are generators of $SU(n-n_1)$ and remaining entries zero, or which are diagonal phase matrices with determinant 1. The orthogonal eigenspace is generated by the generators whose entries are all off the diagonal block. By the Cartan decomposition theorem, we can then write any $SU(n)$ matrix in the form

$$U = \begin{pmatrix} U_{n_1} & 0 \\ 0 & U_{n-n_1} \end{pmatrix} \exp(i\mathbf{p}), \tag{B.3}$$

here U_k is a matrix in $U(n_k)$ with $\det U_{n_1} \det U_{n-n_1} = 1$ and where $\mathbf{p}$ is in the Lie algebra of $SU(n)$ and is generated by matrices whose diagonal blocks are zero.

Note that this process can be iterated: we can then decompose U_{n-n_1} in a similar way. Ultimately, the matrix U can be written in the form

$$U = \begin{pmatrix} U_{n_1} & & & \\ & U_{n_2} & & \\ & & \ddots & \\ & & & U_{n_{k+1}} \end{pmatrix} \exp(i\mathbf{p}), \tag{B.4}$$

where $n_1 + n_2 + \cdots + n_{k+1} = n$, $\det(U(n_1)U(n_2)\ldots U(n_k)) = 1$, and $\mathbf{p}$ is a linear combination of generators whose entries are all off the diagonal block. The condition on the determinants can be removed by allowing $U \in U(n)$ rather than $SU(n)$.

The essential result for this work is that a Hermitian matrix with degenerate eigenvalues can be written in terms of fewer parameters than if no degeneracy were present. Let R be a Hermitian matrix that has k degenerate eigenvalues, with the first one, r_{n_1}, being n_1-fold degenerate, the second one, r_{n_2}, being n_2-fold degenerate, and so on. By spectral decomposition, the matrix can be written as

$$R = U^\dagger D U \tag{B.5}$$

here D is diagonal. The matrices U are unitary since R is Hermitian. Now, decompose U using

(B.4). The decomposition yields

$$R = \exp(-i\mathbf{p})U^\dagger DU \exp(i\mathbf{p}) = \exp(-i\mathbf{p})D \exp(i\mathbf{p}), \tag{B.6}$$

such that

$$D = \begin{pmatrix} r_{n_1}1_{n_1} & & & \\ & \ddots & & \\ & & r_{n_k}1_{n_k} & \\ & & & D_{n_{k+1}} \end{pmatrix}, \qquad U = \begin{pmatrix} U_{n_1} & & & \\ & \ddots & & \\ & & U_{n_k} & \\ & & & P_{n_{k+1}} \end{pmatrix}, \tag{B.7}$$

here $D_{n_{k+1}}$ is diagonal matrix and $P_{n_{k+1}}$ is a diagonal matrix of (different) phases. In order to count the number of parameters necessary to describe this matrix, we can count the number of parameters in U before performing the reduction of (B.6) and subtract off the number of parameters removed by decomposing. U is an $n \times n$ unitary matrix, which naïvely has $n(n-1)/2$ real parameters and $n(n+1)/2$ phases. By decomposition, we removed $\sum_j n_j(n_j-1)/2$ real parameters and $\sum_j n_j(n_j+1)/2 + n - \sum_j n_j$ phases. In the counting of the phases, the first sum comes from adding up the parameters in the unitary matrices U_{n_j} and the second two terms come from adding up the phases in $P_{n_{k+1}}$. Furthermore, the number of real parameters in D is $n - \sum_j (n_j - 1)$. Thus, the number of real parameters in R is

$$N_R^{(r)} = \frac{n(n+1)}{2} - \sum_j \left(\frac{n_j(n_j+1)}{2} - 1 \right) \tag{B.8}$$

nd the number of phases in R is

$$N_R^{(i)} = \frac{n(n-1)}{2} - \sum_j \left(\frac{n_j(n_j-1)}{2} \right). \tag{B.9}$$

APPENDIX C

A new CP violating observable for the LHC

C.1 THE ELECTROWEAK SECTOR OF THE MSSM

The charginos and neutralinos are the mass-basis superpartners of the Higgs and Electroweak gauge bosons. Their physics is determined by three components of the Lagrangian:

- The superpotential

$$W = \mu H_u H_d \tag{C.1}$$

  leading to fermion terms

$$\mathcal{L} = -\mu \tilde{H}_u \tilde{H}_d + \text{h.c.} \tag{C.2}$$

- The supersymmetric gauge interactions

$$\begin{aligned}\mathcal{L} = &-\sqrt{2}g\left(H_d^\dagger \frac{\sigma^a}{2}\tilde{H}_d\right)\tilde{W}^a - \sqrt{2}g\tilde{W}^a\left(\tilde{H}_d^\dagger \frac{\sigma^a}{2}H_d\right) \\ &- \sqrt{2}g\left(H_u^\dagger \frac{\sigma^a}{2}\tilde{H}_u\right)\tilde{W}^a - \sqrt{2}g\tilde{W}^a\left(\tilde{H}_u^\dagger \frac{\sigma^a}{2}H_u\right) + \sqrt{2}g'\left(H_d^\dagger \frac{1}{2}\tilde{H}_d\right)\tilde{B} \\ &+ \sqrt{2}g'\tilde{B}\left(\tilde{H}_d^\dagger \frac{1}{2}H_d\right) - \sqrt{2}g'\left(H_u^\dagger \frac{1}{2}\tilde{H}_u\right)\tilde{B} - \sqrt{2}g'\tilde{B}\left(\tilde{H}_u^\dagger \frac{1}{2}H_u\right)\end{aligned} \tag{C.3}$$

- The soft SUSY-breaking interactions

$$\mathcal{L} = -(M_1 \tilde{B}\tilde{B} + M_2 \tilde{W}^a \tilde{W}^a + b H_u H_d + \text{h.c.}) \tag{C.4}$$

Notice that the Higgsino mass is determined only by the superpotential, the gaugino mass only by the SUSY-breaking interactions, and the mixing only by EWSB. This structure means that the mass difference between charginos will always be at least of order m_W. This fact will lead to a suppression of CP violating effects in the chargino-neutralino sector, which are generally suppressed when the mass difference is either much smaller or larger than some other scale set by the width in the process.

The resulting mass matrices after EWSB are [43]

$$M_{\tilde{C}} = \begin{pmatrix} M_2 & \sqrt{2}s_\beta m_W \\ \sqrt{2}c_\beta m_W & \mu \end{pmatrix} \tag{C.5}$$

in the $(\tilde{W}^+, \tilde{H}_u^+), (\tilde{W}^-, \tilde{H}_d^-)^T$ basis and

$$M_{\tilde{N}} = \begin{pmatrix} M_1 & 0 & -c_\beta s_W m_Z & s_\beta s_W m_Z \\ 0 & M_2 & c_\beta c_W m_Z & -s_\beta c_W m_Z \\ -c_\beta s_W m_Z & c_\beta c_W m_Z & 0 & -\mu \\ s_\beta s_W m_Z & -s_\beta c_W m_Z & -\mu & 0 \end{pmatrix} \tag{C.6}$$

in the $(\tilde{B}, \tilde{W}^0, \tilde{H}_d^0, \tilde{H}_u^0)$ basis. These mass matrices are diagonalized by

$$M_{\tilde{C}} = U^T M_{\tilde{C}}^{(D)} V, \qquad M_{\tilde{N}} = N^T M_N^{(D)} N, \tag{C.7}$$

where U, V, and N are unitary matrices.

The electroweak sector of the MSSM, including the Higgs fields, generically violates CP symmetry with new physical phases. We will now count parameters and look at CP-violating invariants in this sector. This analysis has been done in ref. [180], but we reproduce it here with a different emphasis.

The electroweak sector has four complex parameters M_i, μ, b plus the real gauge couplings. We would like to determine how many of these parameters are physical. Note that the electroweak sector without potentials has a $U(1)_R \times U(1)_{PQ}$ global symmetry. The symmetry is explicitly

broken by the superpotential and soft terms. There is no residual symmetry in the electroweak sector. We are thus able to remove two of the four complex phases in the parameters listed. There are two remaining physical phases in this sector.

Field	$U(1)_R$	$U(1)_{PQ}$
H_u	1	1
H_d	1	1

Table C.1: Charges of the (chiral) superfields under $U(1)_R \times U(1)_{PQ}$.

Spurion	$U(1)_R$	$U(1)_{PQ}$
M_i	-2	0
μ	0	-2
b	-2	-2

Table C.2: Charges of the spurions under $U(1)_R \times U(1)_{PQ}$.

Next, we would like to determine the invariants corresponding to these phases. For this, we perform a spurion analysis. The charges of the superfields under the symmetries are summarized in Table C.1. After writing these down, the charges of the spurions can be read off the potentials. The μ term conserves R charge, but violates PQ symmetry. In order to render that term invariant, μ would need to have a charge of -2. The gauginos are invariant under $U(1)_{PQ}$, but they break $U(1)_R$ since they are superpartners of the gauge bosons, which must have R charge 0. The gauginos have R charge 1, so the gaugino masses have a spurious R charge of -2. Finally, the b term violates both symmetries. $U(1)_{PQ}$ is violated as in the μ term, so b has the same R charge as μ. It also violates $U(1)_R$ since it should have R charge 0, not 2 as in the superpotential. b must then have a spurious R charge of 2. The charges of the spurions are summarized in Table C.2.

All observables must be proportional to Hermitian combinations of parameters that have 0 spurious charge. CP violating observables should be proportional to the imaginary part of combinations with 0 spurious charge. The imaginary part vanishes in the CP conserving case and renders the combination real. There are two classes of such observables in the current case. The first is the class of observables formed out of gaugino masses alone: $\mathrm{Im}(M_1^* M_2)$. The other class of observables involves μ. Such observables must also involve b since it is the only other spurion with PQ charge. In particular, we must use the combination $\mu^* b$, which has no PQ charge but has R charge -2.

To form an invariant we must include one of the gaugino masses. However, the two possible such terms (one for each gaugino mass) are not independent since they can be written in terms of just one of the possible combinations, as well as combinations of only gaugino masses. In what follows, we will discuss only the electroweak sector. We will further neglect mixing with Bino for simplicity. This approximation is justified when the mass M_1 is much larger than M_2, μ and b. Then, the only relevant CP violating invariant to study is

$$\mathrm{Im}(\mu^* b M_2^*). \tag{C.8}$$

While there are generally strong bounds on this phase due to the non-observation of electric dipole moments [7], the bounds are model dependent. They come from loops involving the sleptons [181, 182]. We assume that we can make these loops small by, for example, making the sleptons very heavy, so that the region of parameter space we will study is not excluded by indirect measurements.

C.2 DIFFERENTIAL DECAY RATE OF HEAVY NEUTRALINO

We use the notation of Ref. [183]. The differential decay rate of the heavy neutralino via the diagrams Fig. 5.6, $\chi_4^0 \to \chi_1^+ \chi_2^- \chi_1^0$, is given by

$$
\begin{aligned}
\frac{d\Gamma}{dq_{13}^2 dq_{23}^2} \;=\; & \frac{1}{(2\pi)^3}\frac{1}{32 m_0^3} \\
& \left[\frac{1}{(q_{13}^2 - m)^2 + \Gamma^2 m^2}\left[(m_0^2 + m_2^2 - q_{13}^2)(|\lambda_{02}^+|^2 + |\lambda_{02}^-|^2) + 4 m_0 m_2 \mathrm{Re}(\lambda_{02}^+ \lambda_{02}^-)\right]\right. \\
& \left[(q_{13}^2 - m_1^2 - m_3^2)(|\lambda_{31}^+|^2 + |\lambda_{31}^-|^2) - 4 m_1 m_3 \mathrm{Re}(\lambda_{31}^+ \lambda_{31}^-)\right] + (1 \leftrightarrow 2) + \\
& 2\mathrm{Re}\Big\{ \frac{1}{(q_{13}^2 - m^2 + im\Gamma)(q_{23}^2 - m^2 - im\Gamma)} \times \\
& \left[m_0 m_1 (q_{23}^2 - m_2^2 - m_3^2)(\lambda_{32}^- \lambda_{01}^{-*} \lambda_{02}^{-*} \lambda_{31}^{+*} + [+ \leftrightarrow -]^*) + \right. \\
& (q_{13}^2 q_{23}^2 - m_0^2 m_3^2 - m_1^2 m_2^2)(\lambda_{01}^+ \lambda_{32}^- \lambda_{02}^{-*} \lambda_{31}^{+*} + [+ \leftrightarrow -]^*) + \\
& m_1 m_2 (q_{13}^2 + q_{23}^2 - m_1^2 - m_2^2)(\lambda_{02}^+ \lambda_{32}^- \lambda_{01}^{-*} \lambda_{31}^{+*} + [+ \leftrightarrow -]^*) + \\
& m_0 m_3 (q_{13}^2 + q_{23}^2 - m_0^2 - m_3^2)(\lambda_{31}^- \lambda_{32}^- \lambda_{01}^{-*} \lambda_{02}^{-*} + [+ \leftrightarrow -]^*) + \\
& m_0 m_2 (q_{13}^2 - m_1^2 - m_3^2)(\lambda_{01}^+ \lambda_{02}^+ \lambda_{32}^- \lambda_{31}^{+*} + [+ \leftrightarrow -]^*) + \\
& m_1 m_3 (q_{13}^2 - m_0^2 - m_2^2)(\lambda_{01}^+ \lambda_{31}^- \lambda_{32}^- \lambda_{02}^{-*} + [+ \leftrightarrow -]^*) + \\
& m_2 m_3 (q_{23}^2 - m_0^2 - m_1^2)(\lambda_{02}^+ \lambda_{31}^- \lambda_{32}^- \lambda_{01}^{-*} + [+ \leftrightarrow -]^*) - \\
& \left. 2 m_0 m_1 m_2 m_3 (\lambda_{01}^+ \lambda_{02}^+ \lambda_{31}^- \lambda_{32}^- + [+ \leftrightarrow -]^*)\right] \Big\}\Big], \qquad \text{(C.9)}
\end{aligned}
$$

where $m = m_{H^+}$, $\Gamma = \Gamma_{H^+}$, $m_0 = m_{\chi_4^0}$, $m_1 = m_{\chi_1^+}$, $m_2 = m_{\chi_2^-}$, $m_3 = m_{\chi_1^0}$, and $\lambda_{ij}^{\pm} = Y^{H^{\pm} \chi_{a(i)}^0 \chi_j^{\mp}}$ with $a(0) = 4$, $a(3) = 1$, and $j = 1, 2$. The notation $[+ \leftrightarrow -]^*$ means exchange $\lambda^{\pm} \leftrightarrow \lambda^{\mp *}$ with the same indices. The differential decay rate for $\chi_4^0 \to \chi_1^- \chi_2^+ \chi_1^0$ can be obtained from (C.9) by interchanging the indices 1 and 2 at all places.

APPENDIX D

Model of leptons from $SO(3) \to A_4$

D.1 MATHEMATICS OF A_4

The non-Abelian discrete group A_4 arises in the context of neutrinos as described in section 6.2. For the purposes of this chapter, we would like to be able to determine the irreducible representations of this group, to determine the result of products of representations, and to decompose reducible representations into irreducible representations. Accomplishing these goals requires some mathematical background.

The group A_4 is defined to be the group of even permutations of 4 objects. It is isomorphic to the group of rotational symmetries of the tetrahedron. The latter description will be used throughout this work. The group is of order 12 with the elements given as follows:

- The identity 1;
- Rotations by 180° about three orthogonal axes (edge-to-edge);
- Rotations by 120° and 240° about 4 different axes (vertex-to-face).

This description gives the defining representation, which clearly has dimension 3 and indicates that A_4 is a subgroup of rotations in 3 dimensions $SO(3)$. Typically, a basis is chosen where the two

generators S and T are given by:

$$S = \begin{pmatrix} 1 & 0 & 0 \\ 0 & -1 & 0 \\ 0 & 0 & -1 \end{pmatrix}, \qquad T = \begin{pmatrix} 0 & 1 & 0 \\ 0 & 0 & 1 \\ 1 & 0 & 0 \end{pmatrix}. \tag{D.1}$$

This basis is chosen such that the three 180° rotation axes are the Cartesian coordinate axes.

Two irreducible representations are immediately seen at this point: the defining dimension 3 representation described above and the trivial representation 1. There are two more irreducible representations of A_4. The $1'$ and the $1''$ are dimension 1 representations that map the 120° rotations onto $\omega = e^{2\pi i/3}$ and $\omega^* = e^{4\pi i/3}$ respectively. The number ω is a cube root of 1 and satisfies

$$1 + \omega + \omega^2 = 0. \tag{D.2}$$

Notice that these representations are not real. The combination $1' \oplus 1''$, however, is a real representation isomorphic to the group generated by a 120° rotations in 2 dimensions. Thus, any real representation of A_4 must contain $1'$ and $1''$ in equal multiplicities.

The products of these representations are as follows:

$$\begin{aligned} 1' \times 1' &= 1'', \qquad 1' \times 1'' = 1, \qquad 1'' \times 1'' = 1', \qquad 1' \times 3 = 3, \\ 1'' \times 3 &= 3, \qquad 3 \times 3 = 3_1 + 3_2 + 1 + 1' + 1''. \end{aligned} \tag{D.3}$$

iven two triplets (x_1, x_2, x_3) and (y_1, y_2, y_3), the results of the multiplication of 3×3 gives

$$\begin{aligned} 1 &= x_1y_1 + x_2y_2 + x_3y_3, \\ 1' &= x_1y_1 + \omega x_2y_2 + \omega^2 x_3y_3, \\ 1'' &= x_1y_1 + \omega^2 x_2y_2 + \omega x_3y_3, \\ 3_1 &= (x_2y_3, x_3y_1, x_1y_2), \\ 3_2 &= (x_3y_2, x_1y_3, x_2y_1). \end{aligned} \tag{D.4}$$

	$0°$	$120°$	$240°$	$180°$
χ_1	1	1	1	1
χ_2	1	ω	ω^2	1
χ_3	1	ω^2	ω	1
χ_4	3	0	0	-1

Table D.1: The character table for A_4, listing the conjugacy classes on the horizontal and the representations on the vertical. Here ω satisfies the equation $\omega^2 + \omega + 1 = 0$. The table is taken from [184].

urthermore, for a $1'$ (denoted by u) and an $1''$ (denoted by v), the multiplications $3 \times 1'$ and $3 \times 1''$ give respectively

$$3 = u(x_1, \omega x_2, \omega^2 x_3), \qquad 3 = v(x_1, \omega^2 x_2, \omega x_3). \tag{D.5}$$

Next we need a way to decompose reducible representations of A_4 into a direct sum of irreducible representations. In order to do this decomposition, we use a theorem about the characters of an element of a representation. Given an arbitrary group G, an element $g \in G$, and a representation ρ of G, the character is defined as

$$\chi_\rho(g) = \mathrm{Tr}\rho(g). \tag{D.6}$$

Since the trace is invariant under similarity transformation, every element of a given conjugacy class will have the same character. There are four conjugacy classes for A_4 given by each of the four possible angles of rotation: $0°$, $180°$, $120°$, and $240°$. The number of conjugacy classes is the same as the number of irreducible representations. This is a general result that holds for any finite group. It allows the construction of a character table listing the characters by irreducible representation and conjugacy class. For A_4, the character table is given in Table D.1.

Given a representation ρ which is not necessarily irreducible, irreducible representations ρ_i and an element $g \in G$, the following relation holds:

$$\chi_\rho(g) = \sum_i n_i \chi_{\rho_i}(g), \tag{D.7}$$

where n_i is the multiplicity of ρ_i in the decomposition of ρ into irreducible representations. In the case of A_4, $i = 1, 1', 1'', 3$. Notice that the number of multiplicities n_i is given by the number of

j	n_1	$n_{1'}$	$n_{1''}$	n_3
0	1	0	0	0
1	0	0	0	1
2	0	1	1	1
3	1	0	0	2
4	1	1	1	2
5	0	1	1	3

Table D.2: Decomposition of the six smallest representations of $SO(3)$ into irreducible representations of A_4. The 4 rightmost columns indicate the multiplicity of the four irreducible representations of A_4.

irreducible representations of G. Such an equation can be written down for each conjugacy class of G. Thus, if we wish to determine the multiplicities n_i, we have the same number of variables as equations given by (D.7). Given the characters in the representation under study and the irreducible representations, it is then possible to determine the decomposition of the representation ρ into irreducible representations. The characters of the irreducible representations are given by the character table. The characters of the representation under study can be computed directly. In our case, we are interested in studying the representations of A_4 induced by irreducible representations of $SO(3)$. In this case, computing the characters is even simpler as a general formula for the characters in $SO(3)$ has been determined [176]:

$$\chi_j(\theta) = \frac{\sin\left[(2j+1)\theta/2\right]}{\sin\left(\theta/2\right)}, \tag{D.8}$$

where j is the spin of the representation and θ is the angle of rotation.

For a spin j representation of $SO(3)$, the decomposition under A_4 proceeds as follows. There are four conjugacy classes of A_4, corresponding to rotations by $0°$, $180°$, $120°$, and $240°$. The characters of these rotations under the representation of $SO(3)$ are given by (D.8). The multiplicities of $1'$ and $1''$ must be equal since the group $SO(3)$ is real. Then, using (D.7), the following set of equations

can be written:

$$\begin{aligned} 2j+1 &= n_1 + 2n_{1'} + 3n_3, \\ (-1)^j &= n_1 + 2n_{1'} - n_3, \\ \frac{2}{\sqrt{3}} \sin \frac{(2j+1)\pi}{3} &= n_1 - n_{1'} + \omega^2 n_3 \end{aligned} \tag{D.9}$$

ote that the last two equations are cyclic in j with period 6. This results in a pattern with that period. The decomposition for the first six representations is given in Table D.2. The pattern for a higher representation j can be determined as follows. Let

$$q = \lfloor j/6 \rfloor, \qquad r = j \bmod 6. \tag{D.10}$$

hen for $i = 1, 1', 1''$ we have

$$n_i(j) = n_i(r) + q. \tag{D.11}$$

or $i = 3$ we have

$$n_3(j) = n_3(r) + 3q. \tag{D.12}$$

or example, the spin $j = 23$ representation has $q = 3$ and $r = 5$, and thus $n_1(23) = 3$, $n_{1'}(23) = n_{1''}(23) = 4$ and $n_3(23) = 12$.

D.2 MINIMA OF THE POTENTIAL OF A 7 OF $SO(3)$

In this appendix, we present the determination of the minima of the potential (6.10) as done in [175]. In order to proceed, it is simplest to reparametrize T^{abc} based on symmetries. Before we do that, however, we start with a simpler example: the case of a triplet. We can write the **3** as the product of a magnitude and a unit vector: $v^a = \alpha x^a$ such that the three parameters are the length of v, denote by α, and the two angles that describe the orientation of v^a. The point to emphasize is that the potential for such a scalar is written as a function of only one of the parameters, the

magnitude α. It is given by

$$V = -\frac{\mu^2}{2} v^a v^a + \frac{\lambda}{4!}(v^a v^a)^2 = -\frac{\mu^2}{2}\alpha^2 + \frac{\lambda}{4!}\alpha^4. \tag{D.13}$$

Furthermore, if $\mu^2 > 0$ and $\lambda > 0$, the resulting vacuum has the residual symmetry of the unit vector x^a, which is $SO(2)$.

For the **7**, the parametrization and potential are both more complicated. There are three orthogonal terms with different symmetries. The first term is invariant under $SO(2)$ as it depends on a single unit vector. The second term is best described geometrically. Consider an arbitrary equilateral triangle in three dimensions. Define three vectors connecting the center of the triangle to each of the three vertices of the triangle. The object defined by these vectors is called a regular 3-point star. Mathematically, it can be written as the symmetric outer product of the three defining vectors. This construction is automatically traceless. The second term is then given by a regular 3-point star defined with unit vectors. Finally, the third term is given by the symmetric product of three orthonormal unit vectors.

Explicitly, the parametrization is

$$T^{abc} = \alpha\left(x^a x^b x^c - \frac{3}{5}\delta^{(ab}x^{c)}\right) + \beta\chi^{abc}_{(3)} + \gamma x^{(a}y^b z^{c)}, \tag{D.14}$$

where $\chi^{abc}_{(3)}$ describes an arbitrary 3 point regular star with unit length vectors, the vectors x, y, z are orthonormal and χ is orthogonal to x. A general tensor written as in (D.14) has 7 parameters as one would expect for a symmetric traceless tensor of rank 3: α, β, γ, the two angles in x^a, the angle of $\chi_{(3)}$ about the x axis, and the angle of y about the x axis. The angle of z is determined by requiring orthogonality. There are two advantages to the parametrization (D.14). The first is that since the terms are orthogonal and normalized, the potential can now be written in terms of the three parameters α, β, and γ rather than in terms of seven parameters. The second is that, once the vacua are determined, it is far easier to determine the symmetries in this parametrization. The three terms in the parametrization have well-defined symmetry groups. The first is invariant under $SO(2)$ (rotations orthogonal to x). The second is invariant under D_3 since a three point star has

the symmetries of a triangle. The third is invariant under A_4, where the three vectors x, y, and z are taken to be the 180° rotation axes. If the basis is chosen such that x, y, and z are along the corresponding axes of the coordinate system, this term is invariant under both S and T given in (D.1).

The potential of Eq. (6.10) written in terms of (D.14) depend only of three out of the seven parameters, α, β, and γ. It is given by

$$V = -\frac{\mu^2}{2}\left(\frac{2}{5}\alpha^2 + \frac{1}{4}\beta^2 + \frac{1}{6}\gamma^2\right) + \frac{\lambda}{4}\left(\frac{2}{5}\alpha^2 + \frac{1}{4}\beta^2 + \frac{1}{6}\gamma^2\right)^2 + c\left(\frac{44}{25^2}\alpha^4 + \frac{1}{25}\alpha^2\beta^2 + \frac{2}{25}\alpha^2\gamma^2 + \frac{1}{24}\beta^2\gamma^2 + \frac{3}{18^2}\gamma^4\right). \quad \text{(D.15)}$$

In order for an A_4-invariant vacuum to exist, there must be a minimum with $\alpha = \beta = 0$ and $\gamma \neq 0$. Indeed, there is such a minimum for a certain portion of parameter space. If $c > 0$, then there is a D_3 invariant vacuum (only $\beta \neq 0$). For $-\lambda/2 < c < 0$, there is an A_4 invariant vacuum. Finally, for $c < -\lambda/2$, the potential has a runaway direction. It is possible to spontaneously break $SO(3)$ to A_4 using a single scalar in a spin 3 representation of $SO(3)$ by picking the second case, $-\lambda/2 < c < 0$.

Bibliography

[1] S. L. Glashow, Nucl. Phys. **22**, 579 (1961).

[2] S. Weinberg, Phys. Rev. Lett. **19**, 1264 (1967).

[3] A. Salam, Conf. Proc. C **680519**, 367 (1968).

[4] D. J. Gross and F. Wilczek, Phys. Rev. Lett. **30**, 1343 (1973).

[5] K. G. Wilson, Phys. Rev. D **10**, 2445 (1974).

[6] A. Casher, J. B. Kogut and L. Susskind, Phys. Rev. D **10**, 732 (1974).

[7] K. Nakamura *et al.* [Particle Data Group Collaboration], J. Phys. G G **37**, 075021 (2010).

[8] M. Baak, M. Goebel, J. Haller, A. Hoecker, D. Ludwig, K. Moenig, M. Schott and J. Stelzer, arXiv:1107.0975 [hep-ph].

[9] M. Ciuchini *et al.*, JHEP **0107**, 013 (2001) [arXiv:hep-ph/0012308].

[10] J. Charles *et al.* [CKMfitter Group Collaboration], Eur. Phys. J. C **41**, 1 (2005) [hep-ph/0406184].

[11] H. Nishino, K. Abe, Y. Hayato, T. Iida, M. Ikeda, J. Kameda, Y. Koshio and M. Miura *et al.*, arXiv:1203.4030 [hep-ex].

[12] K. Abe *et al.* [Super-Kamiokande Collaboration], arXiv:1109.4227 [hep-ex].

[13] K. Kobayashi *et al.* [Super-Kamiokande Collaboration], Phys. Rev. D **72**, 052007 (2005) [hep-ex/0502026].

[14] M. D. Litos, "A Searcb for Dinucleon Decay into Kaons using the Super-Kamiokande Water Cherenkov Detector," PhD thesis, Boston University, 2010.

[15] N. Cabibbo, Phys. Rev. Lett. **10**, 531 (1963).

[16] M. Kobayashi and T. Maskawa, Prog. Theor. Phys. **49**, 652 (1973).

[17] G. L. Fogli, E. Lisi, A. Marrone, D. Montanino, A. Palazzo and A. M. Rotunno, arXiv:1205.5254 [hep-ph].

[18] A. Goobar, S. Hannestad, E. Mortsell and H. Tu, JCAP **0606**, 019 (2006) [astro-ph/0602155].

[19] L. F. Abbott and M. B. Wise, Phys. Rev. D **22**, 2208 (1980).

[20] F. Bossi *et al.* [KLOE Collaboration], Riv. Nuovo Cim. **31**, 531 (2008) [arXiv:0811.1929 [hep-ex]].

[21] M. E. Peskin and T. Takeuchi, Phys. Rev. Lett. **65**, 964 (1990).

[22] Z. Han and W. Skiba, Phys. Rev. D **71**, 075009 (2005) [hep-ph/0412166].

[23] G. Aad *et al.* [ATLAS Collaboration], Phys. Lett. B **710**, 49 (2012) [arXiv:1202.1408 [hep-ex]]; S. Chatrchyan *et al.* [CMS Collaboration], *"Combined results of searches for the standard model Higgs boson in pp collisions at sqrt(s) = 7 TeV,"* arXiv:1202.1488 [hep-ex].

[24] E. Komatsu *et al.* [WMAP Collaboration], Astrophys. J. Suppl. **192**, 18 (2011) [arXiv:1001.4538 [astro-ph.CO]].

[25] D. Clowe, M. Bradac, A. H. Gonzalez, M. Markevitch, S. W. Randall, C. Jones and D. Zaritsky, Astrophys. J. **648**, L109 (2006) [astro-ph/0608407].

[26] F. Zwicky, Astrophys. J. **86**, 217 (1937).

[27] N. F. Bell, A. J. Galea and K. Petraki, Phys. Rev. D **82**, 023514 (2010) [arXiv:1004.1008 [astro-ph.HE]].

[28] M. Markevitch, A. H. Gonzalez, D. Clowe, A. Vikhlinin, L. David, W. Forman, C. Jones and S. Murray *et al.*, Astrophys. J. **606**, 819 (2004) [astro-ph/0309303].

[29] E. W. Kolb and M. S. Turner, Front. Phys. **69**, 1 (1990).

[30] A. D. Sakharov, Pisma Zh. Eksp. Teor. Fiz. **5**, 32 (1967) [JETP Lett. **5**, 24 (1967)] [Sov. Phys. Usp. **34**, 392 (1991)] [Usp. Fiz. Nauk **161**, 61 (1991)].

[31] M. Bona *et al.* [UTfit Collaboration], Phys. Rev. Lett. **97**, 151803 (2006) [arXiv:hep-ph/0605213].

[32] J. J. Hudson, D. M. Kara, I. J. Smallman, B. E. Sauer, M. R. Tarbutt and E. A. Hinds, Nature **473**, 493 (2011).

[33] M. Burghoff, A. Schnabel, G. Ban, T. Lefort, Y. Lemiere, O. Naviliat-Cuncic, E. Pierre and G. Quemener *et al.*, arXiv:1110.1505 [nucl-ex].

[34] S. Chatrchyan *et al.* [CMS Collaboration], JINST **3**, S08004 (2008).

[35] G. Aad *et al.* [ATLAS Collaboration], JINST **3**, S08003 (2008).

[36] K. Aamodt *et al.* [ALICE Collaboration], JINST **3**, S08002 (2008).

[37] A. A. Alves, Jr. *et al.* [LHCb Collaboration], JINST **3**, S08005 (2008).

[38] S. Chatrchyan *et al.* [CMS Collaboration], Phys. Lett. B **710**, 26 (2012) [arXiv:1202.1488 [hep-ex]].

[39] G. Aad *et al.* [ATLAS Collaboration], Phys. Lett. B **710**, 49 (2012) [arXiv:1202.1408 [hep-ex]].

[40] F. P. An *et al.* [DAYA-BAY Collaboration], Phys. Rev. Lett. **108**, 171803 (2012) [arXiv:1203.1669 [hep-ex]].

[41] P. Coloma, A. Donini, E. Fernandez-Martinez and P. Hernandez, arXiv:1203.5651 [hep-ph].

[42] F. T. Avignone, III, S. R. Elliott and J. Engel, Rev. Mod. Phys. **80**, 481 (2008) [arXiv:0708.1033 [nucl-ex]].

[43] S. P. Martin, In *Kane, G.L. (ed.): Perspectives on supersymmetry II* 1-153 [hep-ph/9709356].

[44] C. T. Hill and E. H. Simmons, Phys. Rept. **381**, 235 (2003) [Erratum-ibid. **390**, 553 (2004)] [hep-ph/0203079].

[45] M. E. Peskin and T. Takeuchi, Phys. Rev. D **46**, 381 (1992).

[46] B. Holdom, Phys. Lett. B **150**, 301 (1985).

[47] O. Aharony, S. S. Gubser, J. M. Maldacena, H. Ooguri and Y. Oz, Phys. Rept. **323**, 183 (2000) [hep-th/9905111].

[48] L. Randall and R. Sundrum, Phys. Rev. Lett. **83**, 3370 (1999) [hep-ph/9905221].

[49] N. Arkani-Hamed, A. G. Cohen, E. Katz, A. E. Nelson, T. Gregoire and J. G. Wacker, JHEP **0208**, 021 (2002) [hep-ph/0206020].

[50] J. Berger and Y. Grossman, Phys. Lett. B **675**, 365 (2009) [arXiv:0811.1019 [hep-ph]].

[51] J. Berger and Y. Grossman, JHEP **1002**, 071 (2010) [arXiv:0910.4392 [hep-ph]].

[52] J. Berger, M. Blanke and Y. Grossman, JHEP **1108**, 033 (2011) [arXiv:1105.0672 [hep-ph]].

[53] J. Berger, M. Perelstein, M. Saelim and A. Spray, arXiv:1111.6594 [hep-ph].

[54] J. Berger, J. Hubisz and M. Perelstein, arXiv:1205.0013 [hep-ph].

[55] C. Brust, A. Katz, S. Lawrence and R. Sundrum, JHEP **1203**, 103 (2012) [arXiv:1110.6670 [hep-ph]];

M. Papucci, J. T. Ruderman and A. Weiler, *"Natural SUSY Endures,"* arXiv:1110.6926 [hep-ph];

Y. Kats, P. Meade, M. Reece and D. Shih, JHEP **1202**, 115 (2012) [arXiv:1110.6444 [hep-ph]];

N. Desai and B. Mukhopadhyaya, *"Constraints on supersymmetry with light third family from LHC data,"* arXiv:1111.2830 [hep-ph].

[56] L. J. Hall, D. Pinner and J. T. Ruderman, *"A Natural SUSY Higgs Near 126 GeV,"* arXiv:1112.2703 [hep-ph].

[57] H. Georgi and A. Pais, Phys. Rev. D **10**, 539 (1974);
D. B. Kaplan and H. Georgi, Phys. Lett. B **136**, 183 (1984);
D. B. Kaplan, H. Georgi and S. Dimopoulos, Phys. Lett. B **136**, 187 (1984);
H. Georgi, D. B. Kaplan and P. Galison, Phys. Lett. B **143**, 152 (1984);
H. Georgi and D. B. Kaplan, Phys. Lett. B **145**, 216 (1984);
M. J. Dugan, H. Georgi and D. B. Kaplan, Nucl. Phys. B **254**, 299 (1985).

[58] N. Arkani-Hamed, A. G. Cohen, E. Katz and A. E. Nelson, JHEP **0207**, 034 (2002) [hep-ph/0206021].

[59] For reviews and further references, see M. Schmaltz and D. Tucker-Smith, Ann. Rev. Nucl. Part. Sci. **55**, 229 (2005) [hep-ph/0502182]; and M. Perelstein, Prog. Part. Nucl. Phys. **58**, 247 (2007) [hep-ph/0512128].

[60] R. Contino, Y. Nomura and A. Pomarol, Nucl. Phys. B **671**, 148 (2003) [hep-ph/0306259];
K. Agashe, R. Contino and A. Pomarol, Nucl. Phys. B **719**, 165 (2005) [hep-ph/0412089];
R. Contino, L. Da Rold and A. Pomarol, Phys. Rev. D **75**, 055014 (2007) [hep-ph/0612048].

[61] C. Csaki, J. Hubisz, G. D. Kribs, P. Meade and J. Terning, Phys. Rev. D **67**, 115002 (2003) [hep-ph/0211124].

[62] H. -C. Cheng and I. Low, JHEP **0309**, 051 (2003) [hep-ph/0308199];
H. -C. Cheng and I. Low, JHEP **0408**, 061 (2004) [hep-ph/0405243].

[63] M. Schmaltz, D. Stolarski and J. Thaler, JHEP **1009**, 018 (2010) [arXiv:1006.1356 [hep-ph]].

[64] E. Katz, A. E. Nelson and D. G. E. Walker, JHEP **0508**, 074 (2005) [hep-ph/0504252].

[65] M. Perelstein, M. E. Peskin and A. Pierce, Phys. Rev. D **69**, 075002 (2004) [hep-ph/0310039].

[66] B. Grinstein, R. Kelley and P. Uttayarat, JHEP **0909**, 040 (2009) [arXiv:0904.1622 [hep-ph]].

[67] S. R. Coleman and E. J. Weinberg, Phys. Rev. D **7**, 1888 (1973).

[68] J. Hubisz, P. Meade, A. Noble and M. Perelstein, JHEP **0601**, 135 (2006) [hep-ph/0506042].

[69] R. Barbieri, B. Bellazzini, V. S. Rychkov and A. Varagnolo, Phys. Rev. D **76**, 115008 (2007) [arXiv:0706.0432 [hep-ph]].

[70] Z. Han and W. Skiba, Phys. Rev. D **71**, 075009 (2005) [hep-ph/0412166].

[71] K. Nakamura *et al.* [Particle Data Group Collaboration], J. Phys. G G **37**, 075021 (2010).

[72] J. Y. Lee, JHEP **0412**, 065 (2004) [hep-ph/0408362].

[73] J. Hubisz, S. J. Lee and G. Paz, JHEP **0606**, 041 (2006) [hep-ph/0512169].

[74] A. J. Buras, A. Poschenrieder and S. Uhlig, Nucl. Phys. B **716**, 173 (2005) [hep-ph/0410309].

[75] M. Blanke, A. J. Buras, A. Poschenrieder, C. Tarantino, S. Uhlig and A. Weiler, JHEP **0612**, 003 (2006) [hep-ph/0605214].

[76] M. Bona *et al.* [UTfit Collaboration], JHEP **0803**, 049 (2008) [arXiv:0707.0636 [hep-ph]]; G. Isidori, Y. Nir and G. Perez, Ann. Rev. Nucl. Part. Sci. **60**, 355 (2010) [arXiv:1002.0900 [hep-ph]].

[77] W. -j. Huo and S. -h. Zhu, Phys. Rev. D **68**, 097301 (2003) [hep-ph/0306029].

[78] M. Misiak *et al.*, Phys. Rev. Lett. **98**, 022002 (2007) [hep-ph/0609232].

[79] A. J. Buras, A. Poschenrieder, S. Uhlig and W. A. Bardeen, JHEP **0611**, 062 (2006) [hep-ph/0607189];
M. Blanke, A. J. Buras, A. Poschenrieder, S. Recksiegel, C. Tarantino, S. Uhlig and A. Weiler, JHEP **0701**, 066 (2007) [hep-ph/0610298].

[80] R. Aaij *et al.* [LHCb Collaboration], *"Strong constraints on the rare decays $B_s \to \mu^+\mu^-$ and $B^0 \to \mu^+\mu^-$,"* arXiv:1203.4493 [hep-ex].

[81] M. Aliev, H. Lacker, U. Langenfeld, S. Moch, P. Uwer and M. Wiedermann, Comput. Phys. Commun. **182**, 1034 (2011) [arXiv:1007.1327 [hep-ph]].

[82] J. Alwall, M. Herquet, F. Maltoni, O. Mattelaer and T. Stelzer, JHEP **1106**, 128 (2011) [arXiv:1106.0522 [hep-ph]].

[83] T. Han, H. E. Logan, B. McElrath and L. -T. Wang, Phys. Rev. D **67**, 095004 (2003) [hep-ph/0301040].

[84] S. Chatrchyan *et al.* [CMS Collaboration], *"Search for heavy, top-like quark pair production in the dilepton final state in pp collisions at sqrt(s) = 7 TeV,"* arXiv:1203.5410 [hep-ex].

[85] S. Chatrchyan *et al.* [CMS Collaboration], Phys. Rev. Lett. **107**, 271802 (2011) [arXiv:1109.4985 [hep-ex]].

[86] The CMS Collaboration, *"Search for t' pair production in lepton+jets channel"*, CMS-PAS-EXO-11-099.

[87] The CMS Collaboration, *"Inclusive search for a fourth generation of quarks with the CMS experiment"*, CMS-PAS-EXO-11-054.

[88] G. Aad *et al.* [ATLAS Collaboration], *"Search for pair-produced heavy quarks decaying to Wq in the two-lepton channel at sqrt(s) = 7 TeV with the ATLAS detector,"* arXiv:1202.3389 [hep-ex].

[89] G. Aad *et al.* [ATLAS Collaboration], *"Search for pair production of a heavy quark decaying to a W boson and a b quark in the lepton+jets channel with the ATLAS detector,"* arXiv:1202.3076 [hep-ex].

[90] T. Sjostrand, S. Mrenna and P. Z. Skands, JHEP **0605**, 026 (2006) [hep-ph/0603175].

[91] J. Conway, `http://physics.ucdavis.edu/ conway/research/software/pgs/pgs4-general.htm`.

[92] The CMS Collaboration, *"Performance of the b-jet identification in CMS,"* CMS-PAS-BTV-11-001.

[93] S. Godfrey, T. Gregoire, P. Kalyniak, T. A. W. Martin and K. Moats, *"Exploring the heavy quark sector of the Bestest Little Higgs model at the LHC,"* arXiv:1201.1951 [hep-ph].

[94] G. F. Giudice, C. Grojean, A. Pomarol and R. Rattazzi, JHEP **0706**, 045 (2007) [hep-ph/0703164];

J. R. Espinosa, C. Grojean, M. Muhlleitner and M. Trott, *"Fingerprinting Higgs Suspects at the LHC,"* arXiv:1202.3697 [hep-ph].

[95] T. Han, H. E. Logan, B. McElrath and L. -T. Wang, Phys. Lett. B **563**, 191 (2003) [Erratum-ibid. B **603**, 257 (2004)] [hep-ph/0302188];
C. -R. Chen, K. Tobe and C. -P. Yuan, Phys. Lett. B **640**, 263 (2006) [hep-ph/0602211].

[96] A. Birkedal, A. Noble, M. Perelstein and A. Spray, Phys. Rev. D **74**, 035002 (2006) [hep-ph/0603077].

[97] U. Baur, A. Juste, L. H. Orr and D. Rainwater, Phys. Rev. D **71**, 054013 (2005) [hep-ph/0412021].

[98] T. Abe *et al.* [American Linear Collider Working Group Collaboration], *"Linear collider physics resource book for Snowmass 2001. Part 3. Studies of exotic and standard model physics.,"* hep-ex/0106057.

[99] C. F. Berger, M. Perelstein and F. Petriello, *"Top quark properties in little Higgs models,"* hep-ph/0512053.

[100] G. D. Kribs, A. Martin and T. S. Roy, Phys. Rev. D **84**, 095024 (2011) [arXiv:1012.2866 [hep-ph]].

[101] K. Harigaya, S. Matsumoto, M. M. Nojiri and K. Tobioka, *"Search for the Top Partner at the LHC using Multi-b-Jet Channels,"* arXiv:1204.2317 [hep-ph];
A. Girdhar and B. Mukhopadhyaya, *"A clean signal for a top-like isosinglet fermion at the Large Hadron Collider,"* arXiv:1204.2885 [hep-ph].

[102] G. Aad *et al.* [ATLAS Collaboration], *"Search for squarks and gluinos using final states with jets and missing transverse momentum with the ATLAS detector in sqrt(s) = 7 TeV proton-proton collisions,"* arXiv:1109.6572 [hep-ex];
S. Chatrchyan *et al.* [CMS Collaboration], *"Search for Supersymmetry at the LHC in Events with Jets and Missing Transverse Energy,"* arXiv:1109.2352 [hep-ex].

[103] A. Strumia, JHEP **1104**, 073 (2011) [arXiv:1101.2195 [hep-ph]].

[104] C. Brust, A. Katz, S. Lawrence, R. Sundrum, *"SUSY, the Third Generation and the LHC,"* arXiv:1110.6670 [hep-ph].

[105] M. Papucci, J. T. Ruderman, A. Weiler, *"Natural SUSY Endures,"* arXiv:1110.6926 [hep-ph].

[106] Y. Kats, P. Meade, M. Reece, D. Shih, *"The Status of GMSB After 1/fb at the LHC,"* [arXiv:1110.6444 [hep-ph]].

[107] T. Gherghetta, A. Pomarol, Phys. Rev. **D67**, 085018 (2003) [hep-ph/0302001]; R. Sundrum, JHEP **1101**, 062 (2011) [arXiv:0909.5430 [hep-th]]; T. Gherghetta, B. von Harling, N. Setzer, JHEP **1107**, 011 (2011) [arXiv:1104.3171 [hep-ph]].

[108] M. Toharia, J. D. Wells, JHEP **0602**, 015 (2006) [hep-ph/0503175].

[109] G. L. Kane, E. Kuflik, R. Lu and L. T. Wang, *"Top Channel for Early SUSY Discovery at the LHC,"* arXiv:1101.1963 [hep-ph]; B. S. Acharya, P. Grajek, G. L. Kane, E. Kuflik, K. Suruliz, L. -T. Wang, *"Identifying Multi-Top Events from Gluino Decay at the LHC,"* [arXiv:0901.3367 [hep-ph]].

[110] A. Abdesselam *et al.*, Eur. Phys. J. C **71**, 1661 (2011) [arXiv:1012.5412 [hep-ph]].

[111] K. Agashe, A. Belyaev, T. Krupovnickas, G. Perez and J. Virzi, Phys. Rev. D **77**, 015003 (2008) [arXiv:hep-ph/0612015]; B. Lillie, L. Randall and L. T. Wang, JHEP **0709**, 074 (2007) [arXiv:hep-ph/0701166].

[112] M. Perelstein and A. Spray, JHEP **0910**, 096 (2009) [arXiv:0907.3496 [hep-ph]]; JHEP **1109**, 008 (2011). [arXiv:1106.2171 [hep-ph]].

[113] T. Plehn, M. Spannowsky, M. Takeuchi, D. Zerwas, JHEP **1010**, 078 (2010) [arXiv:1006.2833 [hep-ph]].

[114] D. Alves *et al.*, *"Simplified Models for LHC New Physics Searches,"* arXiv:1105.2838 [hep-ph].

[115] R. Essig, E. Izaguirre, J. Kaplan, J. G. Wacker, *"Heavy Flavor Simplified Models at the LHC,"* arXiv:1110.6443 [hep-ph].

[116] M. Perelstein, C. Spethmann, JHEP **0704**, 070 (2007) [hep-ph/0702038 [HEP-PH]].

[117] W. Beenakker, R. Hopker, M. Spira, *"PROSPINO: A Program for the production of supersymmetric particles in next-to-leading order QCD,"*, hep-ph/9611232.

[118] J. Alwall, M. Herquet, F. Maltoni, O. Mattelaer, T. Stelzer, JHEP **1106**, 128 (2011) [arXiv:1106.0522 [hep-ph]].

[119] T. Sjostrand, S. Mrenna, P. Z. Skands, Comput. Phys. Commun. **178**, 852-867 (2008) [arXiv:0710.3820 [hep-ph]].

[120] M. Cacciari, G. P. Salam, Phys. Lett. **B641**, 57-61 (2006) [hep-ph/0512210].

[121] M. Cacciari, G. P. Salam and G. Soyez, `http://fastjet.fr`

[122] D. E. Kaplan, K. Rehermann, M. D. Schwartz and B. Tweedie, Phys. Rev. Lett. **101**, 142001 (2008) [arXiv:0806.0848 [hep-ph]].

[123] G. Bevilacqua, M. Czakon, C. G. Papadopoulos and M. Worek, Phys. Rev. Lett. **104**, 162002 (2010) [arXiv:1002.4009 [hep-ph]]; *"Hadronic top-quark pair production in association with two jets at Next-to-Leading Order QCD,"* arXiv:1108.2851 [hep-ph].

[124] H. Ita, Z. Bern, L. J. Dixon, F. F. Cordero, D. A. Kosower and D. Maitre, *"Precise Predictions for Z + 4 Jets at Hadron Colliders,"* arXiv:1108.2229 [hep-ph].

[125] Signal rates for a SUSY search (in the context of constrained MSSM) using a single top tag were computed in P. Bandyopadhyay, B. Bhattacherjee, Phys. Rev. **D84**, 035020 (2011) [arXiv:1012.5289 [hep-ph]]. However, this paper did not analyze the backgrounds, which are quite strong in this channel.

[126] T. Junk, Nucl. Instrum. Meth. **A434**, 435-443 (1999) [hep-ex/9902006]; A. L. Read, *"Modified frequentist analysis of search results (The CL(s) method),"*, CERN-OPEN-2000-205.

[127] G. J. Feldman, R. D. Cousins, Phys. Rev. **D57**, 3873-3889 (1998) [physics/9711021 [physics.data-an]]; V. Bartsch, G. Quast, *"Expected Signal Observability at Future Experiments",* CERN-CMS-NOTE-2005-004.

[128] J. Bramante, J. Kumar, B. Thomas, *"Large Jet Multiplicities and New Physics at the LHC,"* [arXiv:1109.6014 [hep-ph]].

[129] A. Santamaria, Phys. Lett. B **305**, 90 (1993) [arXiv:hep-ph/9302301].

[130] Y. Nir, [arxiv:0708.1872].

[131] C. Amsler et al., Physics Letters **B667**, 1 (2008) [http://pdg.lbl.gov].

[132] A. W. Knapp, *Lie Groups Beyond an Introduction*, Birkhäuser Boston (1996).

[133] S. Dimopoulos, D. Sutter, Nucl. Phys. **B452**, 496-512 (1995)

[134] H. E. Haber, Nucl. Phys. Proc. Suppl. **101**, 217-236 (2001) [arxiv:hep-ph/0103095].

[135] R. Barbieri, L. J. Hall, S. Raby, A. Romanino, Nucl. Phys. **B493**, 3-26 (1997) [arxiv:hep-ph/9610449]

[136] M. Bona *et al.* [UTfit Collaboration], JHEP **0803**, 049 (2008). [arXiv:0707.0636 [hep-ph]].

[137] M. Raidal, A. van der Schaaf, I. Bigi, M. L. Mangano, Y. K. Semertzidis, S. Abel, S. Albino, S. Antusch *et al.*, Eur. Phys. J. **C57**, 13-182 (2008). [arXiv:0801.1826 [hep-ph]].

[138] G. Valencia, Phys. Rev. **D39**, 3339 (1989).

[139] J. G. Korner, K. Schilcher, Y. L. Wu, Phys. Lett. **B242**, 119 (1990).

[140] B. Kayser, Nucl. Phys. Proc. Suppl. **13**, 487-490 (1990).

[141] W. Bensalem, D. London, Phys. Rev. **D64**, 116003 (2001). [hep-ph/0005018].

[142] A. Datta, D. London, Int. J. Mod. Phys. **A19**, 2505-2544 (2004). [hep-ph/0303159].

[143] J. A. Aguilar-Saavedra, Phys. Lett. B **596**, 247 (2004) [arXiv:hep-ph/0403243].

[144] A. Bartl, H. Fraas, S. Hesselbach, K. Hohenwarter-Sodek and G. A. Moortgat-Pick, JHEP **0408**, 038 (2004) [arXiv:hep-ph/0406190].

[145] P. Langacker, G. Paz, L. -T. Wang, I. Yavin, JHEP **0707**, 055 (2007). [hep-ph/0702068 [HEP-PH]].

[146] G. Moortgat-Pick, K. Rolbiecki, J. Tattersall and P. Wienemann, JHEP **1001**, 004 (2010) [arXiv:0908.2631 [hep-ph]].

[147] A. Pilaftsis, M. Nowakowski, Phys. Lett. **B245**, 185-191 (1990).

[148] M. Nowakowski, A. Pilaftsis, Mod. Phys. Lett. **A6**, 1933-1942 (1991).

[149] G. Eilam, J. L. Hewett, A. Soni, Phys. Rev. Lett. **67**, 1979-1981 (1991).

[150] D. Atwood, G. Eilam, M. Gronau, A. Soni, Phys. Lett. **B341**, 372-378 (1995). [hep-ph/9409229].

[151] I. Bediaga, I. I. Bigi, A. Gomes, G. Guerrer, J. Miranda and A. C. d. Reis, Phys. Rev. D **80**, 096006 (2009) [arXiv:0905.4233 [hep-ph]].

[152] M. Apollonio *et al.* [CHOOZ Collaboration], Eur. Phys. J. C **27**, 331 (2003) [arXiv:hep-ex/0301017].

[153] B. Aharmim *et al.* [SNO Collaboration], Phys. Rev. C **72**, 055502 (2005) [arXiv:nucl-ex/0502021].

[154] M. H. Ahn *et al.* [K2K Collaboration], Phys. Rev. D **74**, 072003 (2006) [arXiv:hep-ex/0606032].

[155] K. Abe *et al.* [Super-Kamiokande Collaboration], Phys. Rev. Lett. **97**, 171801 (2006) [arXiv:hep-ex/0607059].

[156] S. Abe *et al.* [KamLAND Collaboration], Phys. Rev. Lett. **100**, 221803 (2008) [arXiv:0801.4589 [hep-ex]].

[157] M. Bona *et al.* [UTfit Collaboration], JHEP **0507**, 028 (2005) [arXiv:hep-ph/0501199].

[158] C. Amsler *et al.* [Particle Data Group], Phys. Lett. B **667**, 1 (2008).

[159] B. Pontecorvo, Sov. Phys. JETP **26** (1968) 984 [Zh. Eksp. Teor. Fiz. **53** (1967) 1717].

[160] Z. Maki, M. Nakagawa and S. Sakata, Prog. Theor. Phys. **28**, 870 (1962).

[161] P. F. Harrison, D. H. Perkins and W. G. Scott, Phys. Lett. B **530**, 167 (2002) [arXiv:hep-ph/0202074].

[162] K. S. Babu, E. Ma and J. W. F. Valle, Phys. Lett. B **552**, 207 (2003) [arXiv:hep-ph/0206292].

[163] G. Altarelli and F. Feruglio, Nucl. Phys. B **720**, 64 (2005) [arXiv:hep-ph/0504165].

[164] G. Altarelli, arXiv:0905.2350 [hep-ph].

[165] G. L. Fogli *et al.*, Phys. Rev. D **78**, 033010 (2008) [arXiv:0805.2517 [hep-ph]].

[166] G. Altarelli, arXiv:0905.3265 [hep-ph].

[167] E. Ma, Phys. Rev. D **73**, 057304 (2006) [arXiv:hep-ph/0511133]; Mod. Phys. Lett. A **22**, 101 (2007) [arXiv:hep-ph/0610342]; F. Bazzocchi, S. Kaneko and S. Morisi, JHEP **0803** (2008) 063 [arXiv:0707.3032 [hep-ph]]. P. H. Frampton and S. Matsuzaki, arXiv:0806.4592 [hep-ph];

[168] G. Altarelli and D. Meloni, arXiv:0905.0620 [hep-ph].

[169] C. Csaki, C. Delaunay, C. Grojean and Y. Grossman, JHEP **0810**, 055 (2008) [arXiv:0806.0356 [hep-ph]].

[170] G. Altarelli and F. Feruglio, Nucl. Phys. B **741**, 215 (2006) [arXiv:hep-ph/0512103].

[171] G. Altarelli, F. Feruglio and Y. Lin, Nucl. Phys. B **775**, 31 (2007) [arXiv:hep-ph/0610165].

[172] F. Bazzocchi, S. Morisi and M. Picariello, Phys. Lett. B **659**, 628 (2008) [arXiv:0710.2928 [hep-ph]]; F. Bazzocchi, S. Morisi, M. Picariello and E. Torrente-Lujan, J. Phys. G **36**, 015002 (2009) [arXiv:0802.1693 [hep-ph]].

[173] A. Adulpravitchai, A. Blum and M. Lindner, JHEP **0909**, 018 (2009) [arXiv:0907.2332 [hep-ph]].

[174] E. Ma and G. Rajasekaran, Phys. Rev. D **64** (2001) 113012 [arXiv:hep-ph/0106291]; E. Ma, Mod. Phys. Lett. A **17** (2002) 627 [arXiv:hep-ph/0203238]. K. S. Babu, E. Ma and J. W. F. Valle, Phys. Lett. B **552** (2003) 207 [arXiv:hep-ph/0206292]; M. Hirsch, J. C. Romao, S. Skadhauge, J. W. F. Valle and A. Villanova del Moral, arXiv:hep-ph/0312244; Phys. Rev. D **69** (2004) 093006 [arXiv:hep-ph/0312265]; E. Ma, Phys. Rev. D **70** (2004) 031901; Phys. Rev. D **70** (2004) 031901 [arXiv:hep-ph/0404199]; New J. Phys. **6** (2004) 104 [arXiv:hep-ph/0405152]; arXiv:hep-ph/0409075; S. L. Chen, M. Frigerio and E. Ma, Nucl. Phys. B **724** (2005) 423 [arXiv:hep-ph/0504181]; E. Ma, Phys. Rev. D **72** (2005) 037301 [arXiv:hep-ph/0505209]; M. Hirsch, A. Villanova del Moral, J. W. F. Valle and E. Ma, Phys. Rev. D **72** (2005) 091301 [Erratum-ibid. D **72** (2005) 119904] [arXiv:hep-ph/0507148]. K. S. Babu and X. G. He, arXiv:hep-ph/0507217; E. Ma, Mod. Phys. Lett. A **20** (2005) 2601 [arXiv:hep-ph/0508099]; A. Zee, Phys. Lett. B **630** (2005) 58 [arXiv:hep-ph/0508278]; X. G. He, Y. Y. Keum and R. R. Volkas, JHEP **0604** (2006) 039 [arXiv:hep-ph/0601001]; B. Adhikary, B. Brahmachari, A. Ghosal, E. Ma and M. K. Parida, Phys. Lett. B **638** (2006) 345 [arXiv:hep-ph/0603059]; L. Lavoura and H. Kuhbock, Mod. Phys. Lett. A **22** (2007) 181 [arXiv:hep-ph/0610050]; S. F. King and M. Malinsky, Phys. Lett. B **645** (2007) 351 [arXiv:hep-ph/0610250]; S. Morisi, M. Picariello and E. Torrente-Lujan, Phys. Rev. D **75** (2007) 075015 [arXiv:hep-ph/0702034]; M. Hirsch, A. S. Joshipura, S. Kaneko and J. W. F. Valle, Phys. Rev. Lett. **99**, 151802 (2007) [arXiv:hep-ph/0703046]. F. Yin, Phys. Rev. D **75** (2007) 073010 [arXiv:0704.3827 [hep-ph]]; Prog. Theor. Phys. **119** (2008) 583 [arXiv:0801.0181 [hep-ph]]; B. Brahmachari, S. Choubey and M. Mitra, Phys. Rev. D **77** (2008) 073008 [Erratum-ibid. D **77** (2008) 119901] [arXiv:0801.3554 [hep-ph]]; B. Adhikary and A. Ghosal, Phys. Rev. D **78** (2008) 073007 [arXiv:0803.3582 [hep-ph]]; M. Hirsch, S. Morisi and J. W. F. Valle, Phys. Rev. D **78** (2008) 093007 [arXiv:0804.1521 [hep-ph]]. F. Feruglio, C. Hagedorn, Y. Lin and L. Merlo, arXiv:0807.3160 [hep-ph]; F. Bazzocchi, M. Frigerio and S. Morisi, arXiv:0809.3573 [hep-ph]; W. Grimus and L. Lavoura, arXiv:0811.4766 [hep-ph]; S. Morisi, arXiv:0901.1080

[hep-ph]; P. Ciafaloni, M. Picariello, E. Torrente-Lujan and A. Urbano, arXiv:0901.2236 [hep-ph]; M. C. Chen and S. F. King, arXiv:0903.0125 [hep-ph]; G. Altarelli, F. Feruglio and C. Hagedorn, JHEP **0803** (2008) 052 [arXiv:0802.0090 [hep-ph]]; Y. Lin, Nucl. Phys. B **813**, 91 (2009) [arXiv:0804.2867 [hep-ph]]; arXiv:0903.0831 [hep-ph].

G. C. Branco, R. Gonzalez Felipe, M. N. Rebelo and H. Serodio, Phys. Rev. D **79**, 093008 (2009) [arXiv:0904.3076 [hep-ph]].

M. Hirsch, Pramana **72**, 183 (2009).

M. Hirsch, S. Morisi and J. W. F. Valle, Phys. Lett. B **679**, 454 (2009) [arXiv:0905.3056 [hep-ph]].

P. Ciafaloni, M. Picariello, E. Torrente-Lujan and A. Urbano, arXiv:0909.2553 [hep-ph].

[175] B. A. Ovrut, J. Math. Phys. **19**, 418 (1978).

[176] G. Etesi, J. Math. Phys. **37**, 1596 (1996) [arXiv:hep-th/9706029].

[177] T. Inami and C. S. Lim, Prog. Theor. Phys. **65**, 297 (1981) [Erratum-ibid. **65**, 1772 (1981)].

[178] P. Gambino and M. Misiak, Nucl. Phys. B **611**, 338 (2001) [hep-ph/0104034].

[179] P. P. Divakaran, R. Ramachandran, Pramana **14**, 47-56 (1980).

[180] S. Dimopoulos and S. D. Thomas, Nucl. Phys. B **465**, 23 (1996) [arXiv:hep-ph/9510220].

[181] T. Ibrahim, P. Nath, Phys. Rev. **D58**, 111301 (1998). [hep-ph/9807501].

[182] M. Brhlik, G. J. Good, G. L. Kane, Phys. Rev. **D59**, 115004 (1999). [hep-ph/9810457].

[183] H. K. Dreiner, H. E. Haber, S. P. Martin, Phys. Rept. **494**, 1-196 (2010). [arXiv:0812.1594 [hep-ph]].

[184] W. Ledermann, *Introduction to group characters*, Cambridge University Press, 2nd Edition (1987).